AEDC-TR-08-20

RDHWT/MARIAH II
Hypersonic RDHWT/MARIAH II
Hypersonic Wind Tunnel Research Program

Edited by
M. L. Laster, C. C. Limbaugh, and J. L. Jordan
Aerospace Testing Alliance

September 2008

Final Report for Period January 1, 2001 – September 30, 2004

ARNOLD ENGINEERING DEVELOPMENT CENTER
ARNOLD AIR FORCE BASE, TENNESSEE
AIR FORCE MATERIEL COMMAND
UNITED STATES AIR FORCE

NOTICES

DESTRUCTION NOTICE

For unclassified, limited documents, destroy by any method that will prevent disclosure or reconstruction of the document.

APPROVAL STATEMENT

This report has been reviewed and approved.

ROBERT A. WILSON, CAPT
Applied Technology Division
Test Operations Directorate

Approved for publication:

FOR THE COMMANDER

ROBERT T. CROOK
Deputy Chief, Applied Technology Division
Test Operations Directorate

REPORT DOCUMENTATION PAGE

Form Approved
OMB No. 0704-0188

1. REPORT DATE *(DD-MM-YYYY)*	2. REPORT TYPE	3. DATES COVERED *(From - To)*
00-09-2008	Final	January 1, 2001 - September 30, 2004

4. TITLE AND SUBTITLE
RDHWT/MARIAH II Hypersonic Wind Tunnel Research Program Final Report

5a. CONTRACT NUMBER
F40600-03-C-0001

5b. GRANT NUMBER

5c. PROGRAM ELEMENT NUMBER

6. AUTHOR(S)
Editors:
M. L. Laster
C. C. Limbaugh
J. L. Jordan
Aerospace Testing Alliance

5d. PROJECT NUMBER
9498

5e. TASK NUMBER

5f. WORK UNIT NUMBER

7. PERFORMING ORGANIZATION NAME(S) AND ADDRESS(ES)
AEDC/DOT
1099 Avenue C
Arnold AFB, TN 37389-9013

8. PERFORMING ORGANIZATION REPORT NUMBER
AEDC-TR-08-20

9. SPONSORING/MONITORING AGENCY NAME(S) AND ADDRESS(ES)
AEDC/DOT
1099 Avenue C
Arnold AFB, TN 37389-9013

10. SPONSOR/MONITOR'S ACRONYM(S)

11. SPONSOR/MONITOR'S REPORT NUMBER(S)

12. DISTRIBUTION/AVAILABILITY STATEMENT
STATEMENT A: Approved for public release; distribution unlimited.

13. SUPPLEMENTARY NOTES
Available in Defense Technical Information Center (DTIC). Prepared in cooperation with MSE Technology Applications, Inc., Butte, Montana.

14. ABSTRACT
The U.S. Air Force sponsored and the USAF Arnold Engineering Development Center directed the Radiantly Driven Hypersonic Wind Tunnel (RDHWT)/ Magnetohydrodynamic Accelerator Research Into Advanced Hypersonics (MARIAH II) Program. This report primarily covers the research for the period from January 2001 through July 2004. The scope of the research program was to develop enabling technologies for a medium-scale hypersonic wind tunnel (MSHWT) that would provide a Mach 8 to 15 test capability with aeropropulsion testing as the principal need and focus. The USAF research program has been terminated, but work continues under Army sponsorship. Considerable progress has been achieved, and this final report summarizes the work. Key participants in this work were MSE Technology Applications, Inc., the prime integrating contractor; Princeton University; Ring Technical Services (RTS); Lawrence Livermore National Laboratory (LLNL); Sandia National Laboratory (SNL); and Oak Ridge National Laboratory (ORNL) (funded by a separate DoD program).

15. SUBJECT TERMS
Radiantly Driven Wind Tunnel; hypersonic wind tunnel; test facility

16. SECURITY CLASSIFICATION OF:			17. LIMITATION OF ABSTRACT	18. NUMBER OF PAGES	19a. NAMES OF RESPONSIBLE PERSON
a. REPORT	b. ABSTRACT	c. THIS PAGE			Capt. Robert A. Wilson
Unclassified	Unclassified	Unclassified	Unclassified	161	19b. TELEPHONE NUMER *(Include area code)* (931) 454-5261

PREFACE

The work reported herein was sponsored by the Arnold Engineering Development Center (AEDC), Air Force Materiel Command (AFMC), during the period spanning FY98 to FY04. The report contains an edited compilation of published and unpublished work performed by a national research team. Members of the team and authors, with their specific areas of expertise are:

Lawrence Livermore National Laboratory
- Dr. Marc Constantino – Ultra-High-Pressure Technology
- Dr. Ian Boyd – Ultra-High-Pressure Technology

Sandia National Laboratory
- Dr. Ronald Lipinski – Electron Beam Technology
- Dr. Gary Pena – Electron Beam Technology
- Dr. Larry Schneider – Electron Beam Technology

Princeton University
- Dr. Richard Miles – Diagnostics
- Dr. Gary Brown – Gas Dynamics
- Dr. Ihab Girgis – Modeling
- Dr. Dennis Mansfield – Experimental

Ring Technical Services
- Dr. Leon Ring – Systems Integration

MSE, Inc
- Gloyd Simmons – Project Management
- David Lofftus – Project Design and Management
- Steve Tarrant – Operations
- Jean Tourikis – Operations

Oak Ridge National Laboratory
- Dr. C. T. Liu – Materials

Arnold Engineering Development Center (Aerospace Testing Alliance)
- Dr. E. J. Felderman – High-Pressure Technology
- Dr. R. P. Howard – Diagnostics

Other members of the team and editors of this report are Mr. J. L. Jordan, Dr. M. L. Laster, and Dr. C. C. Limbaugh, Aerospace Testing Alliance., Arnold Engineering Development Center, Arnold Air Force Station, Tennessee. The manuscript was submitted for publication in September 2008.

CONTENTS

APPENDIXES

ILLUSTRATIONS

Figure

Figure Page

TABLES

1.0 INTRODUCTION

The United States Air Force (USAF) Arnold Engineering Development Center (AEDC) sponsored the Radiantly Driven Hypersonic Wind Tunnel/Magnetohydrodynamics Accelerator Research into Advanced Hypersonics (RDHWT/MARIAH II) Program. The purpose of the program was to develop enabling technologies for design criteria that will lead to the design of a medium-scale hypersonic wind tunnel (MSHWT) with Mach 8 to 15, true-temperature flight test capabilities. This research program was initiated in fiscal year (FY) 1998 and is based on prior research sponsored by the USAF and National Aeronautics and Space Administration (NASA) on supersonic thermal energy addition and magnetohydrodynamic (MHD) energy addition, respectively. The RDHWT/MARIAH II Research Program was originally expected to require approximately five to eight years and to lead to the development of a Mach 8 to 15 flight duplication test and evaluation (T&E) facility, depending on annual funding levels. The USAF RDHWT/MARIAH II Program was terminated in 2004 after completion of an estimated 50 percent of the required research. However, several aspects of the research are continuing under Army Aviation and Missile Research Development and Engineering Center (AMRDEC) sponsorship. This report is the third summary technical report published on the overall research project and summarizes the research and development (R&D) sponsored by the Air Force with focus on the period from January 2001 through June 2004. Detailed progress has been reported in other publications cited. Research and development results on nozzle materials, sponsored by the Office of the Secretary of Defense (OSD)/Director of Operational Test & Evaluation (DOT&E) Test & Evaluation/Science and Technology (T&E/S&T) Program and related to this effort, are also summarized in this document.

AEDC was responsible for overall program management during this reporting period, while each of the program's technical areas was led by one of the team members. Table 1 shows the primary and support organizations for each of the major facets of the research program. AEDC was responsible for the overall management of the program and contracted directly with MSE Technology Applications, Inc. (MSE), Sandia National Laboratories (SNL), Lawrence Livermore National Laboratories (LLNL), and Oak Ridge National Laboratories (ORNL) for the work. Princeton University (PU) and Ring Technical Services (RTS) were subcontractors to MSE, who served as an integrating contractor.

The ultimate goals of the program are to validate the enabling technologies and develop facility design criteria for a MSHWT. The MSHWT can serve two distinct purposes. First, it will provide a unique capability for testing and evaluation of missile-scale weapons systems. Second, it will validate the advanced technologies required to build a large-scale facility for testing aircraft air-breathing propulsion systems. Development of a MSHWT will provide an affordable capability for research, development, and T&E testing that will be substantially beyond the Air Force test capabilities that exist today. Performance goals of the MSHWT are true temperature, Mach 8 to 15, dynamic pressure of 500 to 2000 psf (24 to 96 kPa), a test section core flow size of 0.5 to1.0 m across, and run times greater than 1 s in clean air.

Near the completion of the R&D program, plans are to build an Integrated Test System (ITS), which is basically a small pilot wind tunnel. The ITS, which will not include MHD augmentation in its initial phase, first will serve to demonstrate a complete RDHWT wind tunnel, and second, will allow identification and solution of any potential problems that may arise from the system integration. Third, the ITS also will give future operators of the MSHWT the opportunity to learn how to operate the facility. Finally, the ITS could serve as a test bed for future technologies that may be spiraled into the MSHWT at a later time, such as MHD augmentation.

Table 1. Organization

Area	Primary	Support
Program Management	AEDC	
Test Requirements	AEDC	All
Concept Development	MSE	PU, SNL, LNL, RTS
UHP	LLNL	MSE
Nozzle Throat Survivability	LLNL, MSE	PU
Nozzle Heat Transfer	PU	AEDC, MSE
Nozzle Throat Materials Development	ORNL	
Electron Beam	SNL	PU
MHD	MSE	PU
Systems Integration	RTS	MSE

Key facility research areas for the MSHWT are ultra-high-pressure (UHP) air supply, nozzle-throat survivability, nozzle boundary layer and cooling, supersonic thermal energy addition, magnetohydrodynamic (MHD) energy augmentation, and system integration. This document summarizes the work and references other documents, where the research is discussed in detail.

Ultra-high-pressure air supply concepts for the MSHWT continued to evolve during this reporting period, culminating in an octahedral module concept that provides air and nitrogen in a coaxial flow to the nozzle. This concept, which consists of two nitrogen intensifier modules, two air modules, a transfer module, and a nozzle module, will operate with plenum conditions of 2100 MPa (305,000 psi) and 750 K (890°F) for run times of 1 to 10 s and a combined nitrogen/airflow rate of 160 kg/s. Development of an experiment to test and demonstrate critical MSHWT air supply components on a small scale was initiated at LLNL. A UHP development path was developed and is summarized in this report.

An experiment named A-2 Lite was designed, and testing was begun but not completed, for proof of principal of the pressure intensifier concept. A UHP test facility (UHPTF) was designed and constructed at MSE to test the A-2 Lite and pressure intensifier components as well as test nozzles at near-MSHWT air and nitrogen stagnation conditions for survivability at the severe flow conditions of the proposed MSHWT. The A-2 Lite components, including the pressure

vessel and piston, were designed and fabricated at LLNL and installed in the UHPTF for testing. Ultra-high-pressure component testing and nozzle survivability testing were initiated in the UHPTF A-2 Lite, and pressures up to 1260 MPa (183,000 psi) were achieved during this reporting period. Tests were planned for the A-2 Lite at pressures up to 2000 MPa (290,000 psi).

Nozzle survivability is a critical element of the RDHWT/MARIAH II technology base. With MSHWT stagnation pressures and temperatures up to 2100 MPa (305,000 psi) and 750 K (890°F), the nozzle is exposed to pressures on the order of 600 MPa (87,000 psi) and wall recovery temperatures up to 1800 K (2780°F). The MSHWT nozzles must survive these extreme conditions for seconds of run time essentially without geometric changes. The RDHWT/ MARIAH II Program has continued nozzle research through experiments, analytical model development, and nozzle materials research and development. Testing of nozzles in the A-2 Lite was initiated, and pressures up to 1034 MPa (150,000 psi) were achieved in a quasi-static blowdown mode from ambient temperature. Nozzle testing was planned for plenum conditions up to 2000 MPa (290,000 psi) and 750 K (890°F) but was not completed. It is hoped that the testing will be continued and completed in the future.

Because of the extreme environment to which MSHWT nozzles will be exposed, materials with high strength at high temperature must be used, and the nozzles must resist oxidation or be protected from oxidation. Material research at ORNL has developed an iridium alloy material that is an attractive candidate for this application; however, the material has not been proven to be capable of withstanding the oxidizing environment at MSHWT conditions. Thus oxidation protection could be required. In this event, the plan is to use a coaxial flow of nitrogen around a core flow of air to protect nozzles from oxidation. Modeling of the air/nitrogen coaxial flow is under way. A high Reynolds number coaxial flow nozzle experiment has been designed by Princeton University. Hardware for this experiment (including the coaxial flow nozzle) has been procured, but the experiments have not been completed.

The proposed MSHWT will operate with nozzle flow Reynolds number up to about 10^{10}. High Reynolds number (about 10^{8}) boundary-layer and heat-transfer experiments have been conducted at Princeton University at plenum pressures up to 136 MPa (20,000 psi) with plans to conduct experiments at plenum pressures up to 207 MPa (30,000 psi). The higher pressures have been plagued by leakage in the nozzle assembly and by pressure transducer failure. Thus far the analytical codes and experimental data on boundary-layer displacement have not agreed. Further analysis of these phenomena is included in this report using other hypersonic wind tunnel nozzle experimental data. Low-pressure (0.5 MPa), two-dimensional (2D) experiments have also been conducted in the Princeton University heat-transfer tunnel to demonstrate thin film injection along a nozzle wall. The 2D nozzle has optical access for evaluating the performance of the film cooling. These experiments have not been completed.

Progress was made in electron-beam (e-beam) thermal energy-addition research, including e-beam accelerator system concept development for MSHWT-scale systems (up to 200 MW),

energy-addition model development, and thermal energy-addition experiments. Princeton University and SNL conducted these experiments, in which e-beam energy addition to a supersonic nozzle flow was demonstrated at power levels up to 700 kW. While the fluid dynamics of the flow appeared to be reasonably stable, fluctuations in e-beam current were observed during the experiments. These fluctuations are believed to be caused by partial impingement of the beam on apertures in the beam accelerator tube. This problem should be correctable by proper design of a new accelerator that is being procured for the next series of experiments, which is to be sponsored by the Army. Thermal energy-addition simulation computer models (developed during this program) were used to evaluate the data from these experiments. However, good agreement could not be obtained, probably because of the unsteady and unknown magnitude of the beam current, which was not measured during the experiments. It is critical that the analytical model be able to predict the energy addition for MSHWT design purposes. This validation is planned for accomplishment in the next series of experiments, which is to be sponsored by the Army.

Sandia National Laboratories continues development of e-beam accelerator system technology, including the development of a 2- to 3-MeV, MSHWT-scale accelerator system concept capable of several seconds' operation. E-beam accelerator systems using thermionic cathodes and a rectified dc power supply appear to be feasible for MSHWT power levels. Additionally, a new 3-MeV accelerator system was designed and fabricated for use in planned 1-MW, 5-ms and 1-s experiments. As previously mentioned, these experiments were planned to be conducted during the next year of the program under Army sponsorship.

Magnetohydrodynamic acceleration of the flow after the thermal energy addition will be required to achieve test conditions for Mach numbers beyond 12. Modeling of MHD accelerator performance and small-scale experiments were accomplished during this reporting period. Magnetohydrodynamic acceleration for this application requires nonequilibrium ionization of the air in the accelerator. The use of e-beam devices in the sidewalls of the accelerator to create the required ionization at low temperature had been proposed but not yet validated. However, experiments were conducted at Princeton University using a high-frequency, high-voltage pulser that demonstrated nonequilibrium ionization and MHD interaction in a low-temperature, low-pressure flow. This is a significant result that gives hope that MHD acceleration can be used to extend the MSHWT performance above Mach 12.

System engineering and integration activities have continued with the purpose of ensuring that the major components of the MSHWT are compatible with each other in terms of operating conditions, scale, and stability of operation, as well as that the total system will meet its performance requirements. MSHWT analyses were conducted, and trade models and cost estimates were developed. A concept for a 20- to 30-MW integrated test system (ITS) demonstrator was developed and is discussed in this report.

At this point in the program, no fundamental flaws in the RDHWT/MARIAH II MSHWT concept have been identified in the experimental and analytical investigations. Additionally, no insurmountable problems were identified during the thermal energy addition and UHP air supply research, although the performance demonstration goals for the air supply, nozzle survivability, and energy addition have not yet been achieved. Thermal energy-addition experiments and modeling have led to the conclusion that stable energy addition to the supersonic flow can be achieved, at least to the power densities achieved in these experiments. While e-beam accelerator technology must be developed to produce an accelerator for the MSHWT with an average power level that is two orders of magnitude greater than those demonstrated to date, experimental results and analysis of accelerator components have led to the conclusion that the concept is viable.

From the UHP testing, it is concluded that pressures sufficient to simulate greater than Mach 10 conditions in a wind tunnel can be reached with a pressure intensifier system. However, fully dynamic operation of the UHP intensifier has not yet been demonstrated and will be required to demonstrate that steady, constant pressure flow can be maintained for at least 1 s. Some components that were thought to be low-risk elements experienced failures during testing. This fact leads to the conclusion that significant development work may be required and that thorough testing and demonstration of components at a sufficiently large scale is needed to reduce the risk in the design and construction of an RDWHT-type wind tunnel that uses high-pressure intensifiers.

Continued development of the UHP air supply, nozzle, e-beam, thermal energy-addition, facility control system, and overall system technologies is required to mature the technologies required for design data of a larger scale, reliable wind tunnel that will achieve the MSHWT performance goals. Specifically, the 1-MW thermal energy-addition experiments should be conducted with the new e-beam accelerator that is under development and data acquired to validate computer codes and (with a continuous dc power supply) to demonstrate a stable and reliable e-beam operation for a duration of at least 1 s. E-beam technology development for MSHWT-scale components should also continue.

In addition, the ultra-high-pressure technology testing should continue to demonstrate a capability to reliably achieve MSHWT pressures in a single-stroke pressure intensification system. Continued nozzle testing is also recommended to find the survivability limits of nozzle throats and to develop survivable nozzle systems. Depending upon the results of the nozzle throat survivability testing currently in progress, a coaxial air/nitrogen flow ultra-high-pressure nozzle demonstration experiment may be needed for a Mach 12 wind tunnel operation.

Development and validation of analytical tools must continue. Since the RDHWT/MARIAH II Program is moving beyond component technology development and toward integrated system demonstration and development of MSHWT design criteria, the system engineering function is becoming more important. System engineering and integration activities should increase in intensity and extent to ensure that the integrated system achieves the required performance and operational reliability.

1.1 BACKGROUND

Hypersonic military and/or commercial flight vehicles, including space access vehicles, fast reaction, global reach (strike and reconnaissance) vehicles, and missile defense systems are envisioned future needs. The USAF Scientific Advisory Board (SAB) (Ref. 1), Air Force 2025 (Ref. 2), Aerospace 2020 (Ref. 3), the Review and Evaluation of the Air Force Hypersonic Technology Program (Ref. 4), the joint NASA/Department of Defense (DoD) Study in 1994 (Ref. 5), and the DoD Aeronautical Test Facilities Assessment study in 1997 (Ref. 6) all indicate the need for hypersonic vehicles and/or the test facilities to develop them. These and other studies, discussed in more detail in Refs. 7 and 8, all reveal that the U.S. lacks the capability to adequately ground test hypersonic propulsion and vehicle concepts. In particular, major facility deficiencies are cited for the ground testing of air-breathing hypersonic propulsion systems above Mach 3.2, which is the current limit of large-scale, clean air, continuous full-scale testing capability.

In order to conduct performance and durability development testing in a ground test facility, it is critically important that the hypersonic flight environment be duplicated in terms of velocity, temperature, pressure, air chemistry, and test time and at full scale test conditions. There are at least five major technical obstacles or issues to the development of higher Mach number ($M > 7$), clean air, true-temperature, hypersonic T&E wind tunnels. They are: 1) introducing sufficient energy into the air while 2) producing the correct air chemistry and 3) entropy, 4) providing sufficient run time, and 5) availability of materials or techniques that will contain the high-temperature, high-pressure test gas. Existing technology for energy addition using ceramic storage heating will allow ground-based clean air testing at speeds only up to about Mach 7. Combustion-heated, vitiated air facilities can provide testing to about Mach 8, but this test medium contains combustion products and is not clean air. A test capability of Mach 9 to 10 (currently limited by pressure capability) can be achieved by heating air with electric arc heaters, but no test capability of adequate size using this technology currently exists, and the test medium is not clean air. Compression heating, such as that used in impulse shock tunnels, can provide up to about Mach 14 to 15 test conditions, but the run time is limited to no more than a few milliseconds, which is entirely too short for operability and durability testing of air-breathing propulsion systems. Gas chemistry issues occur in electric arc-heated and impulse tunnels because of the heating processes and very high temperatures involved. Furthermore, the high stagnation temperatures cause severe heat transfer into the nozzle and unacceptable erosion of the nozzle throat. Currently, the only known approach with the potential to provide the needed true-temperature, relatively clean air, long run-time, Mach 8 to 15 ground test capability is the radiantly driven wind tunnel approach, the subject of this report.

The approach taken in the RDHWT research program is to add the necessary energy to the air downstream of the nozzle throat in the supersonic region of the flow (Ref. 9). The original approach, resulting from Air Force-funded studies of radiantly heating supersonic flow performed between 1992 and 1998, was to use laser or electron-beam energy directed into the airflow, thus raising the static thermal energy content of the air, which could then be converted to added

velocity by the nozzle expansion. The idea of adding energy to the supersonic flow dates back more than 30 years (Ref. 10) but was long considered impractical because techniques to achieve the ultra-high-stagnation pressures required were not known or developed.

Early RDHWT research proved promising, but it also revealed that the concept still had performance boundaries. A pressure of about 2100 MPa (305,000 psi) is currently accepted as a practical design limit for operating pressure vessels using known pressure intensifier technology. This pressure is high enough to provide an upper Mach number limitation of about 12 at a flight dynamic pressure of 2000 psf (96 kPa). For higher Mach numbers, the pressure requirement grows dramatically and quickly becomes impractical to achieve in an operating air supply system.

At the same time as the earlier Air Force studies, NASA was funding studies of an MHD acceleration or energy-addition concept. The results of the NASA studies confirmed earlier Air Force study results that MHD alone was not practical to achieve the needed test conditions, but the NASA studies further concluded that a combination of the RDHWT approach augmented with MHD acceleration could possibly achieve Mach 12 to 15 test conditions (Ref. 11). This approach avoids flight stagnation temperatures ahead of the nozzle throat, and nozzle heat transfer problems are reduced. Also, effects of gas dissociation are reduced since the gas is not heated to high static temperatures (< 2500 K).

Past demonstrations of MHD augmentation required that the test gas be electrically conductive. This effect has been demonstrated at high temperature and low pressure using alkali metal seeding to enhance the conductivity. The approach has been shown to work only if the static temperature of the alkali is greater than about 2500 K (4040°F). This high static temperature leads to too high an air entropy and undesirable air chemistry (NOX formation), both of which make it impractical to reach the desired flight conditions. Additionally, the test gas alkali seed has an unknown and probably undesirable effect on the flight system test objectives.

Out of these research studies, a hybrid concept has been developed to achieve the desired Mach 8 to 15 capability. Electron beam heating of a supersonic flow and subsequent expansion through a nozzle will enable operating a tunnel at speeds up to Mach 12 with clean air. Mach 15 flow velocity would then be achieved by using a second continuously operating electron beam or possibly a diffused electric arc projecting across the acceleration channel to establish the electrical conductivity necessary for MHD acceleration. This method of creating the necessary conductivity will probably avoid the contamination and undesirable high temperatures attendant to seeding.

Two previous AEDC technical reports (Refs. 12 and 13) have been prepared documenting progress on this research through the year 2000. Also, numerous overview technical papers have been presented or published on various aspects of this research (Refs. 7, 8, and 14). The most recent papers prepared (Refs. 14 through 25) covered major facets of the research effort for this reporting period and provide guidance to earlier related papers. These cover the more recent research in the areas of ultra-high-pressure (UHP) air supply; nozzle throat survivability, including nozzle material research; nozzle design, including nozzle boundary-layer development

and cooling; airflow thermal energy addition; airflow chemistry resulting from thermal energy addition; MHD energy addition; system integration; and test requirements definition.

1.2 FACILITY CONCEPT

The RDHWT/MARIAH II program is focused on the technology development and demonstration of an innovative hybrid concept for reproducing hypersonic flight conditions over the Mach 8 to 15 range in an affordable ground testing facility (Refs. 7 and 26 through 28). Figure 1 illustrates this concept and provides a comparison to a conventional wind tunnel in which the gas is heated ahead of the nozzle throat in the stagnation region. The RDHWT/ MARIAH II concept uses a UHP air supply (not shown) operating to 2100 MPa (305,000 psi) to achieve Mach 12 simulation at a flight dynamic pressure of 2000 psf (96 kPa). Higher Mach number duplication would require higher pressures, which are impractical to achieve. Thermal energy is added downstream of the nozzle throat (the selected approach shown uses e-beam energy addition) to reduce the chemical dissociation, heat transfer, and erosion problems associated with the conventional approach.

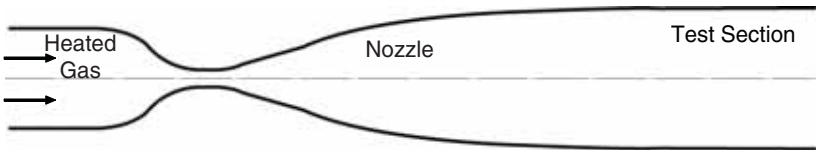

a. Conventionally Heated Wind Tunnel

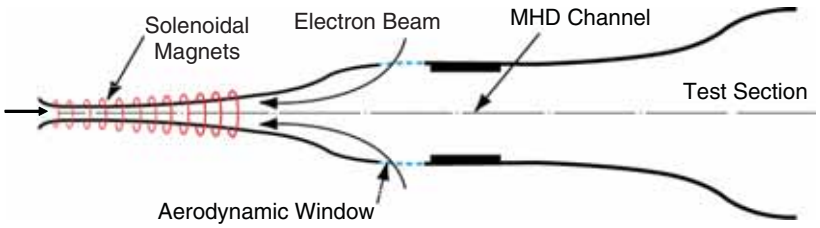

b. E-Beam Supersonic Thermal Energy Addition with MHD Augmentation

Figure 1. Hypersonic Wind Tunnel Concepts

The thermodynamic process for this concept is shown in Fig. 2. The green line in this figure illustrates the performance of the proposed concept overlaid on a Mollier diagram of air for a Mach 14.5 simulation, including MHD augmentation. The illustration starts with air in the plenum pressurized by a UHP system to 2000 MPa (290,000 psi) and a temperature of 900K (1200°F). The air expands isentropically through the facility nozzle to about Mach 1.5 to 2 (~ 200 MPa, 450 K). Thermal energy from the e-beam source is absorbed by the high-density air at nearly constant Mach number. Energy continues to be added in a controlled manner to achieve the final enthalpy level (~3500 kJ/kg). The nozzle and energy deposition profile are tailored to avoid thermal choking and to limit the static temperature to 2500 K (4040°F) or less, thus avoiding unwanted chemistry effects, such as the creation of atomic oxygen and NOX. The facility nozzle provides a

final isentropic expansion of the test gas to the desired conditions entering the MHD channel (~300 K). For simulation above Mach 12, MHD augmentation is employed to accelerate the flow using electromotive forces. A nozzle at the exit of the channel expands the airflow to the final desired velocity and altitude simulation conditions. For Mach 12 and below, MHD augmentation is not required to achieve the desired test conditions.

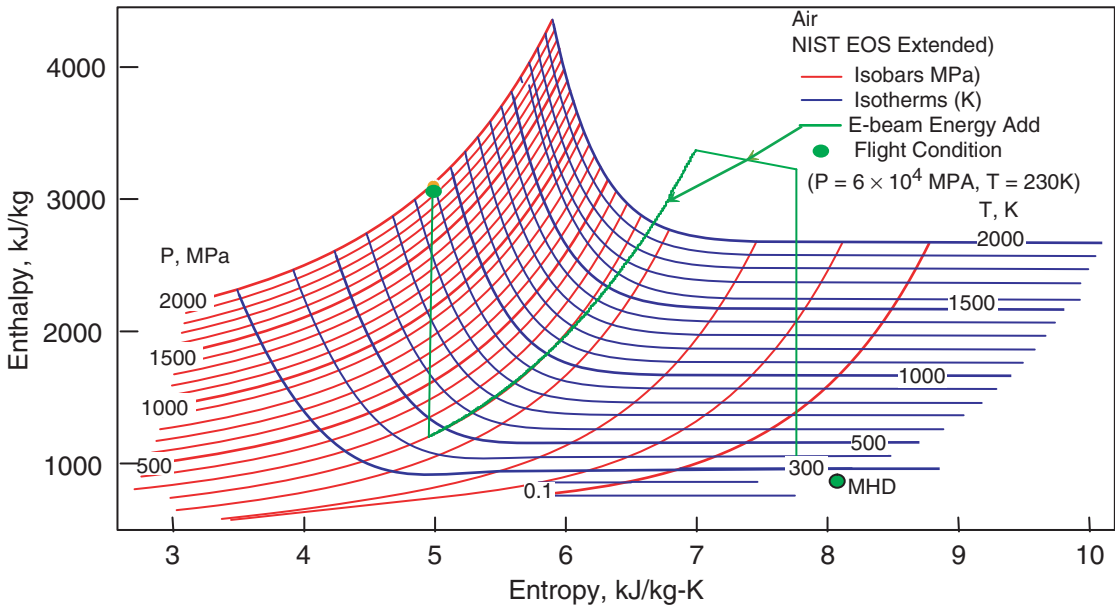

Figure 2. Conceptual Thermodynamic Process

One may note from the Mollier diagram in Fig. 2 that the enthalpy becomes strongly dependent on pressure as well as temperature at the lower entropies. This is a real-gas effect. An important result of this effect is that boundary-layer recovery temperatures can significantly exceed the total temperature of the flow, especially in the vicinity of the nozzle throat. The impact of this phenomenon is discussed in Section 3.

Figure 3 shows one artist's concept of a MSHWT. The figure shows the major facility components as they are presently envisioned, including UHP air supply system, thermal energy-addition system, and MHD channel system. The most recent concept for an air supply configuration is presented in Section 3.

The projected flight duplication performance of the MSHWT facility is shown in Fig. 4 and compared to various types of systems performance envelopes and other classes of facilities. The performance for MHD augmentation is also shown. Note that the MSHWT facility performance limit is denoted "Radiant Facility" on the figure. It should be noted that the RDHWT concept has lower altitude performance potential (for example, Mach 8 at sea level). This feature could be useful for testing any devices that fly at low altitude within this envelope (e.g., low-altitude, rocket-powered missiles).

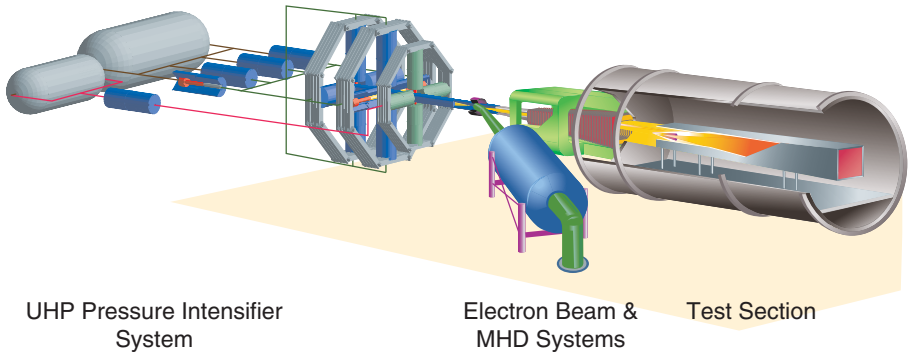

Figure 3. MSHWT Artist's Concept

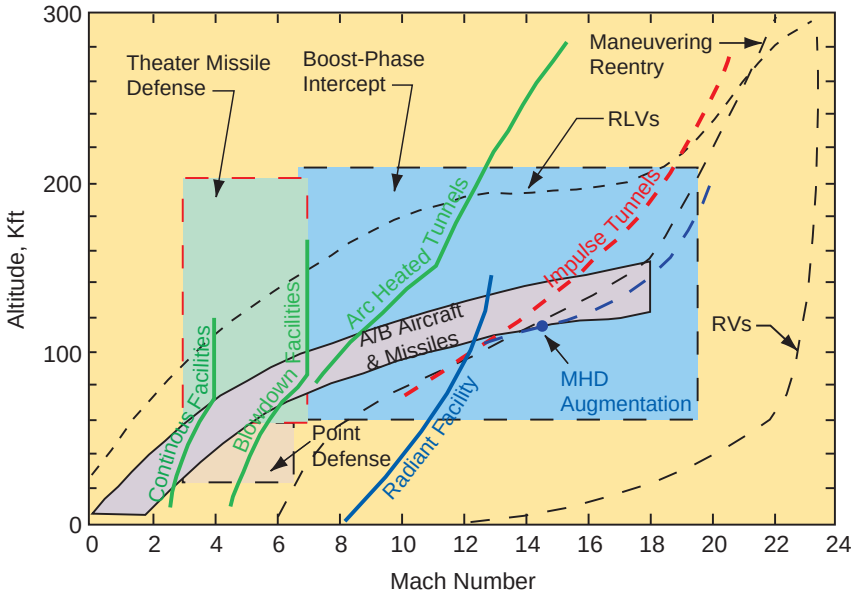

Figure 4. System/Facility Performance for Flight Duplication

Computer models are being utilized extensively throughout the program in preliminary and advanced concept investigations, component trade studies, test planning and preparation, and posttest data analysis and interpretation. The models were adapted, as required, from existing models and are being validated using the test data; thus, they are available for making reliable performance projections for upcoming experiments and, ultimately, for the MSHWT facility. Examples of these modeling efforts are discussed in Sections 3 and 5.

A comprehensive research plan was prepared to guide the program and was updated annually to reflect the latest research findings. The plan addressed key research areas and, within each technical area, addressed requirements, critical technical issues, alternative concepts, key demonstrations, and experiments in some detail. The version of the plan documented in Ref. 7, for example, is considerably outdated.

Section 3 introduces the requirements, critical technical issues, progress, and future plans for the major facility subsystems, including UHP air supply, storage heater, nozzle, thermal energy addition, and MHD.

It should be noted that, during the several years of this research, values used for key parameters have undergone small changes as the work has matured. For example, early work used a target stagnation pressure of 2300 MPa (333,000 psi), whereas the current target is 2100 MPa (305,000 psi). In this report, results from earlier work are reported, and there may be small differences in conditions used to illustrate physical principles or phenomena. Also, as specific hardware has been designed to test specific concepts, final design conditions may differ in detail from the values used initially to understand the phenomena being tested. Since this research effort is intended to extend technology beyond current known physical parameters, such variations should not detract from the understanding of the phenomena being investigated.

2.0 REQUIREMENTS AND NEEDS

2.1 FUTURE HYPERSONIC FLIGHT SYSTEMS AND ASSESSMENT OF TEST NEEDS

Envisioned future needs for military and/or commercial flight vehicles include those that fly at hypersonic speeds in the atmosphere, serve as transporters for space access, and have capabilities of fast response, global reach (strike and reconnaissance), and missile defense. Tentative plans exist in the major categories of hypersonic aircraft and missiles to either improve existing weapons systems or develop new systems over the next 20 years. The National Aerospace Initiative (NAI) program (Ref. 29) is a technology development program with a road map to develop the basic technologies over the next few years with an emphasis on air-breathing propulsion for missiles and aircraft-type systems to Mach 15 in this program. Currently, the development of these type vehicles, which employ air-breathing propulsion, is constrained by the lack of ground-based test facilities that would reduce technical risks to acceptable levels.

The types of vehicles under consideration can generally be classified as follows:

- Aircraft
  - Reconnaissance
  - Interdiction
- Space-Launched, Single and Multiple Stage
- Missiles
  - Tactical
  - Air-Launched Guided
  - Ground-Launched Defense
  - Long-Range Standoff Cruise
- Reentry

This list of vehicle types covers both offensive and defensive systems as well as transportation systems. Generally, for reconnaissance, interdiction, and space launched vehicles, the air-breathing propulsion flight Mach numbers are limited to less than Mach 15 and perhaps to no more than Mach 10 to 12. If air-breathing propulsion is employed, as is proposed in many cases, the flight dynamic pressures usually range between 500 and 2000 psf (24 and 96 kPa). For missiles, the long-range standoff cruise vehicle may also use air-breathing propulsion. Thus far, these vehicles have primarily been considered for cruise Mach numbers less than 10 and use hydrocarbon fuels. For vehicles that use air-breathing propulsion above Mach 10, hydrogen is used as the fuel (Ref. 30).

In the course of planning new hypersonic weapons systems, some vehicles will emerge to be considered for development and deployment. During the development period, critical testing must be accomplished on models and prototype vehicles to validate their design. This will involve computational modeling, ground test, and flight test.

The process for development of air vehicles historically has depended heavily upon both ground and flight test. Experience has taught the air vehicle development community that both are critically important to the successful development of any weapons system. As the need for faster response (i.e., higher flight speeds) and military space activities has evolved, the testing required has become much more demanding and challenging because of the high-thermal environment of hypersonic flight. Existing ground test facilities and test techniques are grossly deficient or even nonexistent for several test disciplines (Refs. 5, 6, 26, 30, and 31). This deficiency has led some to think that development test procedures should be cut short and more dependence be given to flight tests. However, flight test procedures often necessarily limit data fidelity for assessment of performance, operability, and durability capabilities, especially if failures occur. For example, the National Aerospace Plane (NASP) program was heavily weighted toward flight testing because of the nonexistence of adequate ground test facilities. This proved to be a severe limitation and contributed to the demise of the program (Ref. 30).

Studies performed in 1992 and reported in 1994 (Ref. 5) revealed serious gaps in hypersonic test capabilities relative to development test needs for the types of vehicles discussed above. Since these studies were accomplished, there essentially has been no improvement in hypersonic ground test capabilities. Figure 5 (Ref. 5) displays current test capabilities and test needs for the usual classes of test. Figure 5 also shows a summary of the capability limitations or inadequacies that have been identified by comparing the forecasted future test requirements with the existing test capability. As shown in this figure, aeropropulsion test capability above about Mach 7 is completely inadequate. Adequate clean air, large-scale, aeropropulsion test capability exists up to Mach 3.2, and limited capability (with vitiated air) exists from Mach 3.2 to Mach 7. Reasonable aerodynamic test capability exists up to Mach 14, and some limited capabilities exist in the areas of aerothermal, aero-optic, and jet-interaction test capability.

Figure 5 also shows the current NAI science and technology (S&T) off-ramp (Ref. 29) goals in terms of maximum Mach number requirements for development of aircraft/missile systems that employ air-breathing propulsion. Based upon the schedules of the forecasted systems/programs and their operating envelopes, some of these shortfalls present critical deficiencies. For example, the near-, mid-, and far-term off-ramps in Fig. 5 correspond to the years 2010, 2015, and 2020, respectively. Solving some of these shortfalls will require significant advances in the facility state of the art and test techniques. Facility research to develop and demonstrate new facility concepts is necessary in the near term to be ready to meet the test needs in the far term.

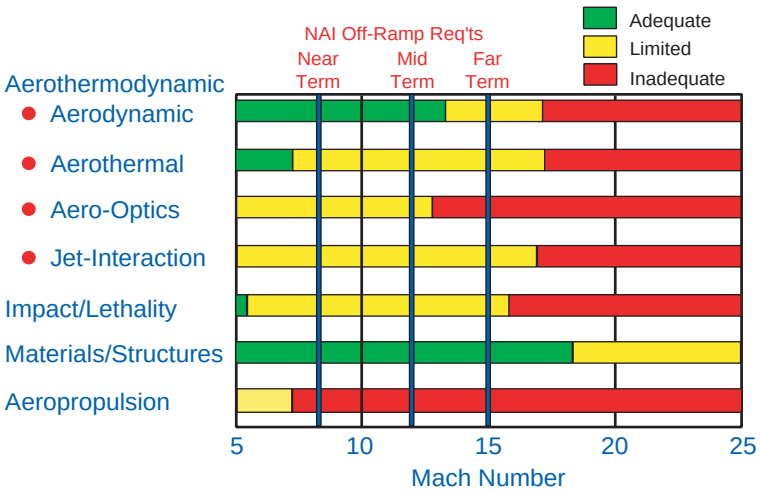

Figure 5. Summary of Current U.S. Hypersonic Test Capabilities (Ref. 5)

2.2 HYPERSONIC FLIGHT SYSTEMS TEST REQUIREMENTS

As a part of the RDHWT/MARIAH II program, studies were sponsored by the Air Force to define technical criteria for development of T&E wind tunnel testing of visionary and future military systems that are expected to fly in the atmosphere and in the Mach 8 to 15 regime (Ref. 27). These technical criteria are needed to establish specific facility technical requirements and approaches that must be pursued in the RDHWT/MARIAH II facility research, to evaluate other proposed facility concept approaches, and to aid in advocacy of any needed new hypersonic facilities. Alternative approaches include, but are not limited to, electric arc-heated and impulse wind tunnels, sled tracks, light-gas gun acceleration devices, modeling and simulation, and flight test. Other studies, not a part of this program, are needed to perform an assessment of alternative solutions.

The scope of test requirements under consideration includes aerothermodynamic, aero-optic, jet interaction, propulsion, thermal-structure, and shroud separation tests. However, the initial emphasis and focus here is on air-breathing propulsion freejet testing, which is the most demanding driver of test requirements. Facility Mach number, enthalpy, pressure, run time, flow path size, flow quality, test productivity, measurement capabilities, facility capitalization cost, and cost of testing have to be considered as a part of facility planning.

2.2.1 Critical Technical Issues

Critical technical issues for aeropropulsion testing include:

1) Combustion phenomena cannot be scaled; therefore, duplication of the desired altitude flight conditions in terms of pressure, temperature, and velocity is required.

2) Test time is critical in establishing facility air storage, energy storage, thermal management, and exhaust management requirements and concepts. Air-breathing propulsion testing objectives are usually classified into three categories: performance, operability, and durability testing, each with a different characteristic testing time.

3) The size of a T&E test facility is determined by test article size requirements. Size and velocity/altitude simulation requirements determine facility mass flow requirements, which (along with test time requirements) determine facility air storage, energy, thermal management, and exhaust management requirements. The focus of the research reported herein is to provide design criteria for a MSHWT but could be extrapolated to a larger scale T&E test facility. The MSHWT is intended to be sized to accommodate testing of "missile size" air-breathing propulsion systems and possibly subsystems of larger systems. Thus, an assessment of the size of selected hypersonic military systems and subsystems that should be tested is also needed.

4) Air chemistry and flow quality requirements for facility testing also must be assessed. The allowable tolerances on these factors are important to selecting a facility concept and to design of components.

2.2.2 Air-Breathing Propulsion Test Requirements

As mentioned above, critical technical issues include test time, test article size, air chemistry, and flow quality as well as duplication of the thermodynamic conditions for flight for air-breathing propulsion testing. Several years ago the Air Force sponsored a study by the Boeing Company to gain some insight into test time and test article size requirements (Ref. 8), and the results of that study are summarized in this section. Some study of air chemistry and flow quality requirements also has been conducted (Ref. 27), but additional study is needed.

The baseline designs considered in the Boeing study are presented in Table 2.

In the Boeing study, the Mach number ranged from 0 to 15, depending upon the specific baseline concept, as shown in Table 2. Pressure altitude was generally 30 km or higher.

Table 2. Summary of Baseline Design Concepts

Concept	Air-Breathing Mach Range	Length, m (ft)	Propulsion
Mach 8 Cruise Missile	4 to 8	4.3 (14)	Hydrocarbon Scramjet
SSTO Space Access with RBCC	0 to 14	62.8 (206)	Hydrogen Ramjet/Scramjet (RBCC)
SSTO Space Access with ODWE	5.5 to 15	65.5 (215)	Hydrogen Oblique Detonation Wave Engine (ODWE)
Dual-Use TSTO/ Cruise Vehicle	0 to 10	63.4 (208)	Hydrocarbon ACETR, Hydrogen Ram/Scramjet

SSTO: Single Stage to Orbit
TSTO: Two Stage to Orbit
RBCC: Rocket-Based Combined Cycle
ODWE: Oblique Detonation Wave Engine
ACETR: Air Core Enhanced Turbo Ramjet

Test time requirements were considered for performance, operability, and durability testing for a Mach 8 cruise missile and the single stage to orbit configuration. It is thought that test time requirements for these configurations will be adequate for most other hypersonic air-breathing propulsion applications. Required test times for the Mach 8 Cruise and SSTO type vehicles are shown in Table 3.

Table 3. Test Time Requirements in Seconds (Ref. 8)

Configuration	Performance	Operability	Durability
Mach 8 Cruise	0.004 to 0.010	10 to 20	525
SSTO	0.008 to 0.02	10 to 20	360 to 1200

The performance time criteria shown in Table 3 are the times needed to establish steady test time based on the “3 slug” rule (i.e., a flow length three times the length of the test article). The operability test time criterion is the time needed to operate moving components of the propulsion system through their operating range. The durability time criterion is the time to reach equilibrium temperature along a trajectory or the time of a long cruise mission.

For a blowdown-type facility like the MSHWT, meeting the test time criteria for performance testing is well within the facility goals adopted by the program (several seconds of run time). The longer test times for operability and durability testing are largely a function of affordability. The test conditions are not significantly more demanding, but the air supply system becomes much more complex, much more costly, and perhaps impractical. The energy-addition system also may be more complex and costly, and nozzle throat survivability may become an issue although alternative approaches, including film cooling and advanced throat materials, are being investigated.

The Boeing study provided anticipated vehicle size in terms of vehicle length and scale, parameters useful in selecting facility size. As shown in Table 2, vehicle length requirements range from 5 m for the Mach 8 cruise missile to about 70 m for the SSTO configurations. For the Mach 8 cruise missile, full-scale tests are proposed for the flow path and will require a maximum cross-section size of about 0.7 m. Therefore, a 1-m test section for the MSHWT test facility appears to be the minimum for cruise missile development testing. A facility for full-scale testing of the larger SSTO and TSTO configurations may not be affordable, and thus subscale or component testing may be the only affordable approach. The Boeing study suggests that combustor testing should be at least at 50-percent scale while the inlet, nozzle, and nozzle afterbody could be tested at 20-percent scale. With these criteria, an estimate of the minimum facility test section cross-section size requirement is about 1.5 to 2.0 m, with a test section length of about 6 m. Further analysis is needed to fully convert these criteria to facility test section size, and the affordability of a facility in this size range is yet to be determined.

On the basis of these studies, it was decided to use a 10-s run time with a 1-m test section for the MSHWT baseline, which will provide capability for performance and operability testing. Durability testing will require significantly longer run times; however, how much longer is not clear. Opinions range from 30 to 40 s to several minutes. Thus, the issue needs further study and resolution. The RDHWT/MARIAH II program identified concepts to increase run times if the need and funding should exist.

3.0 MSHWT TEST FACILITY RESEARCH

This section summarizes the major research activities conducted under the RDHWT/ MARIAH II project since January 2001. The technology development is expected to require about three to four years of additional work to complete, assuming adequate funding is available. The research is organized according to the major technical areas requiring technology development. These major technical areas are gas supply, storage heater, nozzle, electron beam energy addition, and MHD.

3.1 OVERVIEW AND RESEARCH STRATEGY

The major goal of this research has been to find a way of achieving an aeropropulsion ground test capability with at least 10 s of run time and speeds up to Mach 15 at a dynamic pressure of 2000 psf (96 kPa), currently believed to be the upper limit of scramjet propulsion. As indicated in Sections 1 and 2, such facilities do not currently exist, although relatively clean-air, freejet propulsion test capability up to Mach 7 exists through use of state-of-the-art air storage systems and storage heaters. Mach 8 true-temperature test conditions are achieved with vitiated air heaters, but the effects of the combustion contamination are generally unknown and/or undesirable. It is also possible to achieve much higher Mach number enthalpies with electric arc heaters, but not at sufficient pressure to achieve more than about Mach 9 freejet flight conditions.

Adding energy to the flow downstream of the nozzle throat reduces the required stagnation enthalpy and potentially increases facility lifetime. Simultaneously, it can reduce static temperature; thus relatively clean air potentially can be produced through the energy-addition processes. Adding energy to the supersonic flow does produce additional issues, however. As shown in Fig. 2, the supersonic energy-addition process increases the flow entropy, and this effect must be compensated for by the use of very high initial pressure (to reduce the initial air entropy) to achieve the correct test pressure, temperature, and velocity conditions.

The initial analysis for the radiantly heated wind tunnel performed in 1995 (Ref. 9) resulted in the establishment of research goals based on the belief that the air supply pressures and temperatures could be achieved, thus allowing Mach 12 true-temperature, freejet performance at 2000 psf (96 kPa) dynamic pressure. It was also determined that, by adding MHD acceleration to the Mach 12 gas, about Mach 15 simulation might also be achieved. Thus, the overall goal of the research has focused on developing technologies to achieve Mach 8 to 15 test capabilities.

Because of the low entropies needed at the start of the gas expansion process, the gas (air and nitrogen) stagnation conditions are in the real-gas regime. These real-gas effects produce elevated nozzle recovery temperatures; thus nozzle throat heat transfer is an important issue and must be considered. For example, calculated nozzle throat recovery temperature is about 1600 K (2420°F) for a 750 K (890°F) stagnation temperature to provide Mach 12 conditions. However, the calculated recovery temperature for conventional stagnation heating approaches about 8000 K (13,940°F). Even though the RDHWT approach significantly lowers the recovery temperature compared to conventional stagnation heating, the 1600 K (2420°F) recovery temperature at the ultra-high-pressure conditions presents serious material strength and fugacity concerns. Therefore, since there is no practical experience or heat-transfer information with regard to nozzles operating in the real-gas regime at the ultra-high pressures needed, the practical limits of nozzle throat survivability must be established by experiment. In relation to this challenge, an effort has been undertaken under a separately funded project by the Oak Ridge National Laboratory (ORNL) to develop a material with high strength (higher strength than steel) and resistance to oxidation that potentially would satisfy the MSHWT nozzle throat strength, heat transfer, and fugacity requirements. This effort is discussed below.

Of the nozzle survivability issues, the effect of the fugacity (the effect of the partial pressure of oxygen on the material) is probably the most uncertain. Because of this uncertainty, a parallel nozzle survivability research effort has been initiated. This research will investigate the use of nitrogen as film protection to avoid excessive oxidation and erosion of the nozzle material. Helium was also considered for film protection but was discarded from further consideration in favor of nitrogen because nitrogen gas properties are similar to those of air; consequently, nitrogen would be easier to use in shielding the nozzle walls.

To establish the limits of nozzle throat survivability, the strategy is to test representative nozzle throat materials, including any new materials developed by ORNL, in an ultra-high-

pressure flow experiment with both air and nitrogen and thus establish the respective safe operating limits of each of the materials. As of September 2004, tests had been conducted successfully with maraging steel nozzles to approximately 1200 MPa (~12,000 atm), well short of the 2000-MPa (~20,000-atm) goal, but nevertheless encouraging.

The initial research studies showed that about 2300-MPa (~23,000-atm) total operating pressure with an air or nitrogen gas supply may be achievable with pressure intensifiers, although only about 2046 MPa (20,200 atm) is needed for Mach 12 operations at 2000 psf (96 kPa) dynamic pressure. The operating mass flows and test times needed for a facility will require multiple pressure intensifiers operating in parallel, which technique is discussed below. The research strategy has been to prove that a single pressure intensifier could operate successfully and reliably to 2000 MPa (~20,000 atm) pressure with a 1-s run time. Concurrently, design concepts for a pressure intensifier system that can be used for the MSHWT have been developed. These concepts also are discussed below.

Validated boundary-layer models are needed at the high Reynolds numbers (order of 10^{10}) anticipated in the MSHWT nozzle for both air and coaxial air/nitrogen flows. The strategy is to develop and validate models with high Reynolds number (order of 10^{8}) flow experiments at Princeton University. Similar experiments are planned to be conducted at near-MSHWT conditions using the A-2 Lite modified, also described in this section.

The strategy in the electron beam energy-addition research has been to perform modest pressure flow experiments [up to 2600 psi (17,900 kPa)] in rough order-of-magnitude power increases from low power (10 kW) at a few milliseconds up to 1 MW. The 1-MW experiments are to be conducted with the electron beam on at run times of up to 1 s. The experiments accomplished and reported herein are all at millisecond run times. The 1-MW, 1-s experiments are yet to be conducted. The results obtained thus far to about 700-kW power at millisecond run times have been used for comparison with computational models (Refs. 16 and 23).

Real-gas energy-addition experiments are planned at high pressures and densities near those expected in a MSHWT facility up to near Mach 12 enthalpies. These experiments are necessary because the research for each of the subsystems for the energy addition (UHP, electron beam, and steering magnets) has been done without the presence of the other systems. Final validation of the energy addition at the high enthalpies with the electron beam, UHP air supply, and magnets operating together is necessary. It is anticipated that the power levels for this system demonstration will be 20 to 30 MW.

3.2 ULTRA-HIGH-PRESSURE GAS SUPPLY CONCEPT DEVELOPMENT

The UHP development path, illustrated in Fig. 6, has four major experiments, which culminate in the Integrated Test System (ITS) and design specifications for the MSHWT. (In this figure and in subsequent figures of this type, the color shading represents the status at the time of Air Force program termination.) The A-2 Lite is intended to demonstrate basic 2000-MPa

(~290,000-psi) pressure containment, nozzle survivability, and system control; the MSHWT UHP component experiment is intended to demonstrate MSHWT component performance; it also includes an octahedral module subscale experiment to demonstrate the octahedral geometry concept. The A2-Lite Modified (A2LM) experiment demonstrates coaxial air/nitrogen flow up to 900 MPa (~130,000 psi) and may include a storage heater and valve downstream of the pressure intensifier and ahead of the nozzle. The A-2 Lite hardware exists and is being used in experiments that will be discussed in future documentation. The component test rig is in design and fabrication at LLNL. The A2LM and the ITS experiments are planned, but no hardware has been designed or fabricated at this point. The preliminary concept for the A2LM experiment is to modify the existing ultra-high-pressure test facility (UHPTF) (discussed in Section 3.3) and A2 Lite to accommodate a UHP coaxial nitrogen/airflow experiment along with a storage heater and valve.

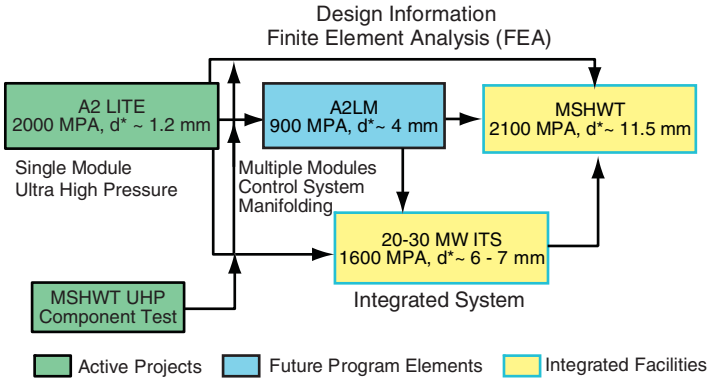

Figure 6. UHP Gas Supply Development Roadmap

3.2.1 Background

The MSHWT will require seconds of run time (10 s is the chosen baseline) and relatively large mass flows for air and nitrogen. This implies relatively large fluid volumes at the highest practicable static pressure and temperature. The primary difficulties for the mechanical design are connecting multiple volumes at pressures of up to 2100 MPa (~305,000 psi) and temperatures of about 750 K (890°F), fabricating high-strength steel sections approximately 2 meters in a typical dimension, and reacting the pressure-related forces in the system. Further, the economics of capital construction, operational costs, and amortization of the UHP hardware over its fatigue lifetime introduce additional constraints on the design. Fortunately, UHP design principles are well understood, and sophisticated finite element analysis (FEA) computer codes are available to model the thermal and mechanical responses for relatively complex geometries. The UHP gas supply design concept has evolved steadily over the past six years, resulting in an "octahedral module" pressure intensifier approach (Section 3.2.3.1) which, according to analysis, meets the current MSHWT UHP subsystem gas supply requirements described above.

Material properties, operability, lifetime costs, wind tunnel systems integration, and a low-to-moderate risk design strategy constrain the pressure-temperature design envelope. A total stagnation enthalpy of 2500 kJ/kg (~1100 Btu/lbm) results from the selection of a specific operating pressure and temperature, which has evolved to 2100 MPa (305,000 psi), 750 K (890°F) for the air stagnation condition. This results in a calculated recovery temperature in excess of 1,600 K (2420°F) at the nozzle throat wall; thus some means of protecting the throat wall from the high-temperature, high-fugacity oxygen in the airflow may be required, as previously mentioned. Film cooling by an outer, coaxial flow of cooler, relatively inert nitrogen to separate the hot, reactive airflow from the nozzle wall is being investigated, but this introduces significant complexity to the UHP design.

Steady total flows on the order of 160 kg/s (353 lbm/s) for run times of 1 to 10 s establish the total system volume for a single-cycle process. A selected length/diameter ratio of approximately 12 for the UHP piston and a maximum UHP bore diameter of approximately 200 mm (8 in.) (limited by the ability to fabricate large forgings of high-performance steel) establish the size and number of UHP intensifiers. Fabrication, operability, and gas supply subsystem costs result in selection of a three-layer compound cylinder approach for the UHP containers. Finally, environmental, safety, and health; operability; and gas supply subsystem costs result in selection of a 35-MPa (5,000-psi) nitrogen storage system for the process energy and an approximately 100:1 pressure ratio for the UHP intensifier.

3.2.2 Critical Technical Issues

The critical technical issues for the UHP air supply system are common to the performance requirements of the MSHWT with supersonic thermal energy addition. They are as follows:

1) Designing, fabricating, demonstrating, and connecting large volumes (liters) for pressure service up to 2100 MPa (305,000 psi);

2) Managing the thermal environment to acceptable levels of heat transfer from the air to its surroundings and maximizing material strength;

3) Developing a design with materials that will ensure pressure vessel and nozzle throat survivability in approximately 500 MPa (72,500 psi) partial pressure (in the pressure vessel) of oxygen and total pressures of 2100 MPa (305,000 psi) at stagnation temperatures from 750 to 1000 K (890 to 1340°F);

4) Developing a design to contain 2100 MPa (305,000 psi) upstream of the nozzle throat while accommodating the magnets to produce a magnetic field of up to 10 Tesla at the throat;

5) Developing a functional design concept(s) that will provide air for run times ranging from 1 to 30 s test time for a MSHWT scale facility;

6) Developing and demonstrating a combination air supply and an air and nitrogen gas heater (electrical resistance or storage) to achieve 2100 MPa stagnation pressure and stagnation temperatures from 750 to 1000 K (890 to 1340°F);

7) Developing a starting valve for the air supply and heater system.

3.2.3 Progress

Current progress on the UHP technology and facility is included in Refs. 17 and 21 and is summarized below.

3.2.3.1 UHP Facility Development

3.2.3.1.1 Octahedral Gas Supply Module Concept

Joining UHP volumes in a geometry that meets other systems requirements implies cross-bore connections, which break the cylindrical symmetry desirable for UHP design. Cross bores create a stress concentration that reduces the maximum design pressure that can be obtained using a compound cylinder approach. Thus the first challenge to be met is joining multiple intensifiers with acceptable deviatoric stresses in the cross-bore region. The solution to this problem has evolved steadily, resulting in an "octahedral module"* approach that meets the current MSHWT UHP subsystem requirements. In the octahedral module concept, four UHP intensifiers, Figs. 7a to g, and two UHP manifolds, Fig. 7h, are arranged in an "octahedral" geometry to form a module, shown in Fig. 8. For this, four UHP intensifiers and two UHP manifolds are arranged in "octahedral" symmetry. An external load frame reacts pressure and redirects the pressure-related forces to form the cross-bore connection. Figure 9 shows how multiple modules connect to make up the required total volume and mass for a process gas. Whereas the intensifier octahedral module satisfies the total UHP volume requirements for the air and nitrogen process streams, the UHP subsystem requires two other UHP components (described

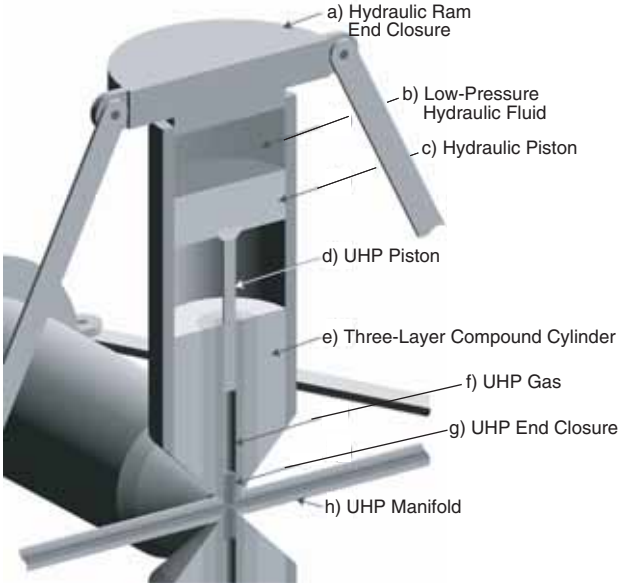

Figure 7. UHP Intensifier

* The MSHWT Module Three perpendicular axis geometry does not, in fact, have octahedral symmetry. However, the two legs of the manifold added to the hexagonal outer structure give an eight-member structure; hence, it is convenient to describe the geometry as "octahedral."

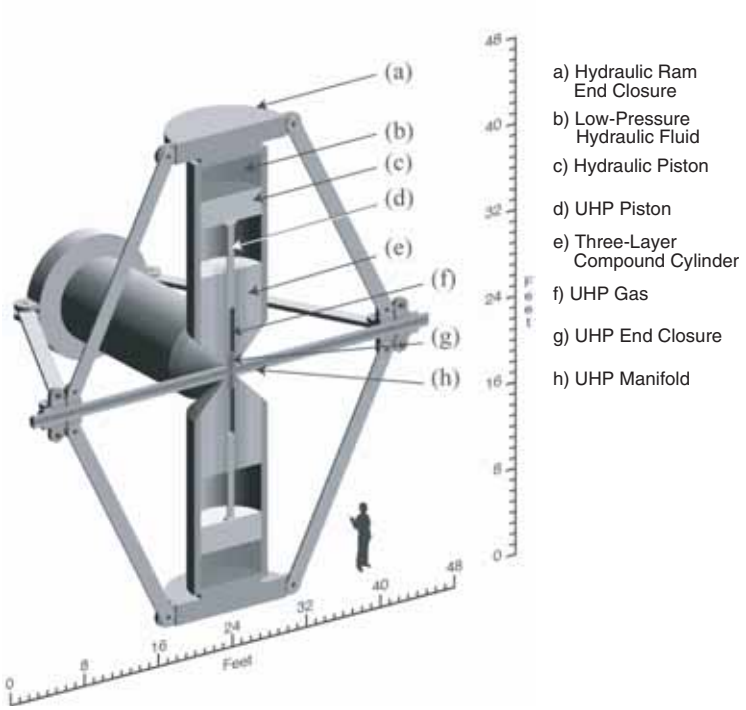

Figure 8. Cutaway Schematic of the MSHWT Design Concept "Octahedral" Module

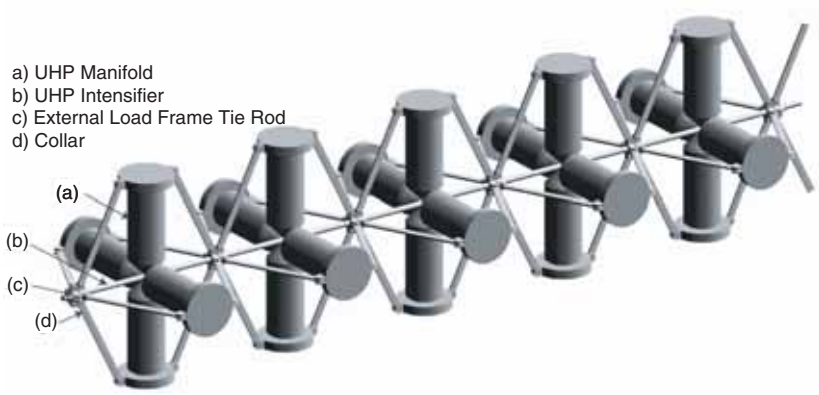

Figure 9. Illustration of Connection of Multiple Octahedral Modules to Make Up the Required UHP Gas Volume

below), as well as low-pressure energy storage, distribution, and control infrastructure for a final facility design.

The end closures of the hydraulic ram (a, in Fig. 7) in the UHP intensifier are free to move axially. The pressure force on the end closure is from the low-pressure hydraulic fluid driving the ram and is proportional to the pressure in the UHP vessel. This force is reacted by two load frame tie rods, shown in Fig. 8 (not called out) and Fig. 9d. One tie rod from each of the four intensifiers

connects to a collar on a manifold. One manifold reacts half the total axial forces of the four intensifiers using a 2:1 tie rod manifold length ratio. Whereas a UHP intensifier is force neutral (except for gravitational forces), the end closure of the intensifier (Fig. 7g) is free to move axially in response to the pressure forces of the UHP gas, just as the end closure to the hydraulic ram is free to move in response to the low-pressure hydraulic fluid. The axes of the four UHP end closures lie along two perpendicular axes in a plane, meeting in the cross-bore region at the origin. The two manifolds lie along a line normal to this plane and also meet in the cross-bore region near the origin. The forces on each of these six components have the same magnitude, within variations attributable to friction and mechanical tolerances; thus the contact stresses they produce can be adjusted and balanced to provide both a low deviatoric stress and pressure seals at the interfaces in the cross-bore region.

Figure 10 shows the results of an FEA of the cross-bore region to demonstrate this design concept. The end closures of the four UHP intensifiers and the three-layer compound cylinder manifolds meet to form a cross bore. Gas from the intensifiers flows through the manifolds to adjacent gas supply modules. The von Mises stresses in the cross-bore region are within the allowable stress of the pressure vessel material. The contact stresses between the components are greater than the gas pressure to make the pressure seals.

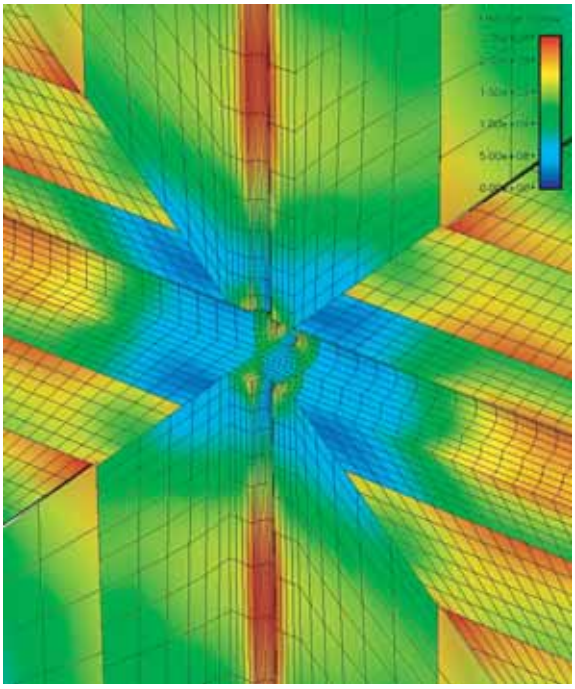

Figure 10. Illustration of von Mises Stresses Calculated with FEA of Octahedral Gas Supply Module Cross-Bore Region at Gas Pressure of 2100 MPa

Two important features of this geometry are passive control of the stresses in the cross-bore region and the self-alignment of the six UHP components. A disadvantage is that it is vulnerable to buckling. The seals at the interfaces between the intensifier end closures and manifolds are "brute force" pressure seals, which require the normal stress at the interface to be greater than the pressure. In conventional laboratory-scale UHP work, these seals have a pressure limit of about 1400 MPa (203,000 psi), owing to strength of materials. In this design, however, the normal stress at the interface increases in proportion to the gas pressure inside the cross bore, so that the deviatoric components of the total stress at all gas pressures are well within the failure limit of the material. The self-aligning feature, which ensures that the normal stresses at the junction interfaces remain similar as the pressure changes, is possible because of the symmetry and the axial degree of freedom of the intensifier end closures. However, the vulnerability of the intensifer to buckling as well as operational convenience in assembling, testing, and moving the gas modules requires surrounding the intensifiers and manifolds with a space frame (not shown). The space frame provides rigidity in the buckling directions, but it must have a degree of freedom along the axis of each intensifier and manifold. The frame also provides a means to satisfy module seismic stability and movement requirements. These are nontrivial, since a MSHWT octahedral module having a 200-mm (8-in.) bore diameter UHP vessel weighs more than 1 MN (110 tons). Furthermore, the space frame defines a volume "footprint" for the module, which can be used to house such infrastructure components as the low-pressure vessels that store the process energy and local barricading to contain blast and fragments.

3.2.3.1.2 Facility Arrangement Concept

As stated above, Fig. 9 shows how multiple modules may be joined to provide the required UHP volume for the process gas. Although each module is force neutral (except for gravitational forces), thermal and elastic strains result in large displacements that require a degree of freedom along the line of modules. Adjacent air supply modules join at the ends of their respective manifolds. (The manifolds are UHP pipes that transfer the working fluid from one UHP module to another, and then to the nozzle.) This means the assembly of modules required to provide the total gas mass must be linear, or at least must have linear segments that must be connected at right angles because of the octahedral cross-bore geometry. This geometry constraint becomes important in the laying out of the MSHWT facility since it precludes arrangements that make better use of floor space and reduce the cost of the building housing the UHP gas supply. If the air mass requirement results in more than one air UHP module, a "transfer module" directs the flow from the arrangement of air modules to a "nozzle module," which is described below.

Figure 11 shows how the modules can be arranged for a facility air supply. Since film cooling of the nozzle is anticipated, this conceptual design includes this, using nitrogen as the cooling gas. A "transfer module" (Fig. 11b) collects the airflow from the linear array of UHP air modules and turns it 90 deg into a manifold along the wind tunnel nozzle axis. This transfer module is somewhat smaller than the gas supply modules and does not contain UHP intensifiers. The manifold connects to the second, additional UHP component, the "nozzle module"

(Fig. 11d), which collects the nitrogen flow from the linear array of UHP nitrogen modules, joins the air and nitrogen flows coaxially, and makes the connection to the wind tunnel nozzle.

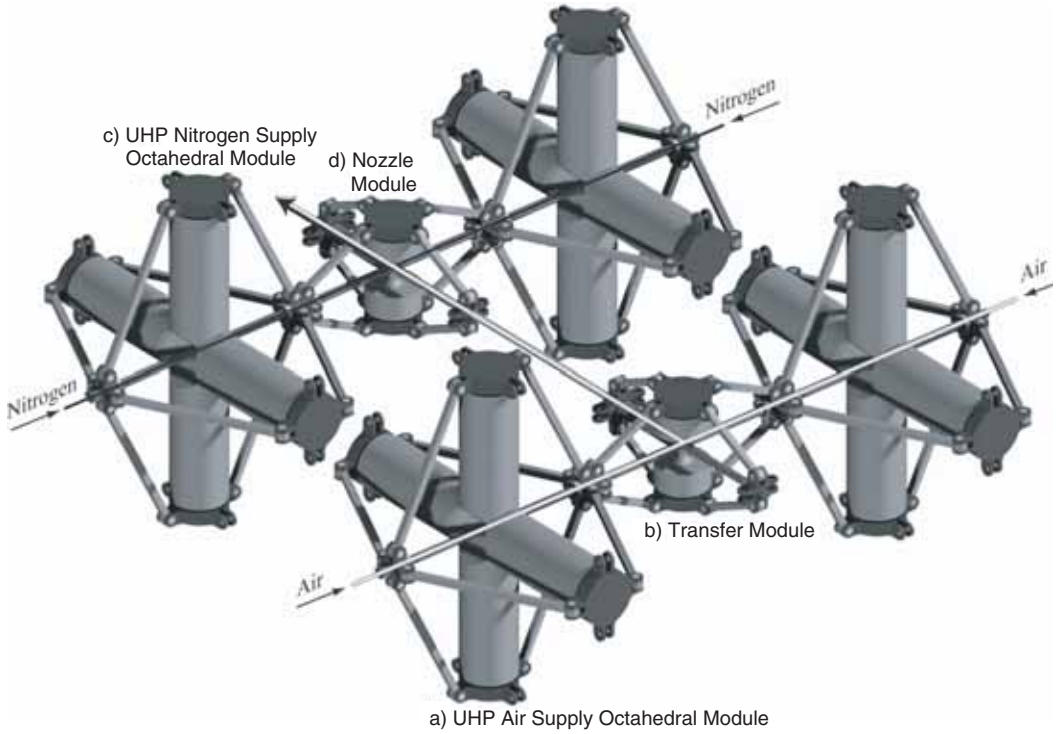

Figure 11. Facility Air Supply Concept, Including Transfer and Film-Cooling Nozzle Modules

3.2.3.1.3 Transfer Module

The transfer module (Fig. 11b) functions primarily as a right-angle connection [a 2100-MPa (305,000-psi) "cross"] that changes the direction of the UHP airflows. In this module (Fig. 12), which is smaller than a UHP gas supply module, two hydraulic ram components provide the forces along two of the six octahedral directions. Ultra-high-pressure manifolds provide the forces in the four remaining directions, and the tie rod geometry of the external load frame adjusts distribution of the forces from the rams. The same low pressure supplied to the hydraulic rams is supplied to the UHP gas supply

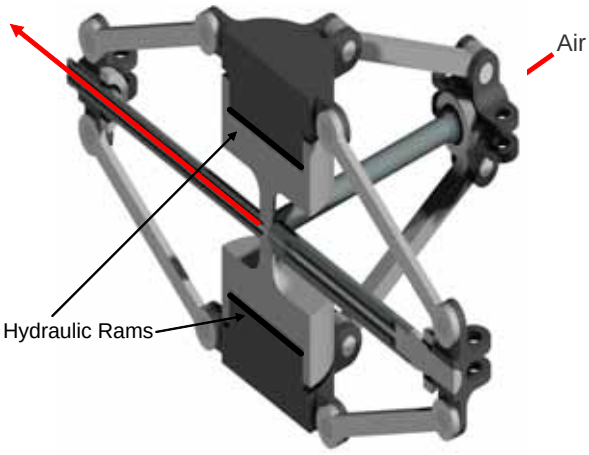

Figure 12. Transfer Module Concept

modules, so the normal stresses that provide the stress balance and sealing functions at the octahedral junction of the module are the same as those in the gas module.

At least two of the four manifolds in the transfer module are used for gas flow. The remaining two can be used to connect one or two other linear arrays of UHP modules or for other purposes. These include 1) bringing to ambient the electrical signals from diagnostics in the UHP environment; 2) pressurizing or depressurizing the UHP volume in normal and off-normal conditions; and 3) passing a mechanical linkage from ambient conditions to the UHP environment. All of these functions are necessary in the complete MSHWT design, although some may be satisfied using the single free manifold at the terminating UHP gas supply module in a linear array.

3.2.3.1.4 Nozzle Module

As discussed in Section 3.3, nitrogen film cooling may be required to protect the nozzle throat from excessive heat transfer and material oxidation. In this event, nitrogen must be provided at ultra-high pressure to the nozzle, as must air, from its own array of pressure intensifiers.

The "nozzle module" from Fig. 11d (shown in Fig. 13) is the second special-purpose octahedral module in the MSHWT UHP gas supply. Its three functions are to 1) combine the flows from the UHP nitrogen modules, 2) join this nitrogen flow coaxially to the core airflow, and 3) connect the UHP gas supply system to the wind tunnel. This third requirement is extraordinarily challenging since the space within a distance of about 50 cm of the nozzle throat must accommodate a 2100-MPa (305,000-psi), 750 K (890°F), 160-kg/s (353-lbm/s) coaxial fluid flow; a nozzle that supports a flow; and a multi-Tesla magnetic field that focuses the counterflow electron beam into the core air flow.

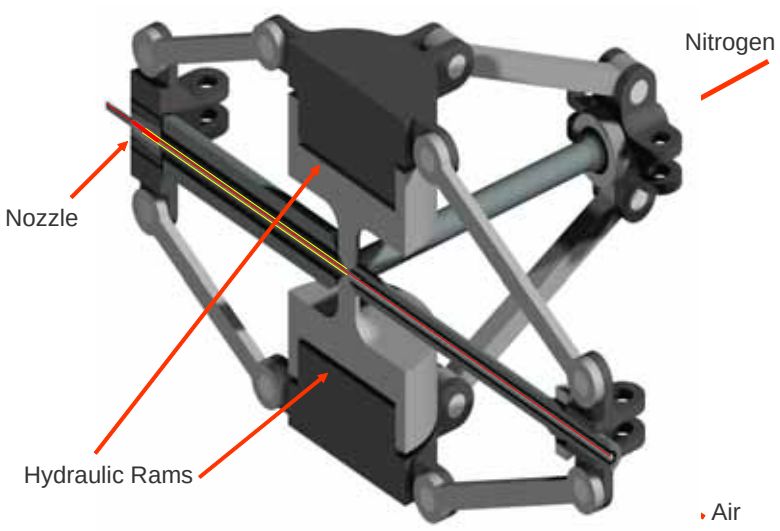

Figure 13. Nozzle Module

Since the nitrogen mass flow will be about the same as the air mass flow in the present concept, the arrangement shown in Fig. 11 satisfies these functions. The manifold from the transfer module connects to a nozzle module manifold along the nozzle (and wind tunnel) axis. The connection, which uses pressure seals similar to others in the UHP subsystem, constrains the

airflow to a central pipe. The nitrogen flow comes through the two manifolds orthogonal to the airflow manifold into the coaxial region outside the pipe. It stagnates at this point and then flows coaxially and joins the airflow at the nozzle converging section, as shown in Fig. 14. Minimizing the mixing of the converging air and nitrogen flows upstream of the throat requires keeping their pressures equal, so that the central pipe separating them does not have to sustain a high pressure differential. However, since the temperatures of the two flows may differ by as much as 100 K, the pipe must support as large a radial thermal gradient as possible.

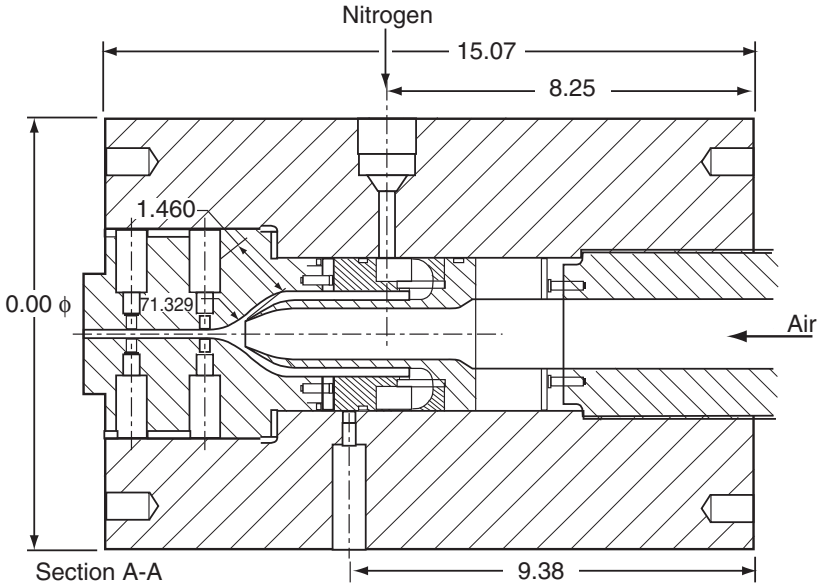

Figure 14. Schematic of Film-Cooling Nozzle Concept

The third major function of the nozzle module is to connect the UHP gas subsystem to the wind tunnel. This is another area of high complexity resulting from conflicting requirements. The first of these conflicting requirements arises from providing a strong focusing magnetic field for the electron beam in a UHP gas at the nozzle throat. The gas pressure in the converging section of the nozzle is 2100 MPa (305,000 psi); it then falls to about 550 MPa (80,000 psi) at the nominal 1.2-cm (0.5-in.)-diam nozzle throat and remains at about 200 MPa (29,000 psi) for about 20 cm (8 in.) in the downstream energy-addition region. The confining magnetic field in this region is solenoidal and coaxial to the nozzle, with a maximum strength of several Tesla near the throat. It probably will be generated using a superconducting magnet with a limit on the magnet core open space of about 10 to 15 cm (4 to 6 in.). This means the pressure vessel containing the 2100-MPa (305,000-psi), 750 K (890°F) flow has a marginal outside diameter/inside diameter ratio of near 10. Fortunately, use of paramagnetic materials for the nozzle is permitted, since the saturation time for the field is short compared to the flow time. The second conflicting set of requirements is attributable to the high Reynolds number of the flow and the assumption that the nozzle will have to be serviced frequently. The high Reynolds number requires exceptional nozzle surface smoothness (thought to be a few tenths of a micrometer), and servicing implies removing the nozzle from the wind tunnel. Additionally, since the nozzle represents one “end closure”

termination of the pressure manifold, the design must provide for reaction of an axial pressure force of about 20 MN (4.5×10^6 lbf). Furthermore, present schemes to contain the air and nitrogen at about 300 MPa (43, 500 psi) before the operating cycle to 2100 MPa (305,000 psi) involve a flow starting valve either immediately upstream or downstream of the throat. The connections on the upstream UHP end to the nozzle module and on the downstream end to the remainder of the wind tunnel must meet these requirements with acceptable operating costs and efficiency.

3.2.3.2 UHP Technology Demonstration Experiments

The high symmetry inherent in the UHP design and state-of-the-art FEA codes significantly reduces the risk in the UHP subsystem design. However, none of the high-risk components has been demonstrated at 2100 MPa (305,000 psi) and 750 K (890 °F) in air, even on a laboratory scale. One technology demonstration experiment (Fig. 6) is in progress, and several others are planned that reduce risk in the specification for the MSHWT. These experiments are:

1) *A-2 LITE Experiment*. A single UHP intensifier having a bore diameter of 63.5 mm (2.5 in.) is operated to 2000 MPa (290,000 psi) and 750 K (890°F). It demonstrates the compound cylinder design, a moving UHP seal, and control of the energy flow from the low-pressure nitrogen storage to the gas flow through the nozzle. Its primary functions are to demonstrate an operational pressure intensifier and to provide a 1-s flow of air for the evaluation of the MSHWT nozzle materials (See Section 3.3). These experiments are in progress, and a more detailed discussion is included below.

2) *MSHWT Component Experiment.* This experiment is planned to test MSHWT full-scale manifold sections and end closures to demonstrate, at room temperature, the connection between two UHP octahedral modules, the end closure used to introduce the process gas, and the clamping shells used to join octahedral modules and to react the manifold end forces. The design concept was accomplished during this reporting period.

   The MSHWT Component Experiment, Fig. 15, consists of three major components: a) two 2100-MPa (305,000-psi), three-layer, compound cylinder UHP vessels; b) a hydraulic ram; and c) an end closure containing a 2100-MPa (305,000-psi) valve.

   The connection between the two UHP vessels is the same as that for the MSHWT full-scale design connection between the manifolds of adjacent gas supply modules. The remaining opening for one vessel contains a gland seal that permits relative motion between the UHP piston and the vessel. The remaining opening for the second vessel contains an MSHWT full-scale, 2100-MPa (305,000-psi) valve. The valve is a “brute force” design, in which a commercial hydraulic ram forces a valve stem into a seat. It permits isolation of the UHP volume during the operational cycle after precharging it with the process gas. It also provides a means of releasing the process gas in off-normal conditions. The hydraulic ram provides MSHWT-design 100:1 pressure intensification

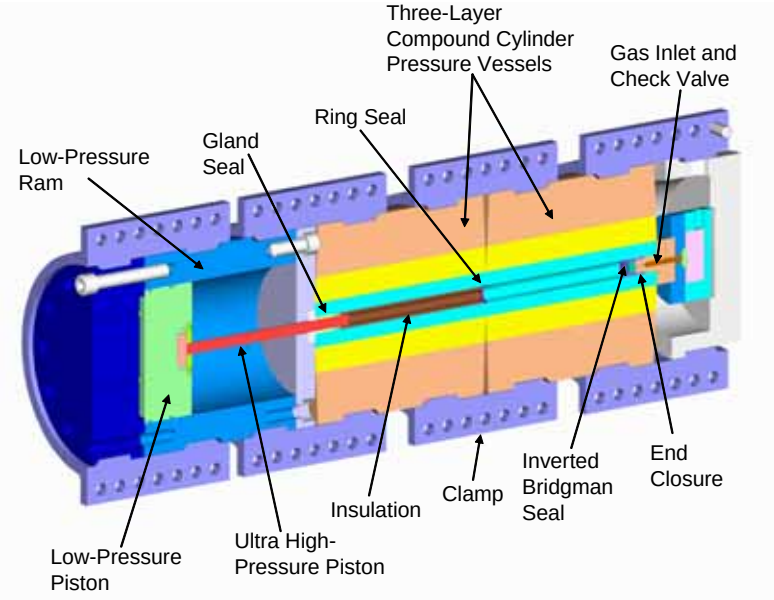

Figure 15. UHP MSHWT Component Experiment

through a tungsten carbide UHP piston having an MSHWT-design length/diameter ratio. Four MSHWT full-scale "clamping shells" connect and align the three components and react the pressure-related forces at the ends of the assembly.

The UHP seal at the connection between the two vessels is a "triangle" cross-section O-ring-type seal that has been demonstrated to 1500 MPa (218,000 psi) in laboratory-scale fluid systems (Ref. 32) and that permits easy separation of an octahedral gas supply module from adjacent modules. This addresses an essential element of the MSHWT design strategy of controlling the operational costs of the wind tunnel UHP subsystem. Since UHP operations at the extremes of material properties in an industrial environment demand a rigorous surveillance and maintenance program, there must be cost-effective access to the UHP components, such as the pressure vessel bores, seals, and nozzle. The modular design of the gas supply system permits efficient maintenance and replacement, but it is usable only if a reliable UHP seal connects the modules.

Operation of the MSHWT for steady, 2100-MPa (305,000-psi) flows greater than 1 s requires some means of keeping the plenum pressure constant as mass passes through the nozzle. This is accomplished using a moving piston in each UHP intensifier, which will require a UHP seal that supports relative motion. A classic Bridgman "mushroom" seal, used in the A-2 LITE, is reliable but requires a moving contact with a smooth pressure vessel bore. Since thermal barrier coatings are not likely to survive the more than 1-percent radial strain of the bore, use of the Bridgman seal probably will require bore

wall temperatures equal to the gas process temperature, degrading the bore material properties and contributing an unwelcome thermal compressive stress at the end of an operational cycle. The static seal at the end of the UHP component experiment bore is a "gland seal" that permits use of a bulk insulator between the process gas and the bore at the cost of an increased bore diameter. One seal configuration has been demonstrated on a laboratory scale using a fluid pressure medium (Refs. 33 and 34), but it has not been used with a gas medium. The gland seal in the Component Experiment is a variant of this geometry, suggested by Prof. S. M. Stishov, the Director of the Russian Academy of Sciences Institute for High-Pressure Physics.† The gland seal in the MSHWT Component Experiment is smaller in outside dimension than the MSHWT design, but it has approximately the same annular (outside diameter minus inside diameter) and height dimensions.

3) *Subscale Octahedral Module Experiment* (not shown in Fig. 6 but included in the component experiment plans; see above). The Subscale Octahedral Module Experiment planned is a room-temperature, standalone, approximately 1/8th MSHWT-scale UHP gas supply module. One manifold termination permits precharging the working fluid and discharging the fluid in normal and off-normal operations. The second manifold termination is for pressure and temperature diagnostics. The device initially is operated quasistatically under manual control, although it can be modified for closed loop, dynamic control with an operational cycle time on the order of seconds. Finally, certain off-normal events, such as a catastrophic loss of pressure caused by a seal failure or fracture of a UHP piston, can be caused to assess their effects on mechanical stability, noise, and blast.

4) *A-2 LITE Modified (A2LM), Nitrogen/Air Coaxial Flow Experiment.* A second A-2 LITE system is added to provide steady flows of air and nitrogen through a coaxial nozzle at 900 MPa (130,000 psi) and 750 K (890°F) for 1 s. This planned experiment also may include demonstration of a storage heater (see Section 3.3.3.4).

5) *Integrated Test System.* An integrated test facility operating to 1600 MPa (230,000 psi) and 750 K (890°F) for 1 s with a dynamic pressure (q) of 2000 psf (96 kPa).

These planned experiments are discussed in greater detail in Section 4.

3.2.3.3 A-2 Lite Facility and Experiment

The A-2 Lite pressure vessel was designed and fabricated by LLNL on the basis of a design concept for the MSHWT intensifiers.‡ Objectives for the A-2 Lite experiments using the UHPTF

† S.M. Stishov, Private Communication. 6 September 2000.

‡ The A-2 Lite is being tested in the UHPTF at the MSE Mike Mansfield Advanced Technology Center in Butte, Montana.

include testing of critical UHP design, construction, and operation techniques to reduce the technical, environmental, safety, health, and programmatic risk for the MSHWT UHP subsystem, as well as the demonstration of survivable nozzle subsystems. A-2 Lite maximum operational requirements (Ref. 17) are a plenum pressure of 2000 MPa (290,000 psi) and a temperature of 750 K (890°F), a flow rate of 1 kg/s (2.2 lbm/s) for a constant pressure run time of 1 s, and use of air and nitrogen as the working gases. These requirements resulted in a total UHP gas volume of 2.1 *l* (128 in.^{3}) for the A-2 Lite pressure vessel.

3.2.3.3.1 A2-Lite Design Concept And Hardware

The UHP intensifier is a hydraulically driven piston pressurization system consisting of the intensifier pressure vessel (A-2 Lite), intensifier piston and seal, external support vessel, alignment system, and diagnostic instrumentation. Figure 16 shows the design concept for the A-2 Lite pressure intensifier in a vertical orientation although it is installed in a horizontal orientation. This concept is expected to be scaled for use in a full-scale MSHWT. The ultra-high pressure is produced by the approximately 100:1 intensification between the low-pressure hydraulic driving fluid and the pressure within the compound cylinder.

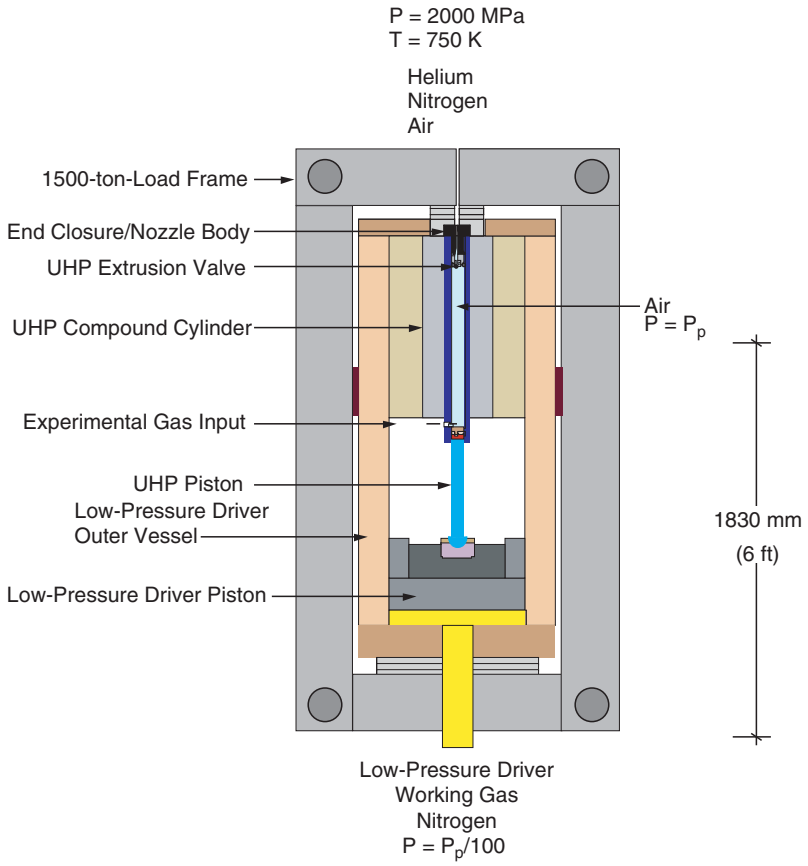

Figure 16. Design Concept for High-Pressure Intensifier

A three-layer compound cylinder pressure vessel design, Fig. 17, is expected to achieve the required UHP pressures. This pressure vessel was constructed as a right circular cylinder with a 6.35-cm (2.5-in.) inside diameter (ID), 66-cm (26-in.) outside diameter (OD), and a nominal length of 113 cm (44.5 in.). Layer 1, or the center core of the pressure vessel, was constructed of Vascomax 350 CVM maraging steel, biconically tapered with a 1-deg half angle on the outside with a maximum OD of 15.2 cm (6 in.) and a 6.35-cm (2.5-in.) ID. Ten rings, each comprised of two layers (Layers 2 and 3) fabricated from 4340 steel with a 1.27-cm (0.5-in.) stainless steel safety ring around the outside, were pressed onto the center core (Layer 1). Figure 18 shows a single ring consisting of a safety ring surrounding Layers 2 and 3 pressed together with the center core, Layer 1, in the background. The completed A-2 Lite pressure vessel (ready for installation in the UHPTF) is shown in Fig. 19. The intensifier system, including the A-2 Lite pressure vessel and piston, is located in the light gray cylindrical section of the UHPTF shown in Fig. 20.

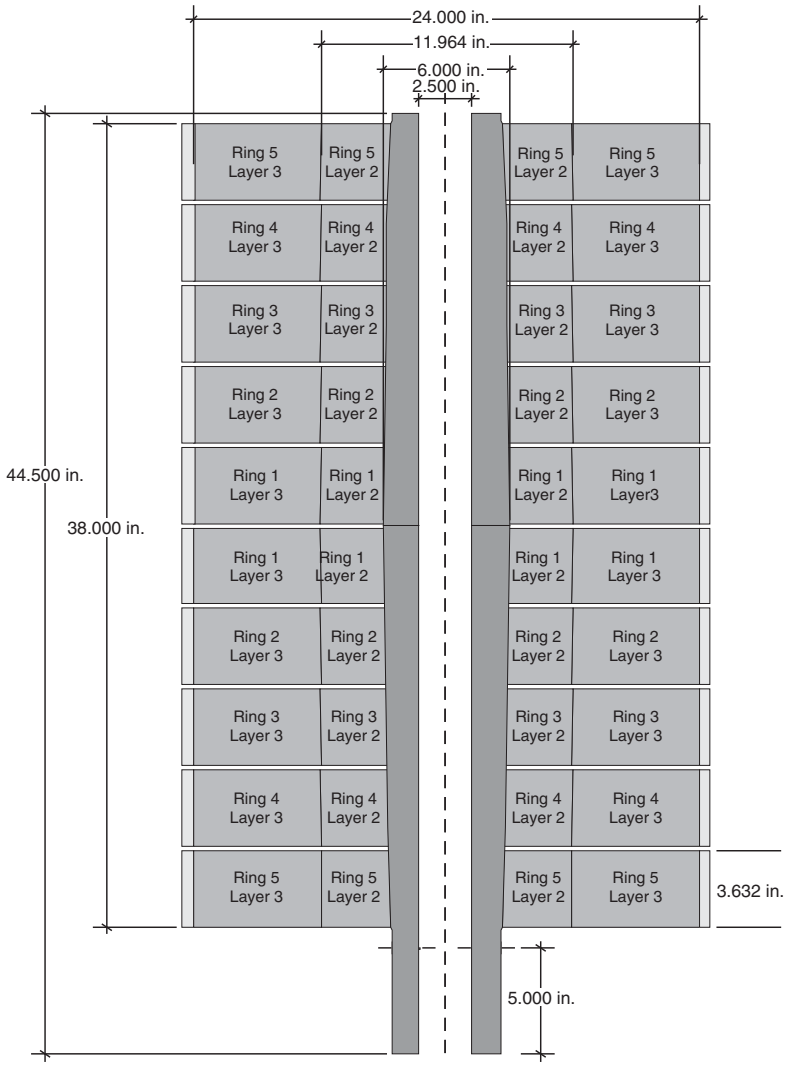

Figure 17. A2 Lite Compound Cylinder

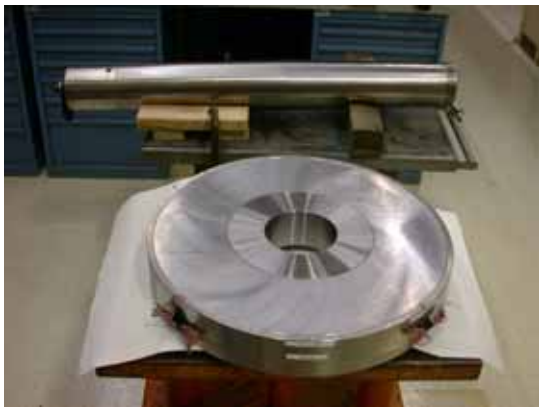

Figure 18. Pressure Vessel Ring with a Safety Ring, Layer 2 and Layer 3 Pressed Together and Layer 1 in the Background

Figure 19. Completed A-2 Lite Pressure Vessel

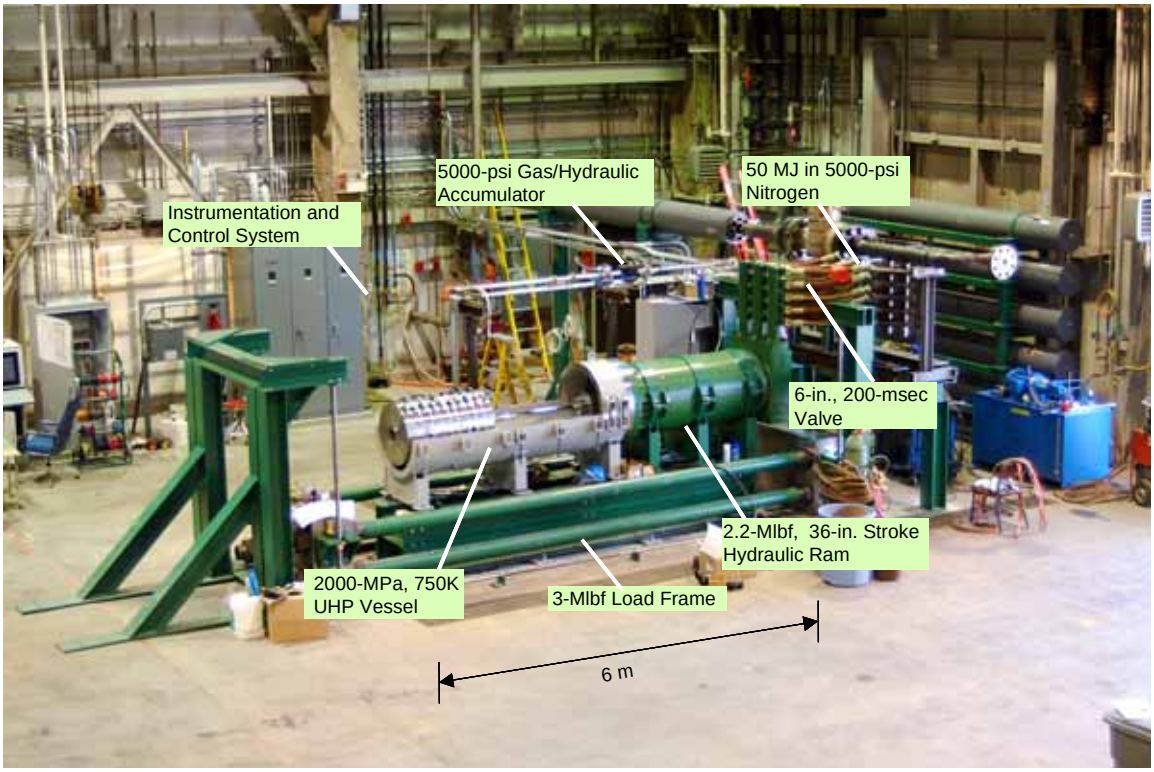

Figure 20. MSE Ultra-High-Pressure Test Facility with A-2 Lite Installed

Pressure vessel fatigue life analyses have been performed by researchers at LLNL and the U.S. Army Benet Laboratories, Watervliet, NY, in order to provide insight into the life expectancy of the present multilayer vessel design. This information is critical to the safety and

operational costs of a production test and evaluation facility. Estimates of over 1000 operational cycles to grow a detectable flaw to failure appear promising but have led to identification of alternative pressure vessel concepts for future study.

In operation, the A-2 Lite intensifier pressure vessel is precharged with the working gas (air or nitrogen) using a skid-mounted, high-pressure compressor/receiver system. The two-stage compressor charges the gas to 20.7 MPa (3000 psi) in Stage 1 and to 310 MPa (45,000 psi) in Stage 2 with a maximum precharge time of 20 min. An intermediate receiver in the compressor system stores the compressed gas from the first-stage compressor for input to the second stage. The working gas is delivered into the intensifier pressure vessel through a manifold and three isolation valves that allow for the appropriate gas (nitrogen or air) to be selected. (Use of helium was discontinued early in the testing program because it is believed that nitrogen will serve as an adequate nozzle protection film if needed.) Most tests to date have been conducted with nitrogen, but tests with air are planned to determine the limits of nozzle survivability with air only. A 0.3-micron filter removes contaminants from the incoming working gas before it enters the compressor.

Compression of the working gas to the test pressure is accomplished using a hydraulic ram to push the intensifier piston and seal into the intensifier pressure vessel. The hydraulic ram (see Figs. 16 and 20) was designed and constructed with a 61-cm (24-in.)-diam piston to achieve a compression ratio of 92:1 in the intensifier. This allows the intensifier to achieve the required ultra-high working pressure with a relatively low hydraulic ram maximum cylinder operating pressure of 34.5 MPa (5000 psi). Compression is achieved by pushing a tungsten carbide piston into the UHP intensifier at a nominal velocity of 0.3 to 0.5 m/s (1 to 1.64 ft/s) with a maximum velocity of 1.0 m/s (3.28 ft/s) through a maximum stroke of 91.4 cm (36 in.). Working gas pressures up to 2140 MPa (310,500 psi) can be achieved. For the A-2 Lite test series, the maximum nominal pressure will be limited to 2,000 MPa (290,000 psi).

Hydraulic fluid for the ram is supplied by a hydraulic piston accumulator through a control valve. High-pressure nitrogen, at pressures up to 34.5 MPa (5000 psi), is stored in receivers and used to pressurize the hydraulic accumulator. Compressed nitrogen gas is stored in five high-pressure receiver vessels (shown on the wall at the right-hand side of Fig. 20). These vessels are filled to the precharge pressure with the hydraulic accumulator in the completely extended position (discharged). Prior to a test, hydraulic oil is pumped into the downstream end of the accumulator to drive the piston to the charged position, thus forcing nitrogen from the accumulator into the receivers, increasing the receiver pressure and providing a volume of high-pressure hydraulic fluid for driving the ram. To fully charge the accumulator prior to a test requires approximately 20 min. The accumulator is seen above and behind the hydraulic ram in Fig. 20.

Hydraulic control valves are used to control the flow of the hydraulic fluid from the accumulator to the hydraulic ram. Two valves [a 15-cm (6-in.)-ID "main" valve and a 5.1-cm (2-in.)-ID "trim" valve] are configured in parallel to provide the flow necessary to attain the desired piston velocity. The valves are hydraulically driven and can be controlled to any position between

fully closed and fully open with a full-stroke time of 200 ms. These valves, which can be seen on the right-hand side of Fig. 20, are used to throttle the hydraulic fluid flow to obtain piston velocities in the intensifier between 0 and 1 m/s (0 and 40 in./s) with a back force of as much as 8 MN (1.8 million pounds).

A momentum trap is located at the nozzle end of the intensifier (not shown in Fig. 20) to capture pieces and particles of various materials exiting the intensifier during a normal test and potentially large pieces in the event of a component failure. Materials ejected during a normal test include pieces of the shear disk, steel punch, and retractable Bridgman seal components used as a starting valve. Nozzles or fractured nozzle pieces and other components could be ejected during component failures.

A load frame designed with a maximum axial load capacity of 13.3 MN (3,000,000 lbf) is used to restrain/support the axial load resulting from pressurization of the UHP intensifier. The load frame may be lowered significantly below the centerline of the vessel and hydraulic ram to allow ergonomic access for the installation and removal of nozzles and shims as well as the performance of posttest inspections and maintenance. The load frame consists of four 15-cm (6-in.)-diam steel bars (two on each side of the load train, as seen in Fig. 20) connecting large steel end platens on either end of the load train.

Process control, data acquisition, and remote monitoring of the process are accomplished through a local area network (LAN) using Ethernet media and through an Allen Bradley Data Highway 485 protocol. The LAN consists of a central server and the Computer Operator Station located in the Central Control Room, which is connected to three clients via Ethernet media including:

The Remote Computer Operator Station, located near the UHPTF and used to control and monitor the UHP components during maintenance, pretesting, and initial system checkout.

The Remote Monitoring Station, located in the Central Control Room and used to monitor the UHP components during tests.

The Data Acquisition System, located near the UHPTF and used to acquire and store component information during tests.

3.2.3.3.2 UHPTF Testing

The first objective of UHP testing was proof-of-concept testing of the UHPTF itself. UHP testing was divided into approximately 20 separate test sequences that would gradually bring on line various UHPTF components and incrementally increase the plenum pressures in both a static and a quasi-static mode of operation and be followed by dynamic testing. In all, 184 test attempts were conducted over a period of approximately 19 months; testing occurred on approximately 74 days during that 19-month period. Figure 21 illustrates the flow of the testing program, and a summary of the UHP tests is included as Table 4.

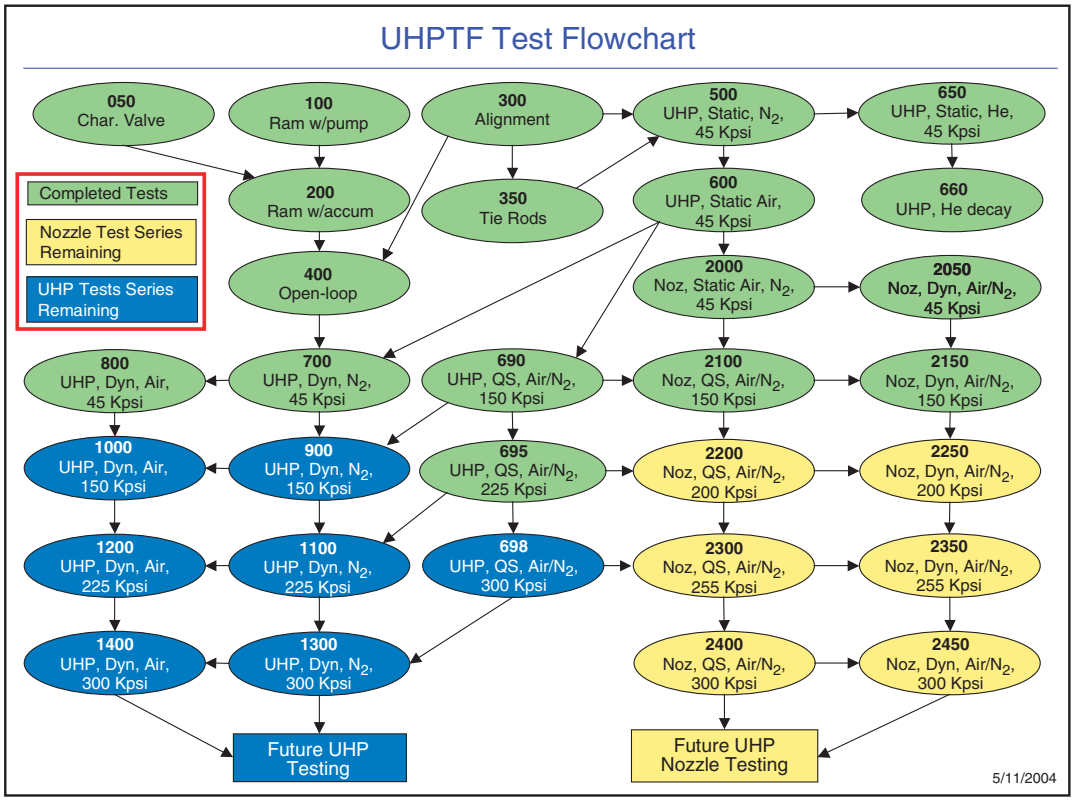

Figure 21. UHPTF Test Flowchart

Before the UHP test series was begun, seven system operating test procedures (SOTPs) were performed to operationally check out both the facility systems and supporting test systems prior to pressurizing the plenum UHP vessel.

The initial UHP development plan called for static and then dynamic pressurization tests to 1500 MPa (217,000 psi) to shake down and test the pressure, instrumentation, and control systems. These tests are conducted with the diagnostic end plug installed and instrumented to measure pressure and temperature in the A-2 Lite UHP gas. Static and dynamic measurements of deformation of critical components were made throughout the shakedown phase using an array of strain gages installed on the rings of the UHP vessel and on the load frame tie rods for comparison to design predictions. Additionally, critical measurements were made of the test equipment to ensure proper alignment of the vessel with respect to other test components.

The initial maximum pressure was set at 1500 MPa (217,000 psi), which provided a safety factor of approximately 1.5 on the maximum design pressure of 2300 MPa (333,000 psi) while permitting nozzle survivability experiments at meaningful pressures. Pressures of 310 MPa (45,000 psi), 1034 MPa (150,000 psi), 1213 MPa (176,000 psi), and 1380 MPa (200,000 psi) were planned as intermediate points in the testing. Other intermediate points were also planned later in the testing program.

Table 4. Summary of UHP Tests

Series No.	Test Series Title	Maximum Pressure, psi	Intermediate Pressures, psi	No. of Test Attempts	Test Type	Gas Used
050	Characterize control valve.	3000	1000 1500 2000	26	N/A	Nitrogen
100	Operate hydraulic cylinder with pump, no piston installed.	Nominal	N/A	1	N/A	Nitrogen
200	Operate hydraulic cylinder from accumulator. Work up to full speed of 0.5 m/s (20 in./s), no piston installed.	3000	N/A	30	Quasistatic	Nitrogen
300	Perform initial alignment procedure.	N/A	N/A	10	N/A	N/A
350	Perform tie-rod strain checks and alignment.	N/A	N/A	1	Static	Nitrogen
400	Move piston within intensifier with open end. Work up to full speed of 0.5 m/s (20 in./s).	45,000	N/A	24	Quasistatic	Nitrogen
500	Pressurize intensifier using precharge pump with nitrogen to 45,000 psi.	45,000	N/A	11	Static	Nitrogen
600	Pressurize intensifier using precharge pump with air to 45,000 psi.	45,000	N/A	2	Static	Air
650	Pressurize intensifier using precharge pump with helium to 45,000 psi.	45,000	N/A	1	Static	Helium
660	Pressurize intensifier using precharge pump with helium to 5000, 15,000, and 45,000 psi and watch decay rate with the diagnostic plug in place.	45,000	5000 15,000 45,000	2	Static	Helium
690	Slow speed (quasistatic) pressurization of the plenum to 10,000 atm (150,000 psi) using the hydraulic pump only.	150,000	70,000 90,000 110,000 130,000	19	Quasistatic	Nitrogen Air
695	Slow speed (quasistatic) pressurization of the plenum to 15,000 atm (225,000 psi) using the hydraulic pump only.	225,000	176,000 210,000	7	Quasistatic	Nitrogen Air
700	Dynamically pressurize intensifier to 45,000 psi with nitrogen.	45,000	N/A	48	Dynamic	Nitrogen
800	Dynamically pressurize intensifier to 45,000 psi with air.	45,000	N/A	2	Dynamic	Air
900*	Dynamically pressurize intensifier to 150,000 psi with nitrogen.	150,000	N/A	0	Dynamic	Nitrogen
1000*	Dynamically pressurize intensifier to 150,000 psi with air.	150,000	N/A	0	Dynamic	Air

Table 4. Concluded

Series No.	Test Series Title	Maximum Pressure, psi	Intermediate Pressures, psi	No. of Test Attempts	Test Type	Gas Used
1100*	Dynamically pressurize intensifier to 225,000 psi with nitrogen.	225,000	N/A	0	Dynamic	Nitrogen
1200*	Dynamically pressurize intensifier to 225,000 psi with air.	225,000	N/A	0	Dynamic	Air
1300*	Dynamically pressurize intensifier to 300,000 psi with nitrogen.	300,000	N/A	0	Dynamic	Nitrogen
1400*	Dynamically pressurize intensifier to 300,000 psi with air.	300,000	N/A	0	Dynamic	Air
TOTAL UHP TESTS ATTEMPTED				184		

* Test series not performed during this contract but planned.

Candidate nozzle materials are planned to be tested to the full 2000 MPa (290,000 psi) after a UHP test to this pressure. Because of uncertainty in the design and fabrication assumptions for this extension of the art, the risk of pressure vessel failure at 2000 MPa (290,000 psi) was thought to be sufficiently great that nozzle testing at lower pressures should be completed before full-pressure testing is attempted

Static tests were performed for plenum pressures of less than 310 MPa (45,000 psi). The purpose of these tests was to pressurize the plenum using only the precharge pump. The first of these static tests were Test Series 500, 600, 650, and 660. Nitrogen, air, or helium was used as the working gas. For quasi-static testing, the hydraulic ram pushed the piston into the plenum using only precharge pressure at a very slow rate to attain plenum pressures greater than 310 MPa (45,000 psi).

Test Series 100, 300, and 350 were performed in preparation for testing at higher plenum pressures. In Test Series 100, the hydraulic ram was operated quasi-statically by the hydraulic system. It was necessary to test the stroke of the piston prior to performing any tests at approximately 310 MPa (45,000 psi) to ensure proper alignment and stroke. Test Series 300 pertained to the alignment of the UHP vessel to ensure that the piston would not bind at higher pressures and would not buckle during dynamic testing. The load frame tie-rod strains were evaluated and adjusted during Test Series 350 in an effort to ensure that load frame strains were evenly distributed.

Test Series 050, 200, and 400 were performed in preparation for dynamic testing. The purpose of Test Series 050 was to characterize the performance of the two set points in the control of hydraulic valves to ensure that they operated as designed. The piston was operated automatically using the programmable logic controller (PLC) for Test Series 200 and 400. In Test Series 200, the piston was not installed, and no pressure was accumulated in the plenum. For Test Series 400, the piston and diagnostic end plug were installed, and pressure was accumulated in the plenum. The plenum pressure was released by retracting the piston and venting through the vessel vent.

Test Series 700 was the first dynamic testing performed at the UHPTF. The objectives of Test Series 700 were to incrementally and dynamically pressurize the intensifier up to 310 MPa (45,000 psi) using piston position and velocity as the control set points. Position or control set point profiles were established, and the valves were automatically operated to achieve the predetermined set points. Nitrogen was used as the working gas. A maximum piston velocity of 10 cm/s (4 in./s) was tested in Test Series 700. In Test Series 800, a velocity profile tested in Test Series 700 was repeated with air used as the working gas.

Test Series 900, 1100, and 1300 are identical to Test Series 700, and Test Series 1000, 1200, and 1400 are identical to Test Series 800, with the exception that greater velocities, piston travel, distance, and pressures are to be attained. These test series have not been conducted but are still planned.

In summary, the RDHWT/MARIAH II A2 Lite pressure vessel has been successfully tested up to a static pressure of approximately 1250 MPa (180,000 psi), and nozzle blowdown testing has been successfully completed up to 1000 MPa (150,000 psi) with both nitrogen and air used as the working gas. Following these tests, no nozzle erosion damage was detected, including any damage to the maraging steel nozzles. However, UHP leaks, seal failures, and nozzle containment structure failure did occur, and the nozzle containment structure was redesigned and operated successfully. More work is needed to develop successful seals. Full dynamic nozzle testing was successfully demonstrated at 83 MPa (12,000 psi), at which time testing was stopped because of scheduling and funding constraints.

The UHP research has made good progress with the designs and hardware noted above, but reference to the plan depicted in Fig. 6 indicates that none of the UHP test programs has been completed. Although no pressure limit has yet been reached, demonstration of the UHP capability to support the full Mach 12 to 15 MSHWT concept remains to be achieved. The moving Bridgman seal used to contain the UHP gas appears to be the limiting component in the present design, and alternatives are being considered. See Ref. 21 for a full description.

3.2.3.4 Storage Heater

3.2.3.4.1 Background

As has been indicated, it is expected that heating of the gas will be required to reach the desired stagnation conditions. Original plans were to use a resistance heater internal to the UHP portion. However, during the reporting period of this research, it was suggested that an inline storage heater be used to achieve the needed stagnation temperature of the air entering the nozzle. It was thought that this would not only reduce cost, but also would markedly improve flow quality. Flow quality is an issue with the internal resistance heater approach because of heat losses in the supply lines of varying lengths between the individual intensifier modules and the facility nozzle, for example. Thus plans are to study the concept in more detail and, if indicated, conduct small-scale demonstrations as a part of the A2LM experiments.

3.2.3.4.2 Approach

Each of the heating concepts is schematically illustrated in Fig. 22. The original approach, which used resistance heaters internal to the UHP segment, is called the “Base Concept.” As envisioned, the storage heater would be an inline unit, with a fairly large L/D ratio, using a core matrix of small tubes.

The method of operation for the base concept is expected to be:

1) Charging the UHP vessel, not to exceed 345 MPa (50,000 psi).

2) Heating the air at constant volume to 550 K (530°F) with a UHP internal resistance heater.

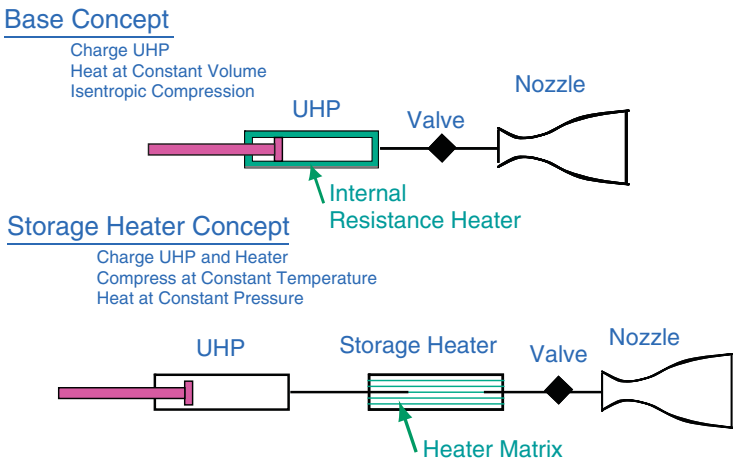

Figure 22. UHP Heater Options

3) Isentropic compression to the operating pressure and temperature.

4) The hydraulic system pushes the air out through the nozzle at constant pressure for operation.

The 50,000-psi compression limit corresponds to that of available commercial compressors.

The method of operation for the storage heater concept is expected to be:

1) Heating the storage heater core matrix to the facility operating temperature.

2) Charging the UHP vessel plus the storage heater, not to exceed 345 MPa (50,000 psi). [The air in the UHP vessel will be at room temperature (293 K, 68°F), which is also the UHP vessel temperature.]

3) Compressing at constant temperature to the operating pressure with the valve closed. The compression will be slow so that the air will again be cooled to the steel temperature with only a minor rise in the temperature of the steel.

4) Heating the air at constant pressure to the operating temperature as it passes through the storage heater.

5) The hydraulic system, with valve opening, pushes the air out through the nozzle at constant pressure for operation.

3.2.3.4.3 Preliminary Performance Calculations

The air enters the storage heater at T_i and exits at T_o. The heater matrix is initially at T_o and cools to T_i at the entrance as it heats the air. The matrix remains at T_o at the heater exit. A

"cooling wave" moves down the length of the heater during operation, and the run is over when the wave reaches the heater exit. With such a design, a high fraction of the matrix heat (decreasing the core from T_o to T_i) is extracted from the core. With this concept, the heater size is only weakly dependent on the incoming air temperature. Thus, a very slow compression cycle can be used so that the heat of compression is taken out by the steel and conducted into the UHP vessel, with the steel never increasing significantly in temperature.

Performance calculations were made of the required volumes of the base system and the storage heater system. The storage heater performance was computed with the following assumptions:

1) Heater matrix core “packing factor,” the ratio of the matrix volume to the total heater volume, of 62.5 percent. Industry conventions suggest that a well-designed heater should have a packing factor as high as 80 to 85 percent. However, because of the short run times, the lower, more conservative value was used.

2) Heater matrix “heat extraction factor,” the fraction of the heat in the matrix that is delivered to the air by the end of the run, of 80 percent.

3) Heater matrix characteristics were computed on the basis of stainless steel material properties, with a normalized volume (density x heat capacity) of 4.0 MJ/m^3-deg.

On the basis of these assumptions, the required volumes of the UHP vessel and the storage heater vessel were computed and shown as ratios in Fig. 23. The ordinate in Fig. 23 is the ratio of the storage heater gas volume to the base system UHP vessel gas volume. For these calculations, consistent with other MSHWT facility performance calculations, the facility operating temperature was taken as 1000 K up to a pressure of 1200 MPa, then reduced to 900 K at 1500 MPa, and taken as 750 K above 1900 MPa.

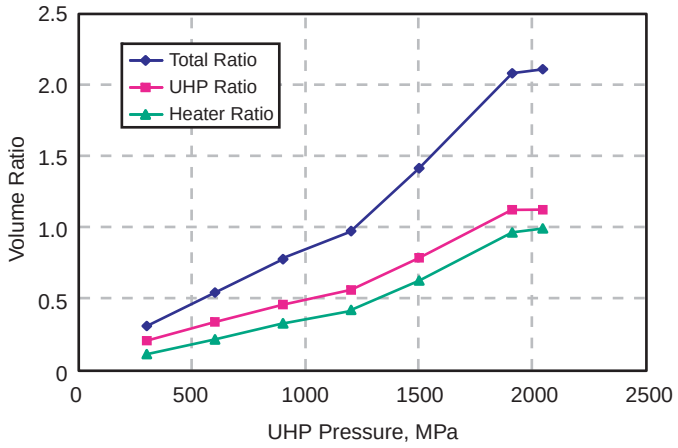

Figure 23. Volume of UHP and Storage Heater as a Ratio of the Volume of the Base Concept UHP

It is seen that the total volume (UHP volume plus the storage heater volume) is 30 percent of the base concept UHP volume at 300 MPa, increases to 100 percent at about 1200 MPa, and becomes 211 percent at 2045 MPa, the MSHWT operating pressure. The basic reason is that the storage heater concept allows higher charge pressures and thus a smaller volume for the UHP vessel to contain the required air mass. As the MSHWT operating pressure is approached, both the base system and the storage heater system are limited in charge pressure to the 345-MPa (50,000-psi) compressor limit.

Results of these preliminary rough order-of-magnitude (ROM) estimates suggest the storage heater concept offers significant advantages, including:

1) The potential for greatly increased flow quality – particularly constant temperature with time.

2) Increased margin of safety for the UHP vessel – because of holding the steel at room temperature.

These results suggest that further detailed study of the use of a storage heater for stagnation heating is warranted. There also appears to be a potential for cost savings since the intensifier volume decreases with the use of a storage heater downstream of the intensifiers.

3.2.4 Future Work

The technology demonstration experiments that are outlined in Section 3.2.3.2 and address the critical technology issues need to be completed or conducted. This means that the A-2 Lite validation, nozzle survivability, and UHP coaxial mixing experiments need to be completed or accomplished, as do MSHWT component experiments. Work is continuing toward fabrication of nozzles from an Ir alloy material being developed at ORNL. This material and associated machining methods looks promising. Reducing or eliminating porosity in the cast ingots remains the primary challenge.

As previously discussed, the fundamental feature of the MSHWT UHP subsystem design is the forces' having an "octahedral" symmetry to manage the deviatoric stresses in a cross-bore connection. This scheme simultaneously connects UHP volumes and solves the cross-bore stress concentration problem. The primary risk is the six UHP "brute force" pressure seals at the contacts between the four UHP intensifiers and the two manifolds. The probability of failure attributable to this risk is proportional to the total number of seals, which, for a baseline Mach 12, 10-s run-time facility with nitrogen film cooling, is 72. Demonstration of the sealing concept which underlies the MSHWT UHP subsystem design is therefore prudent. Since risk reduction using a full-scale MSHWT octahedral gas supply module is cost prohibitive, a subscale module having identical stress fields will be used.

The A2LM coaxial flow experiments should be conducted following the completion of the A-2 Lite Experiments if the A-2 Lite experiments show their necessity. Much of the A-2 Lite

experimental hardware can be used for this experiment with the addition of a second pressure intensifier for the nitrogen gas injection.

Finally, the preliminary work on using a storage heater concept for stagnation heating suggests that there may be advantages to the approach. Further engineering studies should be completed to guide the selection of the stagnation zone heating mechanism. Experimental validation of an approach could be conducted as a phase of the A2LM experiments.

3.3 NOZZLE DEVELOPMENT

The ultra-high pressures needed to achieve the MSHWT test conditions are expected to cause unusually stressful conditions in the nozzle throat regions, both corrosive (high oxygen partial pressure) and erosive (high density). Additionally, model and code validations for the boundary-layer growth at these high Reynolds numbers have not been accomplished. A roadmap of the nozzle technology development (including survivability and film protection technology development) is shown in Fig. 24.

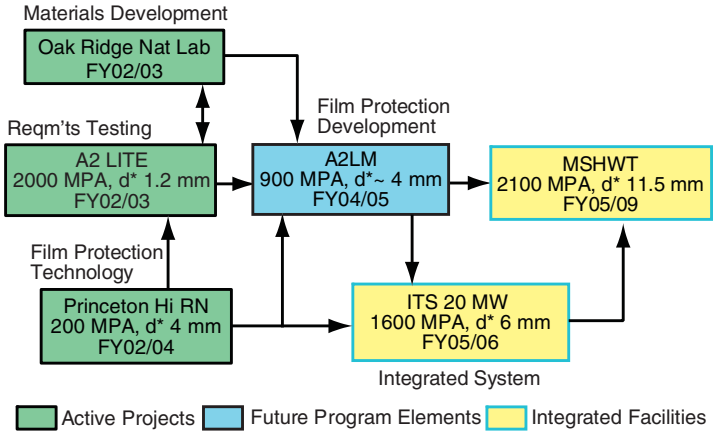

Figure 24. Roadmap for Nozzle Development

As before, the green blocks represent active efforts to date, all of which are continuing or incomplete, and the blue block (A2LM) represents a planned research effort. The "ITS-20MW" block represents the planned total systems technology demonstration, which includes UHP, nozzle, and energy-addition subsystems. Each of these technology efforts (blue and green blocks) is discussed in this section. The ITS demonstrations are discussed in Section 4.

3.3.1 Background

One of the strategic design assumptions for the MSHWT nozzle is that nozzle survivability may be an issue. Consequently, two approaches have been taken: 1) an experimental program to determine the limits of nozzle survivability for candidate nozzle materials and 2) evaluation of a nozzle wall film-cooling approach that will provide protection to the nozzle wall. The approach

for the latter solution is to surround the hot, core airflow with a cooler flow of nitrogen, which has both a lower recovery temperature at the nozzle wall and significantly less reactivity with candidate nozzle materials, and also will prevent or quench oxidation ignition events at the nozzle wall. The latter feature is particularly useful because it is likely that some oxygen will diffuse from the core airflow to the nozzle wall and that perturbations in the electron beam entering the nozzle throat from the downstream portion of the nozzle will result in collision of high-energy electrons with the wall, thereby contributing to wall heating. The discussion below describes an approach to accomplish this film cooling. If the nozzle survivability test program (A-2 Lite nozzle testing) shows that a material will survive the throat conditions in air, these complexities can be removed with significant savings.

It was recognized early that nozzle survivability in the MSHWT was an important technical issue. It is well known that real-gas effects, mentioned earlier, can cause the recovery temperature to rise above the stagnation temperature. The high densities anticipated at the throat (on the order of 1 g/cm^3), coupled with high recovery temperatures at the wall and a high partial pressure of oxygen, are expected to be an extremely stressing environment for materials. Consequently, experiments and measurements of recovery temperatures in very high Reynolds number flows are needed, and some, thus far, have been accomplished. These measurements will serve to aid in development and validation of models for prediction of the recovery temperature in these extreme environments.

Since the failure limits of conventional steel materials (and the newly developed iridium alloy discussed in Section 3.3.3.3) for application to a MSHWT nozzle are unknown, testing to failure of nozzles made of these materials is to be accomplished. In this way researchers can identify the operating regimes and limits of nozzle materials while also obtaining some insight into failure mechanisms.

A design for film cooling of the nozzle wall with nitrogen is being developed and tested. With this approach higher recovery temperatures may be acceptable. The current concepts and status of film-cooling experiments are described herein (Section 3.3.3.2).

Also, a materials research program produced an iridium alloy with high strength and oxidation resistance for a new nozzle material. The current status of this work also is included herein (Section 3.3.3.3).

Finally, work to determine boundary-layer growth at high Reynolds number and to validate models is being conducted (Section 3.3.3.5). This work is being undertaken because the boundary-layer properties are not well understood at high Reynolds numbers, and future design efforts will require this knowledge.

3.3.2 Critical Technical Issues

The MSHWT nozzle is required to survive airflow conditions up to a stagnation pressure of 2100 MPa (304,000 psi) and 750 K (890°F) stagnation temperature for run durations of seconds. The critical technical issues associated with nozzle survivability are as follows:

3.3.2.1 Recovery Temperature at the Nozzle Wall

In the UHP regime, the recovery temperature at the nozzle is calculated to be significantly higher than in the plenum because of real-gas effects, as previously mentioned. How much higher is dependent upon the recovery factor (Prandtl number). At MSHWT Reynolds numbers the boundary layer is fully turbulent. The heat transfer is highest at the nozzle throat although the nozzle recovery temperature is higher downstream of the throat. For example, see Fig. 25. In this example, taken from Ref. 19, calculations indicate that for plenum stagnation conditions of 2300 MPa (334,000 psi, a higher maximum stagnation pressure than MSHWT) and 750 K (890°F), the throat recovery temperature is 1640 K (2952°F). (As discussed above, the recovery temperature is much higher than the stagnation temperature as a consequence of real-gas effects whereby the enthalpy is a strong function of pressure as well as temperature at these stagnation conditions.) Thus the survivability of a throat material at MSHWT conditions is a substantial issue and is further exacerbated by the heat transfer in the nozzle caused by the direct heating by the scattered electron beam. The fluid mechanical heating is highly dependent on the actual turbulent Prandtl number (or recovery factor) at the Reynolds number of the facility. There are some indications from recent work (Ref. 19) that these estimates of wall temperature may be too high since recent high Reynolds number experiments have led to the derivation of a lower Prandtl number, which would result in lower wall temperatures. This result is encouraging, but further study of this issue is needed.

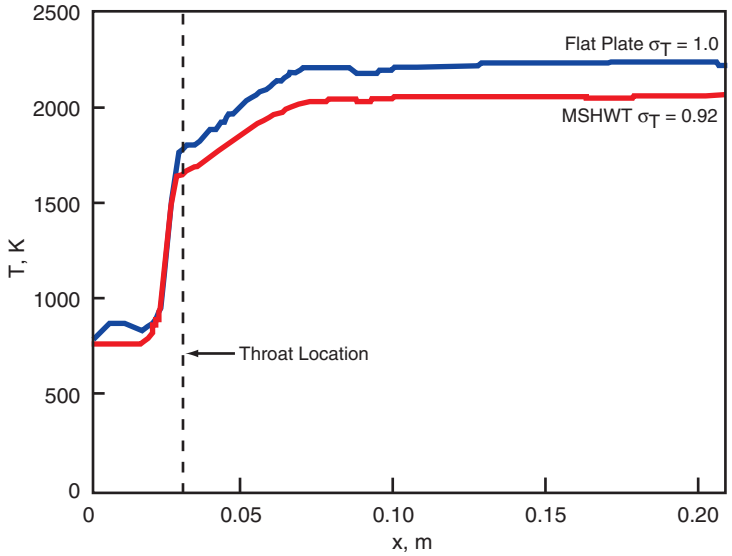

Figure 25. MSHWT Throat and Recovery Temperature (Throat and Heated Region)

3.3.2.2 Electron Beam Heating of the Nozzle Wall

Relatively low-energy scattered electrons are expected to impinge upon the nozzle walls as the return path of the current. This is expected to add heat to the walls in addition to the fluid

mechanical heating mentioned above. The amount of electron heating is not known at present and must be determined.

3.3.2.3 Material Properties and Strength

The nozzle material must be able to survive multiple test runs at the conditions mentioned above. The material must be able to sustain hoop stress levels up to about 600 MPa (87,000 psi) at the nozzle throat recovery temperature. The shear stress at the nozzle throat wall may be the critical factor for throat survivability. Mechanical erosion of the throat wall material is expected to worsen as material properties degrade with increased temperature. Other issues include whether or not an inert gas (nitrogen) could be used to eliminate the partial pressure of oxygen near the wall at the throat without contaminating the core airflow in the facility test section, and whether a lower stagnation temperature and recovery temperature for the inert gas would allow the high heat-transfer coefficient of the boundary layer to transport heat away from the wall in the heat addition region of the nozzle. The nozzle material properties must be resistant to oxidation if no inert or nitrogen gas film protection is used.

3.3.3 Progress

3.3.3.1 Measurements of Recovery Factor

Experiments were conducted at Princeton University to measure the recovery factor at very high Reynolds number. Details on these experiments are given in Ref. 19. Blowdown experiments were conducted with pressure and temperature being measured near the nozzle throat and at one location downstream of the throat. The Mach number was determined to be 0.8 at the throat measurement location because of boundary-layer displacement and nominally 1.4 at the downstream location. The stagnation pressure ranged up to 200 MPa (30,000 psi), and the stagnation temperature was nominally at room temperature. At these total pressures, real-gas effects are definitely present, as can be observed from the Mollier diagram for air (Fig. 26).

In the Princeton experiments the stagnation temperature was nominally room temperature (about 300 K). For a Prandtl number of 1, note that the recovery enthalpy at the wall of the throat would be the same as the stagnation enthalpy. In Fig. 26 this is represented by the horizontal green line, the beginning of which (on the left) is the stagnation pressure and the end of which (on the right) is the throat static pressure. The green line represents the constant total enthalpy thermodynamic process from the outer edge of the boundary layer to zero velocity at the wall in the throat. It is immediately apparent that for Prandtl number 1 the recovery temperature is approximately 380K (224°F) if the stagnation pressure is 207 MPa (30,000 psi), whereas at 69 MPa (10,000 psi), it is 300K (80°F).Thus real-gas effects are present at 207 MPa (30,000 psi) stagnation pressure but are of little consequence at 69 MPa (10,000 psi) stagnation pressure for 300 K stagnation temperature.

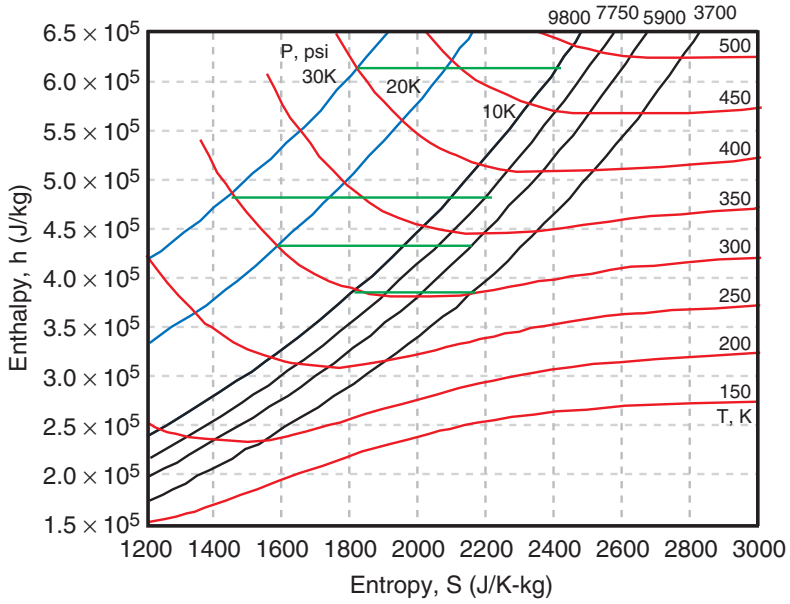

Figure 26. Mollier Diagram for Air

For the results to date, the recovery factor at the physical throat is approximately 0.84 to 0.87. For the MSHWT this would lead to a throat temperature of 1483 K (2210°F) and not 1640 K (2492°F), as shown in Fig. 25. This result certainly lends hope that the MSHWT nozzle throat survivability issue may not be as severe as was first feared. The A-2 Lite experiments should include determination of the recovery factor and temperature with wall temperature and pressure measurements at near MSHWT Mach 12 real-gas conditions.

3.3.3.2 Film Cooling

3.3.3.2.1 Nitrogen Film Protection - Theoretical Considerations

The actual throat diameter for the MSHWT has been chosen somewhat arbitrarily to be twice the ideal one-dimensional diameter in order to keep the direct heating losses to the wall from the scattered e-beam to a low value. The total mass flux is therefore four times the ideal one-dimensional value, and it raises the question of whether some significant fraction (perhaps 25 to 50 percent) of this could be nitrogen for oxidation protection of the wall, especially in light of the predicted wall recovery temperatures. Since it is anticipated that the ultra-high-pressure air will be heated to the stagnation temperature in a heat exchanger, it also raises the possibility that there could be a gradient in total temperature in the nitrogen so that the recovery temperature in the nitrogen boundary layer could be reduced. The issue to be considered is the extent to which the shear layer interface between the nitrogen and the air would cause mixing of the nitrogen with the primary core flow of air given different temperatures and velocities. If in the first instance an inviscid flow with a vortex sheet (mixing layer) between the nitrogen and the air is assumed, it is then a straightforward matter in air to predict the velocity difference across this sheet as a

function of the Mach number in the air from the equation of state for nitrogen, assuming matched (or unequal) velocities upstream in the contraction and matched static pressure.

The relative velocity difference across the sheet is shown in Fig. 27, which is taken from Ref. 19. Stagnation temperature for the air core is 750K, and for the nitrogen it is 400, 450, and 530K. In each case the relative velocity difference remains small (less than 5 percent) even at Mach 3 and with a 350K difference in temperature. The reason is that at very high pressures the density is a relatively weak function of temperature.

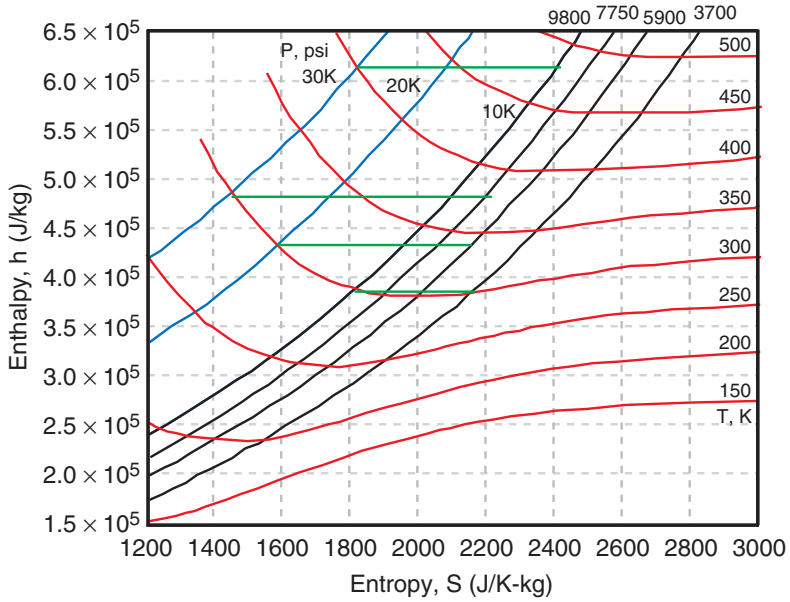

Figure 27. Relative Velocity Difference Across Vortex Sheet (Mixing Layer) as a Function of Mach Number

Brown et al. (Ref. 19) argue that the thickness of the nitrogen/air shear layer should be less than 5 percent of the nozzle throat diameter and that the coaxial nitrogen cooling flow would protect the wall from oxidation, while at the same time it would not contaminate the core flow of air. Whether this holds true far downstream in the facility test section has not been investigated to date. Experiments are needed to confirm the hypothesis and validate turbulent flow models, which include the real-gas equation of state.

3.3.3.2.2 Film Cooling Experiments

A series of film cooling experiments is planned to gather sufficient information to validate analytical models and design a coaxial nitrogen/air injection system for the MSHWT. The planned experiments are outlined as follows:

1) Two-dimensional (2D) nitrogen/air injection system. This is a planar 2D configuration permitting 2D observations of the flow mixing through a nozzle throat. Preliminary

nitrogen film cooling experiments were conducted in the Princeton 2D heat-transfer tunnel. The 2D nitrogen cooling experiments were initiated at Princeton University in their 2D contraction tunnel (Ref. 19) but were not complete as of the writing of this report.

2) High-pressure coaxial film cooling. The purpose of these experiments is to provide data for validation of analytical codes, hardware configuration, and test procedures that can be used in the design and operation of the A2LM UHP experiments and the ITS facility. The intent was to use the Princeton high-pressure blowdown facility for the experiments. The hardware was purchased and assembled, but experiments were not conducted before the termination of this work (Ref. 19).

3) Ultra-high-pressure coaxial film cooling. The purpose of these experiments is to validate a design concept and an operational concept for the ITS and MSHWT nitrogen film cooling systems. The experiments would be conducted using the A2LM in the MSE UHPTF with a coaxial nitrogen/air injection system. Tentatively, the maximum total pressure is 900 MPa, and the total throat diameter would be at least 4 mm to achieve sufficient experimental fidelity for the coaxial flows. Only preliminary plans have been made for the design and fabrication of the experimental hardware.

3.3.3.3 Materials Development

The ORNL undertook an investigation of candidate materials that could be used for the MSHWT nozzle throats that would be better than the baseline 350 maraging steel. The 350 maraging steel is thought to be one of the superior steels for this application, and except for the recovery temperature effects, would probably be satisfactory.

The nozzle throat environment for the MSHWT will be a static pressure of 500 to 600 MPa (72,500 to 87,000 psi), a recovery temperature of as much as 1700 K (2600°F) at the design point of Mach 12, and a dynamic pressure of 2000 psf (96 kPa). As a first approximation, the nozzle throat insert can be considered a thick-walled pressure vessel; therefore, the hoop stress requirement will be approximately 600 MPa (87,000 psi). The thermal loading on the nozzle wall can be expressed as:

$$Q = h(T_r - T_w)$$

Heat loads can be very large since the heat-transfer coefficient (h) is very large at these conditions. However, if the nozzle wall material temperature (T_w) can be allowed to rise to the level of the recovery temperature (T_r), then the heat flux (Q) can be forced toward zero. This can be characterized as a self-limiting heat-sink mode of operation. In this case, the nozzle material would be required to maintain hoop stress strength of 600 MPa (87,000 psi) at 1700 K (2600°F). The objective of this effort was to develop such a material, one that would be oxidation resistant and also would retain the required strength properties at high temperature.

Materials considered for the application included molybdenum-rhenium alloys, molybdenum-silicon-boron alloys, and iridium alloys. Alloys of iridium were the most promising because of their proven oxidation resistance, which has been demonstrated in space power applications. However, pure iridium loses most of its strength at temperatures approaching 1700 K (2600°F). Therefore, it was necessary to find alloying elements that would increase the strength of iridium at elevated temperatures. Several elements were tried, and a number of them significantly increased the strength but had other shortcomings. Two elements, zirconium and hafnium, were found to be the most successful. Other trace elements were added for refinement. An optimized iridium-based alloy with the composition Ir-4.5Zr-0.3W-0.31C-0.005Th (at. percent) was developed. This alloy has demonstrated a yield strength of 700 MPa (100,000 psi) at 1700 K (2600°F), and it has reasonable ductility, good oxidation resistance, and good thermal shock resistance. Oxidation resistance was demonstrated by 10-min exposure to static air at 1700 K (2600°F) as well as to flowing air at a nominal 1-atm pressure. Minimal weight losses/gains were observed. Oxidation resistance at ultra-high pressures were planned to be determined in the A-2 Lite nozzle survivability experiments discussed in Section 3.3.3.4. Thermal shock resistance was demonstrated by heating the material to 1700 K (2600°F) and quenching it in agitated water. No adverse effects on material properties or characteristics were observed.

Small sample ingots for characterization were prepared by a simple arc-heated, drop-casting method. It was known that only limited size ingots could be prepared by this method; consequently, some modifications were made to the drop-casting hardware in order to cast an ingot large enough to machine an A-2 Lite nozzle throat insert. It was demonstrated that throat contours could be machined by electric discharge machining; however, internal porosity was discovered, and this dictated a more sophisticated ingot fabrication technique. Vacuum drip casting was selected because of its ability to fabricate larger, porosity-free ingots.

A minimum of two iridium alloy A-2 Lite nozzle inserts are planned to be tested. The remainder of the 6.35-cm-diam by 11.4-cm-long (2.5-in by 4.5-in) ingots will be available for up to 1) four additional A-2 Lite nozzles or 2) one potentially larger nozzle.

In addition to the iridium alloy developed by ORNL, 350 maraging steel is planned for testing in the A-2 Lite. The test plan objective is to establish the performance limits of each material in terms of stagnation pressure and temperature up to 2100 MPa (304,000 psi) and 750 K (890°F), respectively.

3.3.3.4 Status of Nozzle Throat Survivability Testing

Nozzle survivability testing was undertaken by MSE in the UHPTF. In total, 74 nozzle survivability tests were attempted. Table 5 is a summary of these. Originally nitrogen, helium, and air were to be used as working gases, but helium was eliminated when it was determined not to be needed. Table 5 shows an outline of the nozzle survivability testing program, including tests accomplished and tests planned.

Table 5. Summary of Nozzle Survivability Tests

Series No.	Test Series Title	Maximum Pressure, psi	Intermediate Pressures, psi	No. of Test Attempts	Test Type	Gas Used
2000	Quasistatic tests with nozzle end closure with pressures not to exceed 45,000 psi.	45,000	N/A	39	Static	Nitrogen Air
2050	Plenum dynamic tests with nozzle end closure with pressures not to exceed 45,000 psi.	45,000	N/A	3	Dynamic	Nitrogen
2100	Quasistatic tests with nozzle end closure with pressures not to exceed 150,000 psi.	150,000	70,000 90,000 110,000 130,000	32	Quasistatic	Nitrogen Air
2150*	Plenum dynamic tests with nozzle end closure with pressures not to exceed 150,000 psi.	150,000	N/A	0	Dynamic	Nitrogen Air
2200*	Quasistatic tests with nozzle end closure with pressures not to exceed 200,000 psi.	200,000	180,000	0	Quasistatic	Nitrogen Air
2250*	Plenum dynamic tests with nozzle end closure with pressures not to exceed 200,000 psi.	200,000	N/A	0	Dynamic	Nitrogen Air
2300*	Quasistatic tests with nozzle end closure with pressures not to exceed 255,000 psi.	255,000	N/A	0	Quasistatic	Nitrogen Air
2350*	Plenum dynamic tests with nozzle end closure with pressures not to exceed 255,000 psi.	255,000	N/A	0	Dynamic	Nitrogen Air
2400*	Quasistatic tests with nozzle end closure with pressures not to exceed 300,000 psi.	300,000	N/A	0	Quasistatic	Nitrogen Air
2450*	Plenum dynamic tests with nozzle end closure with pressures not to exceed 300,000 psi.	300,000	N/A	0	Dynamic	Nitrogen Air
Total nozzle survivability tests attempted				**74**		

* Test series not performed during this contract.

Tests are described as:

Static: Only the air compressor is used to create high working gas pressures. This limits the pressure to approximately 310 MPa (45,000 psi).

Quasistatic: The hydraulic pump is used to slowly move the hydraulic ram, which in turn forces the piston into the UHP vessel plenum. Maximum plenum pressures in tests of this nature are limited by test objectives or, ultimately, by UHP vessel strength. Plenum temperatures remain near ambient.

Dynamic: The nitrogen-over-hydraulic accumulator is used to drive the hydraulic ram up to about 1 m/s, which in turn drives the piston into the plenum. Maximum pressures, while theoretically lower than for the quasi-static case, may still be above UHP vessel strength. Temperatures can be greatly increased depending on the precharge pressure applied with the compressor, the final pressure, and the rapidity of the compression.

A major issue with blowdown testing was to develop and successfully test an emergency pressure-relief device capable of releasing pressure should it get trapped in the plenum. Several options were considered, and the most promising option was the retractable Bridgman support (RBS). The RBS uses a short extension to hold a very small Bridgman seal in the throat of the nozzle; when the extension is withdrawn rapidly, the seal releases and gas is released from the plenum. The RBS can be manually operated for an emergency pressure-relief device or automatically operated for nozzle testing. Test Series 2050 was the first dynamic nozzle test where the RBS was automatically activated.

A maximum pressure of 1034 MPa (150,000 psi) was achieved in quasi-static nozzle blowdown testing as part of Test Series 2100. Since this was a quasi-static test, the working gas stagnation temperature was only slightly above ambient. For the tests completed to date, only nozzles made of 350 maraging steel were used. No nozzle material degradation was observed in any tests conducted to date.

3.3.3.5 Nozzle Boundary-Layer Growth

The RDHWT nozzle will operate at very high Reynolds numbers (~10^{10}). Nozzle boundary-layer growth at very high Reynolds numbers is not well established, and boundary-layer turbulence models have not been validated for these conditions. This problem will not invalidate the RDHWT concept, but it does need to be addressed so that realistic nozzle design tools will be available. To this end, high Reynolds number (~10^{8}) experiments (Refs. 19 and 35) have been conducted at Princeton University to gather validation data for boundary-layer growth models. Additionally, nozzle data from the AEDC Tunnel 9 hypersonic wind tunnel at similar Reynolds numbers are being analyzed. The boundary-layer growth data presented in Ref. 36 were for one nozzle position (not stated) and were based on a wall pressure measurement. Although Reynolds number was varied, these data do not reveal any trend in boundary-layer growth with Reynolds number.

The Tunnel 9 data analyzed were taken with the Mach 14 nozzle. A comparison was made of the displacement thickness in Tunnel 9 with that taken by Raman (Ref. 36) at Princeton on this project.

Table 6 below shows the test conditions for the two cases and the calculated displacement thickness, δ*/x, where x is the centerline distance from the nozzle throat.

Table 6. Comparison of Boundary-Layer Growth Between Tunnel 9 and Princeton Experiments

	Gas	Po, psi	To, R	M exit	$\tilde{\delta^*}/x$
Tunnel 9	N2	21,423	3260	~14	0.0081 ± 0.0006
Princeton	Air	2000 to 22,000	~480	~2	0.0057 ± 0.0003

The Tunnel 9 data displayed are for only one test condition. The Tunnel 9 displacement thickness was calculated on the basis of a pitot pressure survey across the nozzle, whereas the Princeton displacement thickness calculations are based on wall pressure measurements. For Tunnel 9, the Reynolds number at the nozzle throat is 6.475E + 07. The nozzle exit Reynolds number is 1.89 E + 07. Further details of the Princeton experiments are found in Ref.36, by Raman.

Raman's data, above, represent several data points. He experimentally observed that the displacement thickness growth was nearly linear with distance from the nozzle throat and was essentially independent of Reynolds number in his experiment, which is indeed curious. The nozzle exit Mach number was about 2. Raman also showed that the displacement thickness growth was roughly double that provided by the smooth-wall computational fluid dynamics (CFD) calculations, using a Baldwin-Lomax turbulence model for a smooth wall. He attributed the difference between the CFD calculations and the experiment to roughness effects in the nozzle.

The Tunnel 9 boundary-layer displacement thickness normalized with the centerline distance from the throat (x) is about 42 percent higher than Raman's empirical result, i.e., 0.0081/0.0057 = 1.42. The unit Reynolds number is higher in the Princeton case because the stagnation temperature is much lower. But the Tunnel 9 nozzle is physically much larger than the Princeton nozzle. The Princeton nozzle throat was about 4 mm, or about 0.157 of the Tunnel 9 throat. Since the stagnation pressures in the two cases are about the same and accounting for the difference in total temperatures, the Reynolds number is of the same order in both experiments, i.e., about 10^8. Since the exit Mach numbers are considerably different—Mach 2 in Raman's case versus Mach 14 for Tunnel 9—so potentially there could be a Mach number effect. The Tunnel 9 nozzle wall is probably much rougher than the Princeton nozzle wall. A comparison of the Tunnel 9 displacement calculation and Raman's calculations is shown in Fig. 28. The Tunnel 9 displacement was calculated on the basis of the pitot survey at the exit of the nozzle, assuming a linear growth from the throat.

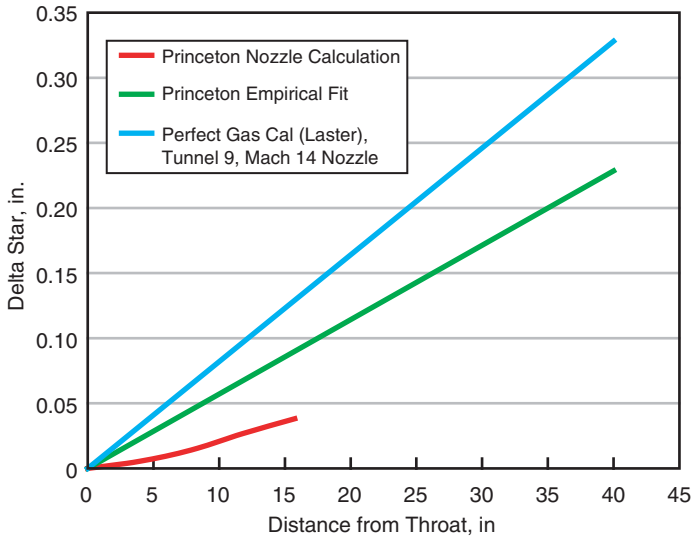

Figure 28. Comparison of Boundary-Layer Displacement Thicknesses

All in all, the Tunnel 9 nozzle is probably more representative of an MSHWT nozzle than is the one used in the Princeton experiments because its physical size and nozzle roughness are probably closer to that of a real MSHWT nozzle.

Additional data were analyzed for Tunnel 9 where both wall pressure and pitot pressure measurements were made. One Reynolds number case is shown in Fig. 29. Displacement thickness calculations were made with both pitot and wall pressure measurements. It should be noted that there is a difference in the calculated value of displacement thickness between the pitot and wall pressure data. The reason is that there is a nonzero pressure gradient across the boundary layer (i.e., the pressure at the wall is higher than the freestream static pressure). This is a normal phenomenon for hypersonic nozzles (Ref. 35). This phenomenon alone perhaps means that in his experimental analysis Raman may be underpredicting the boundary-layer displacement thickness because his analysis calculates displacement on the basis of wall pressure measurements. However, the Mach number is supersonic in his experiments, not hypersonic, and a lateral pressure gradient, if any, is not known.

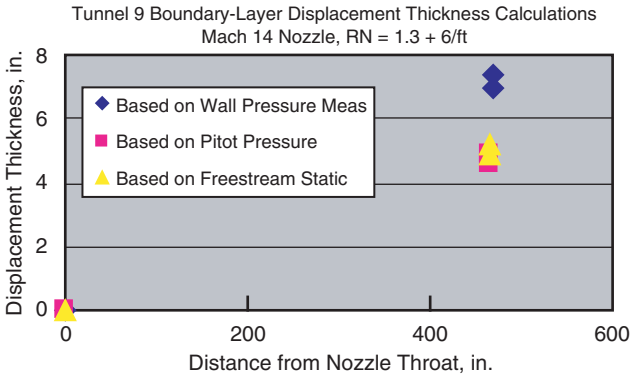

Figure 29. Comparison of Displacement Thicknesses Based on Pitot and Wall Pressure Measurements

The displacement thickness is calculated from the Tunnel 9 pitot pressure and plotted versus Reynolds number as shown in Fig. 30.

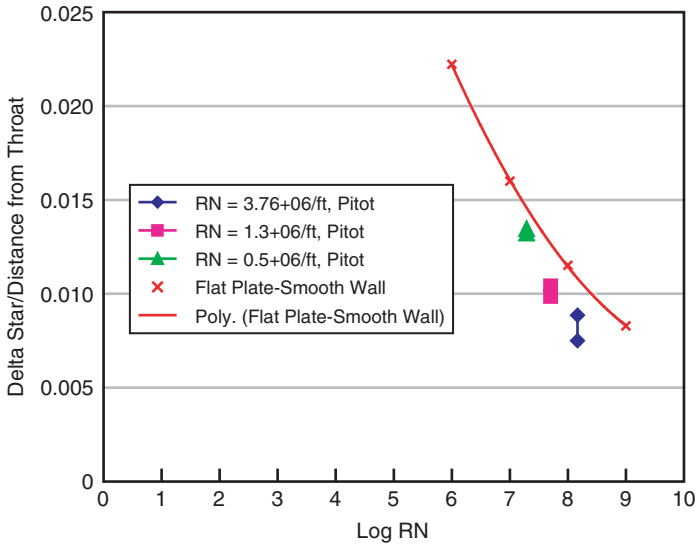

Figure 30. AEDC Tunnel 9 Displacement Thickness as a Function of Reynolds Number

Also shown in Fig. 30 is the flat plate-smooth wall empirical correlation by White (Ref. 37). There is remarkable agreement between the flat plate-smooth wall empirical correlation and the Tunnel 9 rough wall nozzle with a very large favorable pressure gradient. This agreement suggests that, for this hypersonic nozzle, the favorable pressure gradient effect (which retards boundary-layer growth) and the nozzle wall roughness effect (which enhances boundary-layer growth) offset one another. One cannot claim this as a universal finding merely on the basis of this limited set of data, but the data do inspire further investigation. Ideally, one might be able to use this simple flat plate-smooth wall correlation to estimate the boundary-layer displacement thickness in a MSHWT nozzle with first-order accuracy.

3.3.3.6 Future Nozzle Development

The major nozzle development activities to be completed are as follows:

1) Completion of the A2-Lite nozzle survivability experiments to determine the operational limits of maraging steel and the ORNL-developed iridium alloy for nozzle throat application. In these experiments, nozzle temperature and static pressure measurements should be made to determine the recovery factor needed to predict wall temperature and heat transfer.

2) The need for additional film cooling experiments is dependent upon the results of the experiments in 1), above. If it is determined that film cooling is needed, the nozzle film-cooling experiments should be completed as planned, including those in the high-pressure facility at Princeton and the planned A2LM experiments.

3) The determination of nozzle boundary-layer growth in high Reynolds number nozzles for validation of models should be accomplished. It may be possible that these can be done in the 1) or 2) experiments above. However, high Reynolds number boundary-layer growth data from nozzles whose physical size is of the same order as MSHWT nozzles (e.g., Tunnel 9) is believed to provide better experimental data for model validation. Acquisition of these validation data and experiments should be pursued.

3.4 ENERGY ADDITION

The approach taken for the energy-addition experiments is that, insofar as possible, each increment in the experiment would demonstrate technologies that would be appropriate for an MSHWT. Figure 31 illustrates the energy-addition system development plan. These energy addition experiments and supporting experiments provide the proof of principle and the design criteria for the MSHWT. Each of the development steps for these proof-of-principle experiments is taken to test an approach to solve or demonstrate an anticipated full-scale (MSHWT) requirement and simultaneously to accomplish the next energy-addition step. Thus, for example, the design of the e-beam injector for the ITS (Block 3) will be the basis of the design of the injector at 200 MW (Block 8). Two major remaining energy-addition experiments are shown: the 1MW-1s experiment (Blocks 2) and the 20- to 30-MW-1 s ITS system (Block 7) demonstration experiment, with several supporting experiments and developments.

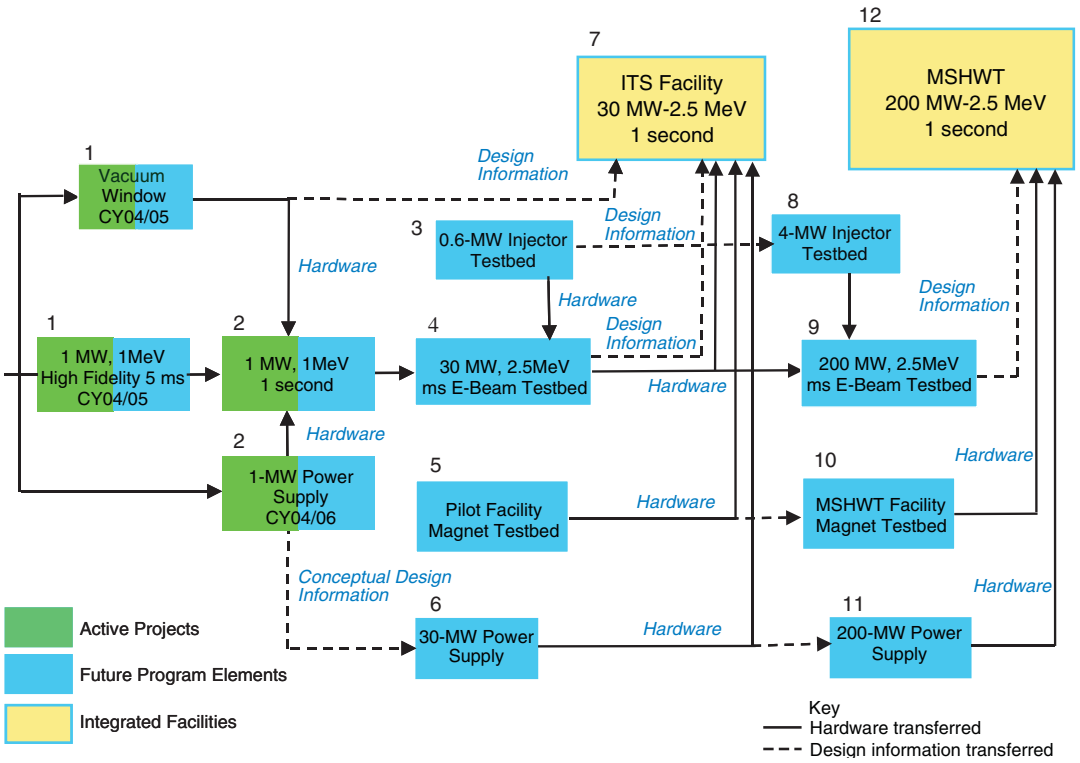

Figure 31. Electron Beam Accelerator Technology Development Plan

3.4.1 Background and Summary

Demonstration of energy addition to the supersonic flows was one of the major issues at the commencement of the research program (Ref. 9). The first successful demonstration of energy addition to supersonic flow was accomplished with a 10-kW CO_2 laser and SF_6-seeded air (Ref. 38). Stable operation at this power level was demonstrated, and code predictions of gas dynamics were validated. Although experiments at higher laser power levels were initially planned, the program team felt that electron beam technology was a more mature technology and had greater promise of achieving the power levels necessary for final facility scale operations (~200 MW) and at least cost. Consequently, subsequent proof-of-principle experiments were accomplished in roughly order-of-magnitude power increments with electron beam energy addition at Sandia National Laboratories in Albuquerque, NM.

The first e-beam energy addition experiment was successfully accomplished at nominally 30 kW (Ref. 39). These experiments were actually performed at several different power levels with energy added to the gas ranging from 10 to 40 kW. The nature of the e-beam equipment that was used necessarily limited these experiments to short durations, and stable operation at the lower power depositions was inferred. The higher power experiments were of too short a duration to establish stable operation, but energy addition at the 40-kW level was successfully demonstrated.

A subsequent experiment at a nominal 100-kW energy addition (power deposition into the gas ranged from 26 kW to 112 kW) (Refs. 40 and 41) was similarly successful with the added energy thermalized. The e-beam pulse was still short (~1 to 2 ms), to avoid rupturing the foil aperture used to maintain vacuum conditions in the accelerator, and to avoid subsequent contamination of the cathode. The flow in the heating region was observed to be stable over the course of the experiments. At the higher power experiments, there appeared to be some fluctuation in the unheated annulus around the central core that was believed to be attributable to the nonuniform heating profile.

Following completion of the 100-kW experiments, the project team began planning for 1-MW power addition experiments. The HAWK electron beam accelerator, which had been used for the 30- and 100-kW tests, was chosen to be modified and upgraded for the 1-MW experiments. Final planning, design, execution, and data analysis for the first series of 1-MW experiments was the major energy addition effort accomplished during this reporting period. Plans for the 1-MW experiment are included in Ref. 42.

3.4.2 Critical Technical Issues

For an MSHWT facility, six technical issues have been identified as critical to the energy addition. These are:

1) **Scaling**. A medium- or large-scale T&E facility will require a very high-power (hundreds of megawatts) e-beam source. This will be provided by either a single e-beam or multiple smaller beams that enter at different locations around the perimeter of the wind

tunnel nozzle. Multiple beams would be merged to deliver the total energy into the high-pressure nozzle region at supersonic flow conditions. Issues associated with scaling to the very high-power single beams or with using a number of smaller beams to achieve the high total power (magnetic confinement of multiple beams, and the energy addition uniformity that can be achieved) must be established before moving to a T&E facility.

2) **Magnetic confinement and focusing of e-beam**. The energy profile across the beam must be controlled to minimize wall heating and ensure that the primary energy deposition occurs uniformly in the core of the high-pressure flow field so that the gas and uniform flow property conditions of flight can be simulated. This will be accomplished with solenoidal magnetic fields to guide the electron beam into the nozzle energy deposition region. The field strengths and dimensions of a large-scale facility represent an extension of the magnetic steering technology and, although thought to be of modest extent, need to be demonstrated.

3) **E-beam insertion through the nozzle wall**. Because of geometric considerations, the e-beam must be inserted into the flow environment through the nozzle wall. This requires development and demonstration of an aerodynamic window that will allow beam insertion without disruption of the nozzle flow.

4) **Dynamic mechanisms in e-beam heating**. Energy deposition in the gas is a consequence of coupling between the high-density gas and the e-beam. The gas density along the e-beam path is a major factor in beam penetration in addition to energy deposition. Nonuniformities in the e-beam lead to nonuniformities in the energy deposition and the subsequent gas properties downstream of the energy deposition region in the lower density flow. This can lead to deeper penetration of the e-beam through the lower density portion of the flow and further nonuniform energy deposition. This may lead to flow instabilities and may also be an important mechanism affecting wall heating. These dynamic mechanisms must be understood for the full-scale facility and can be examined by appropriate modeling with experimental validation.

5) **Flow chemistry and thermalization**. The interaction of the e-beam with the individual gas molecules leads to ionization, electronic excitation, and chemical dissociation. Thermalization of the energy into the flow properties occurs with the subsequent recombination and other chemical processes. Although recombination and other ionic chemistry processes tend to be quite rapid relative to flow times, species are formed that are not typical of flight environment air species. Other thermal chemical and ionic processes are required to complete the thermalization and destroy these atypical species, and these reactions can become slow, relative to flow times. Although the ionization fraction is expected to be small, significant concentrations of contaminant species such as NOX and O_3 may occur. The air density and temperature envelope for thermalization is unknown and must be understood and explored with appropriate, validated codes. The energy-transfer and thermalization processes will occur in a high-density environment and a

very strong magnetic field sufficiently large to affect the intermolecular potential and molecular orientation with unknown effects on the values of reaction rates commonly used in modeling. The effects of the unusual physical environment on the energy-addition air chemistry need to be understood.

6) **Run-time considerations**. For T&E purposes, it is important to have run times at least on the order of seconds and potentially as long as tens to hundreds of seconds. Robust e-beam windows or portholes must be developed that can maintain this continuous power loading, and the e-beam source itself must be capable of operating without significant fluctuations or degradation during this time interval.

The planning for future work is intended simultaneously to provide continued proof-of-principle experiments that provide fundamental data for development of higher power systems and to test technical feasibility of the technical approaches to be used in a final facility design.

3.4.3 Progress

Two areas of work in the energy-addition effort showed significant progress this reporting period: computational modeling and 1-MW energy-addition experiments. The modeling effort has been made in support of the experiments, and, except for a brief overview, results of the modeling are included in the summary of the 1-MW experiment.

3.4.3.1 Modeling

CFD modeling for MSHWT conditions continued throughout the reporting period, building on the earlier work, and progress is described in Ref. 19. A more realistic viscous simulation (Refs. 43 and 44) was developed to deal with condensation conditions calculated by the inviscid code (Ref. 45). Examples of the two codes at near-MSHWT stagnation chamber conditions (2300 MPa, 750 K) are shown in Fig. 32. The condensation region near the nozzle wall is evident in the inviscid solution, and different nozzle flow conditions are predicted by the two codes. Validation experiments for the more realistic code are needed.

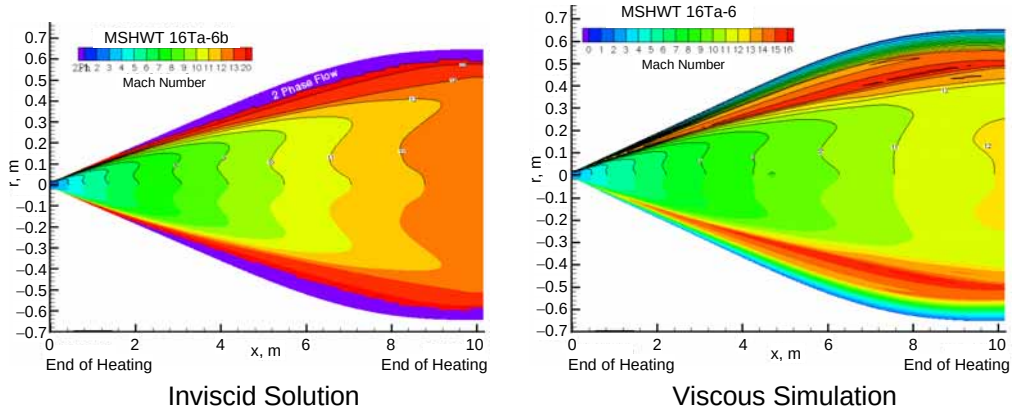

Figure 32. Test Section Simulation, Mach 12 Radiatively Driven Missile-Scale Hypersonic Wind Tunnel

As described below, the 1-MW experiments showed significant transient behavior as measured by the current to ground from the nozzle. Although the experiments were valuable in demonstrating large energy addition to the supersonic air stream by the e-beam, they were not sufficiently repeatable and did not have all the measurements necessary for satisfactory code validations. A fully coupled e-beam-to-fluid dynamics model was developed so that unsteady behavior caused by the time-dependent e-beam flux could be explored (Ref. 23). Some results of this time-dependent modeling are included in the comparisons of experiment and calculations below.

Other modeling pertinent to the energy addition includes studying the effect of different magnetic fields on the energy-addition radial profile. This capability will facilitate examination of different Monte Carlo codes for improvement of the energy deposition model, and it will aid in the design of equipment to obtain a uniform radial heating profile.

3.4.3.2 Experiment

The experimental work included in the period covered by this report was principally directed toward the successful completion of the next increment in energy-addition experiments: energy addition at the 1-MW power level. There were five principal areas of work:

1) Design and upgrade of the high-pressure gas source

2) E-beam accelerator upgrade

3) E-beam window

4) Experiment and diagnostics

5) Data analysis

Initial plans for the demonstration 1-MW experiment are in program planning documents and are summarized in Ref. 42. Emphasis here is on the short-duration energy-addition experiment already accomplished, although planning includes technology demonstration beyond the short-duration 1-MW experiment described here. Progress on these upgrades is described below (Section 3.4.3.3).

Specifically for the short-duration 1-MW experiment, the original objectives of the e-beam upgrades and demonstrations included:

1) Addition of 1 MW of energy to the flow using a 1-Mev beam and 1-A current.

2) Tailoring of the continuous magnetic field over various accelerator structures to minimize growth of beam oscillations, and coupling it with an annular cathode to establish a quasi- “top hat” beam profile (uniform in radial extent) in the energy-addition region. Included is immersion of the cathode in the magnetic field to reduce the transport and reflection losses observed in previous experiments.

3) Bending of the beam through a 45-deg angle into the nozzle.

4) Development of a plasma-aerodynamic window that eliminates the beryllium foil at the vacuum/air interface and allows long-duration, high-power beams.

Included in energy addition and flow quality objectives:

5) Addition of energy to the flow that is about twice the plenum energy to achieve an exit enthalpy ratio (ratio of exit enthalpy to plenum enthalpy) of near 3, comparable to that envisioned for a Mach 12, true-temperature hypersonic wind tunnel (Ref. 45).

6) Validation of energy deposition and e-beam steering models.

7) Establishing the effect of the e-beam on the chemistry of the heated air.

8) Gaining an understanding of the e-beam current return path.

9) Determining whether arc discharges occur in the nozzle and quantifing e-beam-induced wall heating.

3.4.3.2.1 High-Pressure Gas Supply

A heated high-pressure gas source to provide gas flow for the experiment was designed and built. The source is shown schematically in Fig. 33. A picture of the installed hardware is shown in Fig. 34.

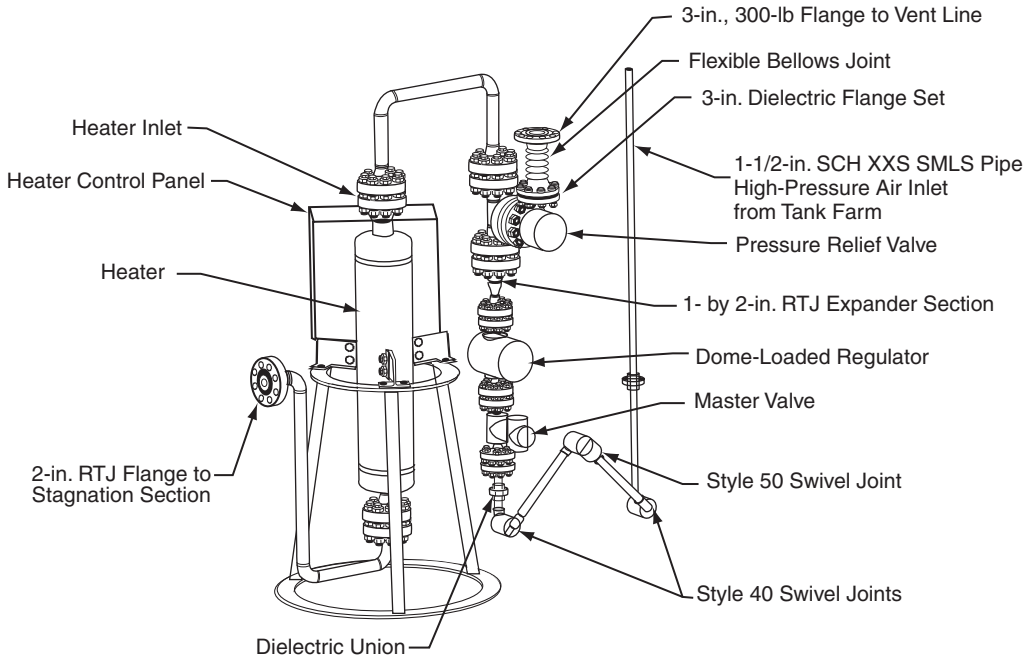

Figure 33. Heater and Piping Assembly Drawing

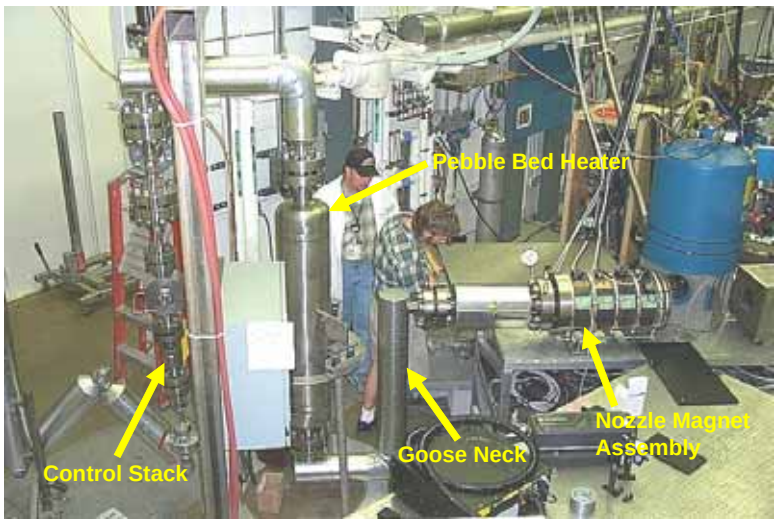

Figure 34. Photograph of the As-Built, High-Pressure Air Delivery System

The system was supplied by 20 compressed gas cylinders able to supply 0.74 m^3 (26 ft^3) at 41 MPa (6000 psi). The system could supply air to the nozzle plenum at 18.3 MPa (2650 psi) and 615 K (647°F). In operation, however, because of other experiment constraints, most data were obtained at nominal operating conditions of 14.8 MPa (2150 psi) and 605 K (629°F).

3.4.3.2.2 Accelerator Upgrade and Electron Beam Window

Upgrade of the sundry elements of the HAWK accelerator to enable it to deliver a 1-MW beam was accomplished. Much of the equipment was the same as that used in the previous 100-kW experiments. Additional capacitance was added to the power supply, and the magnetic field was extended to include the cathode in order to avoid the magnetic reflection problem seen in the 100-kW experiments. A plasma porthole (Ref. 46) was built to replace the beryllium window for beam transport from the HAWK to the atmosphere. As is described below, it was discovered in an initial set of experiments that several aspects of the experiment did not work as expected. These included the plasma porthole and some elements of the HAWK electronics. The plasma porthole was replaced with a mechanical device using differential pumping and an exploding acetate film. The HAWK electronics were modified so that subsequent short-duration experiments could proceed.

3.4.3.2.3 Experiment and Diagnostics

The basic layout of the experiment is shown in Fig. 35. High-pressure air from the gas supply is introduced into a nozzle from the plenum. As the supersonic air expands in the nozzle, energy is introduced into the airflow by a high-power electron beam from the HAWK accelerator. Using externally applied magnetic fields (magnets indicated in green), the e-beam is both bent

into the airflow (satisfying one of the experiment's objectives) and focused away from the nozzle walls. The heated air is subsequently deflected and cooled before being reintroduced into the laboratory. Although not shown in the figure, as indicated above, magnetic coils were designed and built for the HAWK accelerator that immersed the cathode and entire beam creation and transport hardware in a magnetic field tailored for the experiment.

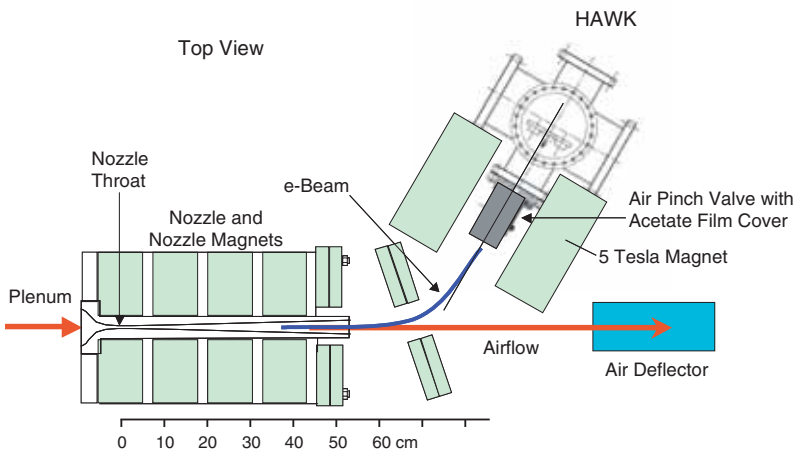

Figure 35. Schematic of Experiment Layout

The initial experiments were unsuccessful in achieving certain objectives. Additional modifications to the HAWK accelerator were required, and the "plasma porthole" concept (Ref. 46) for the plasma-aerodynamic window did not work for this application because of the influence of the magnetic field on the plasma. Measurements of nozzle current to ground were not successful, and refurbishment of some nozzle components was necessary. The HAWK high-voltage deck was modified, and an alternate approach (mentioned above) to the plasma aerodynamic window was used. This alternate approach is indicated in Fig. 35. A second set of experiments was made (Refs. 25 and 47), and successful diagnostic measurements were obtained. Significant transient fluctuations in the nozzle-to-ground current were observed that were linked to beam instabilities resulting from the beam's hitting apertures in the aerodynamic window apparatus. Most data useful for analysis were taken at power additions of less than 400 kW, although up to 890 kW of power were added to the flow in some test runs that obtained useful diagnostic measurements.

Since the power addition pulse in the second series of experiments had an uncontrollable transient component, the utility of the experiment for code validations and flow stability demonstrations was complicated, though still useful. Consequently, additional HAWK modifications are being made, and plans are progressing for a long (1-s) energy-addition experiment (see 3.4.3.3, below). The 1-s, 1-MW experiment will also be used to provide high-quality computer code validation experiments at shorter run times (5 ms).

Several diagnostic systems were used to characterize the flow field both internal and external to the nozzle, as well as with and without e-beam heating. A brief summary of the diagnostics

employed is presented in Table 7, below. Nozzle pressure measurements were carried out with five Optrand® transducers distributed along the length of the nozzle. Airspeed was determined by both direct spark and shadow/spark velocimetry. Shadowgraphs were taken to determine the Mach number, and air density measurements were obtained using Rayleigh scattering. The nozzle return current was measured through a 5.5-Ohm resistor used to electrically float the nozzle. In addition, UV spectroscopy was used to measure NO production during e-beam heating. A special charge-coupled detector (CCD) camera (Princeton Scientific Instruments, Inc.) with a framing rate as high as 1 MHz was employed in several of the measurements. A more complete description of the diagnostic suite is given in Ref. 48.

Table 7. Diagnostics Employed During the 1-MW Experiments

Diagnostic System	Parameter Measured	Comment / Equipment
Omega Pressure Transducer	Plenum Pressure	
Thermocouples	Plenum and Nozzle Temperatures	
Optrand Transducers	Nozzle Pressures	Embedded in nozzle and distributed along length, measured steady-state and transient pressure rise
Shadowgraph	Mach Angle	532-nm CW laser used with PSI fast camera to track shock angle
Direct Spark Velocimetry	Air Speed (with and without e-beam)	Q-switched YAG laser introduces spark in airflow; downstream motion followed with PSI camera
Shadow/Spark Velocimetry	Air Speed and Sound Speed (without e-beam)	YAG laser introduces spark into airflow; shadow of downstream motion followed with PSI camera
Rayleigh Scattering	Air Density	Multi-pulse Q-switched YAG laser used with PSI camera to image air near nozzle exit
Nozzle Return Current	Current through Nozzle to Ground	Nozzle floated by 5.5Ω resistor; virtually all beam current exiting HAWK found to return to ground through the nozzle
Accelerator Exit Return Current	Current Returning to HAWK Exit	Floating (10 Ω) copper disk used at HAWK exit; virtually no return current detected
X-Ray Luminosity	X-Rays from Beam / Air Interaction	Blackened photomultiplier - used to confirm that current fluctuations were caused by beam instabilites
NO Spectroscopy	UV Absorption at 226 nm caused by NO Formation	Xenon lamp used with a UV spectrometer for line-of-sight NO absorption

3.4.3.2.4 Experimental Results Summary

At high e-beam powers (> 450 kW), large fluctuations in the nozzle current generally began about 1 to 1.5 ms into the injection and varied greatly from shot to shot. An example of this behavior is shown Fig. 36. The measured current from two high-power (> 450 kW) and two moderate-power (~380 kW) shots are shown. The behavior of the measured current during the first 2 ms of e-beam injection is clearly improved in the moderate-power shots. As an additional complication, shadowgraph data showed that the nozzle exit flow became subsonic at power levels above approximately 450 kW.

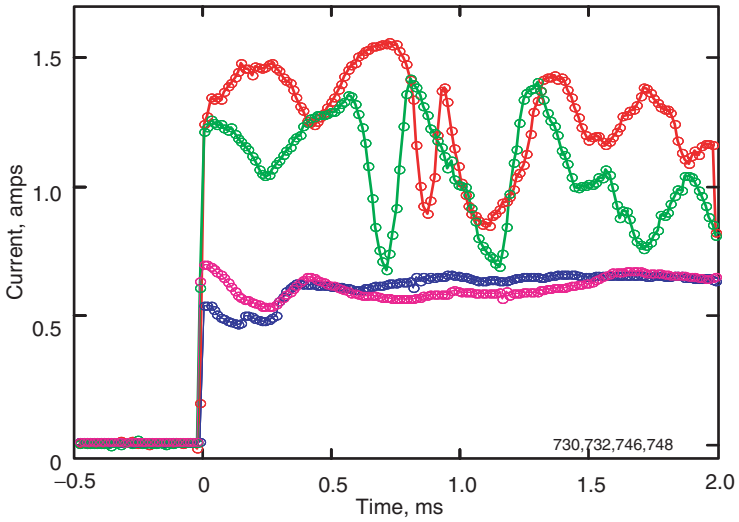

Figure 36. Illustration of HAWK Current Fluctuations at Two High-Power (> 450 kW) and Two Moderate-Power (~380 kW) Shots

Because the flow was observed to become subsonic when the higher powers were added, these data would be of limited use for the supersonic code validations. Thus, a "standardized moderate-power" (SMP) shot with set flow and e-beam parameters and delivering 300 to 400 kW to the flow was chosen that would be used for the majority of data acquisition. Although of lower power than the desired 1 MW, this standard shot would facilitate more useful analysis than a high-power shot that was driven subsonic. One consequence of reducing the power was that penetration of the e-beam into the nozzle would probably be reduced because of lowered voltage.

Nominal plenum pressure and temperature for the SMP shots was set at 14.8 ± 0.2 MPa (2150 ± 25 psi) and 605 ± 3 K (629 ± 5°F), respectively. This operating pressure was chosen by trial and error in the laboratory to allow for reasonably deep penetration of the moderate-power e-beam into the nozzle.

Example shadowgraph measurements for one of the SMP shots are shown in Figs. 37 and 38, below. A scribe was placed in the flow and acted as a sting that generated a shock wave that

traversed the heated region. The shadowgraph in Fig. 37 was taken during an SMP blowdown just before e-beam power addition. A clear and stable shock wave is seen emanating from the sting in the 1-Mhz frame rate video. The Mach number calculated from the measured shock angle for this flow was 3.20 ± 0.12. The error was estimated from the uncertainty in the measurement of the angle.

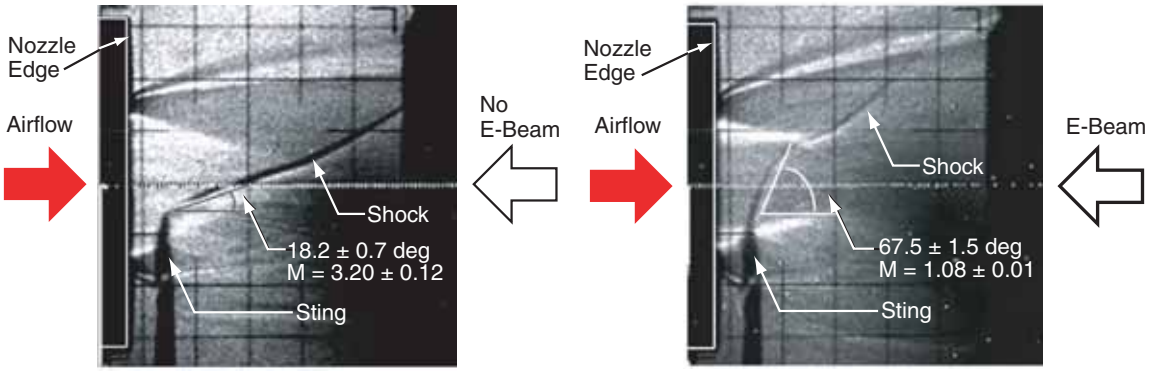

Figure 37. Shadowgraph of Shock in Unheated, Moderate-Power Shot

Figure 38. Shadowgraph of Shock in Heated, Moderate-Power Shot

Figure 38 is a shadowgraph taken during the same blowdown experiment as that of Fig. 37 but well after the establishment of steady airflow during e-beam injection. A clear and stable shock is still seen in the high-speed video, indicating that the flow remains supersonic. The calculated Mach number for this flow was 1.08 ± 0.01.

When the injected power was raised well above the 300- to 400-kW level employed for these SMP shots, the shock angle was observed to approach 90 deg, and the associated shadow was seen to disappear, as would be expected when the flow was driven subsonic.

The predicted Mach number for the unheated flow using the inviscid code was 3.21, compared to the measured value of 3.20 ± 0.12 (Fig. 37). The predicted value during heating for this shot was 1.43, compared to the measured steady-state Mach number value of 1.08 ± 0.01 (Fig 38). This represents a 29-percent difference between prediction and experiment. Hence, it appears that more heating was taking place in these SMP shots than was predicted by the code.

3.4.3.2.5 Data Analysis and Comparisons to Calculations

Examples of modeling of SMP conditions and comparisons to data are presented below.

Figure 39 shows measured and predicted steady-state nozzle pressures with and without e-beam heating. The data are plotted as a function of position along the nozzle axis as measured from the throat. The injected e-beam power for this case was 383 kW. The steady-state values for the heated cases were generated by averaging the injected power over the time interval from 1 to 2.5 ms after beam initiation, when the nozzle current was nearly constant. The predictions are shown as solid-colored lines, green for the unheated case and red for the heated case. The measurements are shown as points (representing the high and low values of the data) with the

corresponding color. The uncertainty in the measurements is represented by the vertical extent of the points and is caused mostly by the slow thermal drift experienced by the pressure transducers.

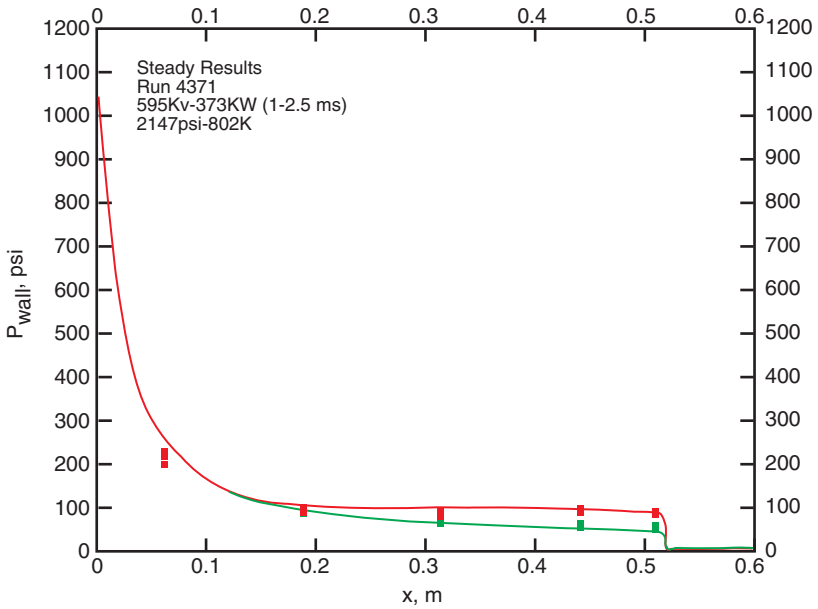

Figure 39. Predicted and Measured Steady-State Wall Pressures (Obtained During an SMP Shot)

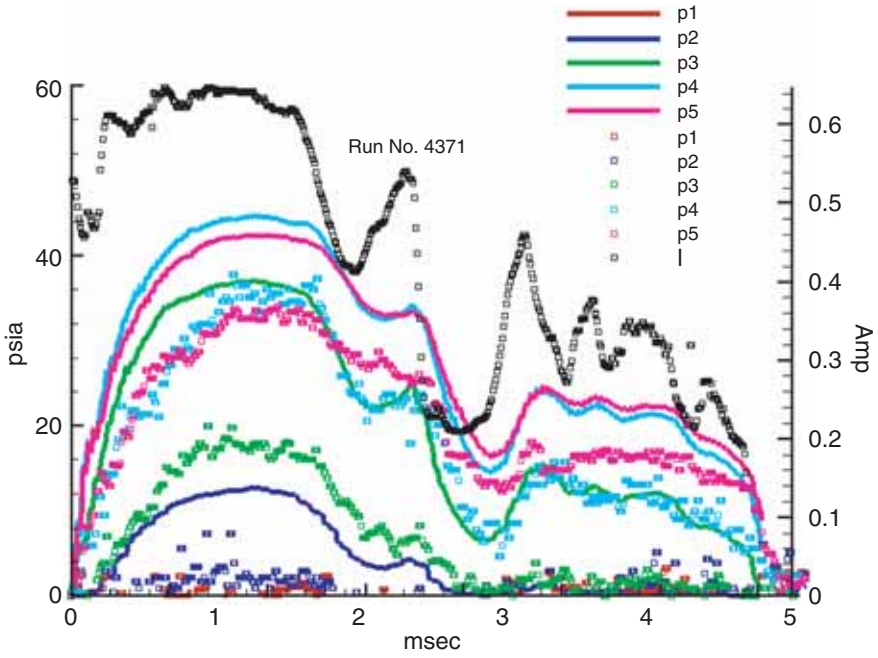

Figure 40. Comparison of Measured and Predicted Changes in Wall Pressure During Energy Addition as a Consequence of the Time-Dependent E-Beam Current for an SMP Shot

Figure 40 shows a comparison of the numerical simulations of wall pressure changes during energy addition to the measured pressure change data from one of the SMP shots. The experimental data are shown channel by channel as colored points, while the corresponding predictions are shown as solid lines of the same color. Also shown in black is the measured nozzle current. Data annotated “p1” are from the transducer nearest the throat; “p5” is the transducer nearest the exit. For this 7-ms shot, the current was approximately constant for the first 2 ms of injection, long enough for steady-state airflow to be established. Although the time-dependent model captures the dynamic features seen in the data, levels are not in agreement. It is interesting to note that the model predicts significantly more penetration of the e-beam towards the throat than was apparent in the data (p1 and p2 data being essentially flat while the prediction for p2 shows a rise in the first three ms).

The high-power shots were more difficult to characterize and more challenging to simulate by CFD. Comparisons of computations to data for one comparatively well-behaved shot are shown in Fig. 41, below. Shown are the measured changes in nozzle pressure resulting from power addition. As in Fig. 40, the experimental data are shown for each transducer as colored points, while the corresponding predictions are shown as solid lines of the same color. Transducer p1 is nearest the nozzle, and transducer p5 is nearest the exit. The measured nozzle current is shown in black. The initial power addition of 700 kW fell to about 480 kW as the current became steadier after the first 2 ms of e-beam injection.

The measured increases in nozzle pressure show some interesting behavior. Initially, the e-beam can be seen to penetrate very deeply into the nozzle because a transient pressure rise is observed on transducer 1 (located 6.3 cm from the nozzle throat). The pressure rise seen in this channel subsides after about 1 ms. It should be noted that the predicted rise in pressure for this channel was zero. Hence it appears that the e-beam penetrates more deeply than predicted, if only temporarily.

It may be noted that, even though the current fluctuations are moderate, there is no time during e-beam injection when the current delivered to the nozzle can be considered constant (as contrasted against the SMP cases discussed above). This particular shot is also interesting because the nozzle pressures measured toward the exit (channels 3, 4, and 5) reach a clear steady state for 2 to 2.5 ms. Because the blowdown airspeed has been measured as about 930 m/s, this 2- to 2.5-ms steady state represents four to five generations of fluid particles passing through the nozzle without the development of a beam-induced instability.

Predictions of the steady-state behavior of the above high-power shot are shown in Fig. 42. Shown are the measured and predicted steady-state nozzle pressures with and without e-beam heating.

Steady-state values for the heated cases were generated by averaging the injected power over the time interval from 2 to 3.5 ms, when the nozzle current was fairly steady (see Fig. 41). Predictions are shown as solid colored lines, green for the unheated case and red for the heated case. The measurements are shown as dual points (high and low values) with the corresponding color. The uncertainty in each measurement is represented by the vertical displacements of the dual data points and is caused mostly by a slow thermal drift in the Optrand pressure transducers.

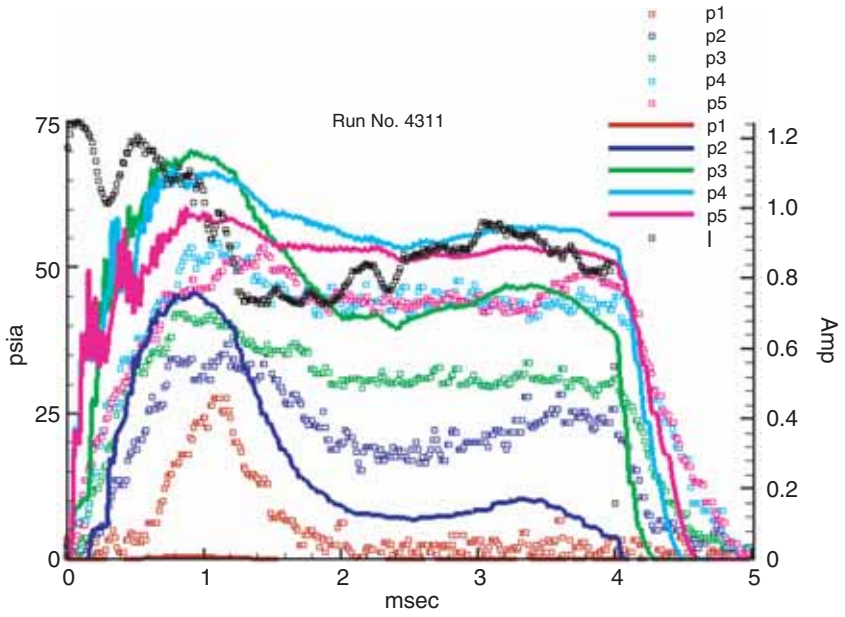

Figure 41. Comparison of Measured and Predicted Changes in Wall Pressure as a Consequence of the Time-Dependent E-Beam Current for a High-Power (~700- to 480-kW) Shot

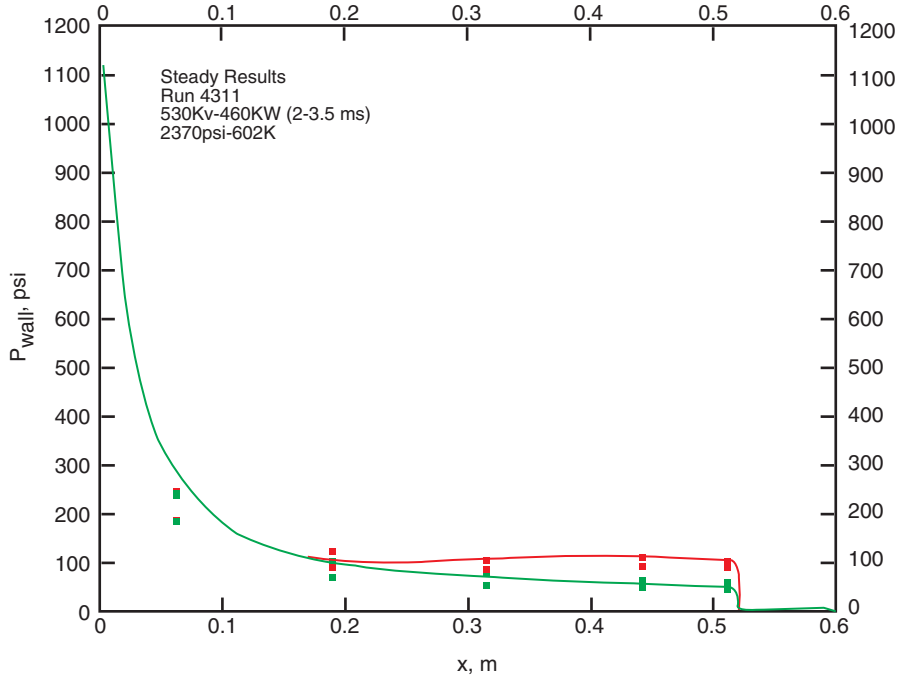

Figure 42. Predicted Steady-State Nozzle Pressures for Shot 699/4311 Compared Against Pressures Measured Using the Optrand Transducers

Tables 8 and 9 show a summary of the comparison of predictions and data. Table 8 is for the unheated case, and Table 9 is for the heated case. Included are the diagnostic measurements used to produce each data point. Note that the exit pressure is shown in Table 8 and the increase in exit pressure is listed in Table 9. Agreement between calculations and data in the unheated case, Table 8, is generally good, with the high exit pressure possibly caused by a thermal effect in the pressure sensor. The agreement in the heated case, Table 9, is not as good, as it shows a significant difference between the measurements and the calculations. The reason for these differences has not been resolved.

Table 8. Comparison of the Predicted and the Measured Airflow Properties of an Unheated SMP Shot

Plenum: P = 2147 psi T = 605 K	**Mach Number**	**Flow Speed, m/s**	**Sound Speed, m/s**	**Pressure @ Exit, psi**	**Density @ 17 mm, kg/m^3**	**Enthalpy, MJ/kg**
Predicted Values	3.21	907	283	45.16	5.44	0.74
Measured Values	[a]3.20±0.12 [b]3.27±0.26	[c]959±63 [b]897±30	[b]274±25	[d]53.5±5.2	[e]5.5 ± 0.8	0.72±0.05

[a]Shadowgraph
[b]Shadowgraph/spark velocimetry
[c]Direct spark velocimetry
[d]Optrand transducer,
[e]Rayleigh scattering

Table 9. Comparison of Predicted and Measured Airflow Properties of an SMP Shot with 380 kW of Heating

Plenum: P = 2147psi T = 605 K	**Mach Number**	**Flow Speed, m/s**	**Sound Speed, m/s**	**∆Pressure @ Exit, psi**	**Density @17 mm, kg/m^3**	**Enthalpy, MJ/kg**
Predicted Values	1.43	907	635	41.24	1.97	1.64
Measured Values	[a]1.08±0.01	[c]926±80	---------	[d]31.5±2.0	[e]2.8±0.5	2.76±0.50

[a]Shadowgraph
[b]Shadowgraph/spark velocimetry
[c]Direct spark velocimetry
[d]Optrand transducer,
[e]Rayleigh scattering

As demonstrated in Figs. 39, 40, 41, and 42, above, as well as in Tables 8 and 9, the results of the inviscid modeling, wall pressure, exit Mach number, exit velocity, and density profile

compared fairly well to the measurements in the unheated cases. On the other hand, for the heated cases, the predicted pressure fluctuations closely followed the measured pressure fluctuations, but with different amplitudes.

3.4.3.2.6 NO Production in High-Power Shots

Triple-pass spectral UV-absorption measurements were used to quantify line-of-sight NO concentrations slightly downstream of the nozzle exit plane. No absorption was observed during the experiments that used SMP shots. This lack of absorption is attributed both to the intrinsically low NO concentrations present in the relatively low-power SMP shots and to problems with the measurement resulting from the shallow penetration depth of the e-beam into the nozzle for these shots. As a result, the NO-UV measurements are not suitable for quantifying NO concentrations at low-to-medium power conditions.

To maximize NO production, a set of operating parameters was chosen that resulted in high-power shots penetrating deep into the nozzle. One shot delivered a relatively stable power addition over the entire 1.2-ms duration of e-beam injection, peaking at about 926 kW and averaging about 813 kW. Examination of the pressure transducer data for this shot leads to the conclusion that the e-beam penetrated the entire length of the nozzle.

NO-UV absorption measurements were made after the e-beam shutoff but during the time e-beam-heated air was still exiting the nozzle. Absorption caused by NO was obvious at 226 nm, as shown in the derived transmittance curve in Fig. 43. The NO-UV transmittances measured during the high-power shots ranged from 0.67 to 0.83.

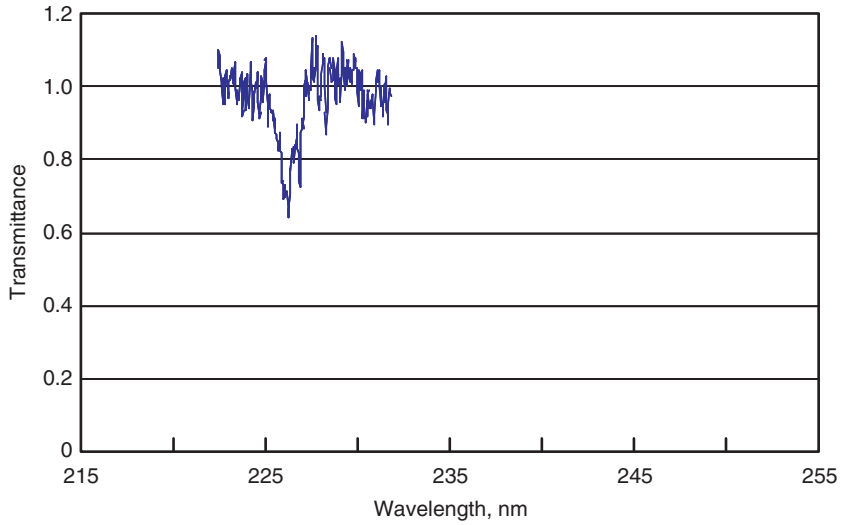

Figure 43. NO Transmittance Measured During High-Power Shot 728/4358 Showing a 30-Percent Absorption

The NO line-by-line radiative transfer modeling code (Ref. 49) employed to deduce NO number density from the NO-UV measurement requires radial and axial static temperature and

static pressure profiles. These were not available from the other diagnostic measurements, and results of the modeling code were used to provide estimates at the nozzle exit ~0.25 ms after e-beam shutdown. These predictions were P_{exit} = 599.8 ± 60 kPa (5.92 ± 0.59 atm) and T_{exit} = 1100 ± 200 K (1520 ± 360°F). Since additional flow calculations predicted essentially uniform properties along the axis within the NO-UV measurement region, the region was treated as a single homogeneous zone of temperature, pressure, and NO number density. The NO number density calculated using these estimated conditions and assuming an absorption path length of 7.62 cm (3 in.) [2.54 cm (1 in.) for each of the 3 passes] was 3.70E+16 (±12%) cm^{-3} for the measured transmittance 0.70 ± 0.03.

The calculated absolute NO density yielded a fractional NO concentration of 0.0010 ± 0.0003 using the estimated 5.92-atm static pressure and 1100 K for the measurement volume. This estimated NO mole fraction of 0.1 percent is in agreement with a-priori chemistry calculations for a 1-MW energy-addition experiment of similar conditions (Ref. 50).

3.4.3.2.7 E-Beam Fluctuations

The nozzle-to-ground current fluctuations present a complication to the understanding of the experiment data, and careful measurements were taken in an attempt to identify their source. A collimated x-ray detector at the end of the differential pumping aperture showed the same temporal fluctuations as the nozzle current fluctuations although there were no significant fluctuations in the cathode current. The energy deposition in the gas was significantly less than the power measured at the cathode. A one-dimensional (1D) analysis of pressure data (Appendix A) suggests that, to be consistent with the measurements, the energy addition must have occurred much nearer the nozzle exit than original code predictions indicated, and at a level significantly below the initial e-beam power. This implies that there were significant losses in the e-beam hardware before the entrance to the nozzle.

Posttest inspection of apertures in the e-beam hardware showed evidence of significant erosion caused by e-beam impact. These observations suggest that the beam was striking the differential pumping apertures and that enough energy was deposited to ablate material from the surface. This high-density cloud of material (gas) would attenuate the beam, leading to a reduction of deposition to the surface and subsequent reduction of ablation products. Once the ablation products were cleared, the deposition would increase and the cycle would begin again.

While some of the beam electrons will be lost in this process (leading to the reduced current transport efficiency), a large fraction will be transported through the system, but with reduced energy and increased transverse velocity because of the scattering off of the ablated atoms and molecules. These electrons will exhibit a decreased range in the nozzle because of their increased transverse energy and resultant helical orbits. Calculations of energy deposition profiles with the beam injected at various angles showed that as the injection angle is increased from 0 to 45 deg, the deposition profile changes from a peak at the throat of the nozzle (0 deg) to a peak at the exit of the nozzle (45 deg). While the experimental beam will have a distribution of entrance angles,

the potential effect of beam scattering is clearly evident. The energy deposition profile resulting from these considerations is generally consistent with the observations of beam penetration and the pressure profiles.

A more complete description of these analyses is given in Refs. 16, 25, and 48 and in Appendix A.

3.4.3.2.8 1-MW Experiment Summary

Included here is a brief summary of the progress towards the objectives accomplished during the 1-MW, short-duration experiments:

1) Addition of 1 MW of power to the flow using a 1-Mev beam and 1-A current.

   Power addition of approximately 900 kW was attained using beam energies of approximately 600 keV and currents of approximately 1.5 A.

2) Tailoring of the continuous magnetic field over various accelerator structures to minimize growth of beam oscillations coupled with an annular cathode to establish a quasi-"top hat" beam profile (uniform in radial extent) in the energy addition region. Included is immersion of the cathode in the magnetic field to reduce the transport and reflection losses observed in previous experiments.

   The magnetic fields and annular cathode concept was successfully demonstrated for the production of a quasi-"top-hat" energy deposition profile. The cathode was immersed in the magnetic field, and reflections were not observed.

3) Bending of the beam through a 45-deg angle into the nozzle.

   Bending of the e-beam by an angle of approximately 45 deg was demonstrated.

4) Development of a plasma-aerodynamic window that eliminates the beryllium foil at the vacuum/air interface and allows long-duration, high-power beams.

   The plasma porthole technology proved unsuccessful, and an alternative approach was developed using a ruptured diaphragm, a fast-acting valve, and differential pumping. This proved successful with a 4-mm window.

5) Addition of energy to the flow that is about twice the plenum energy so that an exit enthalpy ratio (ratio of exit enthalpy to plenum enthalpy) of near 3, comparable to the ratio envisioned for a missile scale hypersonic wind tunnel (2.79), is achieved (Ref. 45).

   At the high-power conditions (approximately 900 kW), the mass averaged enthalpy ratio, $H_{of}/H_{oi,}$ was 3.0, which exceeded the requirement for the MSHWT (2.79). No indications of flow instability were detected in the wall pressure measurements.

6) Validation of energy deposition and e-beam steering models. In the unheated case, measurements of nozzle wall pressure, exit Mach number, velocity, and density profile (Rayleigh scattering) were in close agreement with predictions.

   For both the medium-power shot (~350 kW) and the high-power shot (601 kW), which were modeled in detail, the beam current was fluctuating in time. The measured nozzle wall pressure fluctuations at all five measured stations lagged slightly and smoothed these current fluctuations. The pressure fluctuations predicted on the basis of the measured current also closely follow the measured pressure fluctuations, but with an amplitude at each station along the nozzle that is different in detail from the measured amplitude. The reason for this difference could not be ascertained because no measurements were made of the beam current density profile in situ. A difference in beam penetration was also observed; however, the significance of this difference is not certain, and its cause could not be determined. The predictions were based on an assumption of the same boundary-layer displacement thickness in both the heated and the unheated cases. An additional viscous calculation produced some improvement in the agreement between prediction and experiment for the steady, heated case. Further experiments are now needed with a steady beam current of known profile before the models can be more adequately validated. The current fluctuations were shown to have risen from beam clipping at apertures within the Hawk accelerator and not from interaction with the airflow.

7) Establishing the effect of the e-beam on the chemistry of the heated air.

   Absorption measurements were below measurement threshold at the medium-power (350-kW) shots. While analysis was difficult because of the current fluctuations, an NO mole fraction of 0.1 percent was determined in the high-power (~900 kW) shots, consistent with earlier predictions (Ref. 50).

8) Gaining an understanding of the e-beam current return path.

   Efforts to find any current path from the beam to ground other than through the nozzle wall were unsuccessful. It was also found for the medium-power (350-kW) shots that the product of current to ground and accelerator voltage was close to the measured energy flux in the flow.

9) Determining whether arc discharges occur in the nozzle.

   No spikes in the current to ground from the nozzle were found, and the nozzle remained pristine and undamaged after more than 80 runs with the e-beam. Thus, no discharge arc was found.

3.4.3.3 Accelerator Development

The MSHWT is expected to require an e-beam source capable of 2 to 3 MeV at a total average beam power of approximately 200 MW for several seconds. Although a 200-MW module is a two-order-of-magnitude extrapolation from demonstrated average power levels, the scaling of accelerator components continues to appear feasible. Insofar as possible, design of the experiments will use the technologies that are anticipated to be appropriate in the final MSHWT design.

The e-beam accelerator will be comprised of four subsystems:

1) electron injector and accelerating column

2) beam transport and confinement system

3) beam exit window

4) high-voltage d-c power supply

3.4.3.3.1 E-Beam Accelerator

Following a review of existing accelerator technologies, it was decided to pursue d-c accelerator technology using thermionic cathodes. Thermionic cathodes can support the injector current density requirements of a 50- to 200-MW single accelerator module with several thousand-hour lifetimes. A d-c accelerator concept is simple, scalable, and can be extremely efficient (near 100 percent with a high-precision magnetic field). Additionally, d-c accelerators require only a simple rectifying transformer as a power supply and a linearly graded vacuum stack that is readily available from industry. Space charge limitations in a d-c accelerator with a 50-keV injector were reviewed, and results indicate that this concept remains viable into the few hundreds megawatt range at reasonable beam diameters.

A 2.5-MeV, 200-MW accelerator module will require approximately 80 A of beam current. At an accelerating potential of 50 keV, this injector will generate a 4-MW beam. Because of space charge limitations, a conventional Pierce-type injector cannot deliver this current in a reasonable beam diameter; consequently, a numerically designed high-perveance injector will be required. Preliminary simulations were completed for a 50-A injector, and although this injector will require development, no physical constraints are known that will prevent this objective from being achieved.

Based on the 1-MW experiments accomplished to date, a key challenge of the accelerator column and injector will be to keep any of the beam from impacting apertures. An applied solenoidal magnetic field along the entire length of the accelerator will serve to confine the beam as it leaves the finite divergence injector and accelerates through the column. This will allow the column apertures to be increased in diameter to provide additional clearance around the beam. It is believed that the axial magnetic field is a key requirement to extend the beam current into the tens-of-amperes regime.

Figure 44 shows components of the new accelerator system that will be used during a second series of 1-MW, 5-ms experiments and for a 1-MW, 1-s experiment. The accelerator column, which appears toward the right in Fig. 44, is rated at 3 MeV, which is identical to MSHWT facility requirements.

Figure 44. New 1-MeV Accelerator System for 5-ms, l-s Blowdown Experiments at 1 MW, Shown Opened for Maintenance

3.4.3.3.2 Beam Transportation and Confinement System

The e-beam will be guided from the accelerator's cathode to the expansion nozzle through a series of solenoidal magnets, as shown schematically in Fig. 45. Since high-energy electrons cannot be allowed to impact the wall of the nozzle, the beam scattered by the high-pressure nozzle flow must be compressed radially as it enters the nozzle. This will be accomplished using a series of multi-tesla (T) solenoidal magnets.

To overcome reflection of the electrons in the high B-field in the nozzle requires that the electrons be immersed in a continuous solenoidal B-field back to the cathode electron source. The collisional effects in the high-pressure nozzle were modeled using CYLTRAN. [CYLTRAN is the cylindrical version of the Integrated Tiger Series code (Ref. 51), which determines the bulk energy transfer to the gas from the electron beam along a density profile without regard to the detailed product species.] Results of the calculations are used to establish the magnitude of the solenoidal B-field in the energy injection region from which the B-field profile back to the cathode is designed.

This design and optimization of the axial magnetic field back to the cathode requires numerical modeling techniques. The high perveance injector configuration and imperfect electric fields through the accelerator column are expected to produce a beam with tens of milliradians' (mrad) divergence at the exit of the accelerator column. If one assumes 40-mrad divergence and Bmax = 20 T at the energy injection region, then the B-field at the cathode will need to be on the

order of 0.03 T and must increase to 20 T. Minimizing the equivalent divergence in the injector and accelerator column will be important to reducing the cost of the integrated magnet system.

3.4.3.3.3 Beam Exit Window

As has been shown in previous experiments, the e-beam is far too intense to use a conventional foil window between the vacuum of the accelerator high-pressure path and the energy addition region. A vacuum window for this application has been designed and tested. Differential pumping techniques will be used to pass the beam from the 10^{-8} Torr environment in the accelerator into the approximately 0.17 MPa (1 atm) environment as it enters an aerodynamic opening in the side of the expansion nozzle. The vacuum window with its differential pumping stages is shown in Fig. 46. This system has demonstrated essentially steady-state operation with a beam aperture of 1.2 cm (0.47 in.).

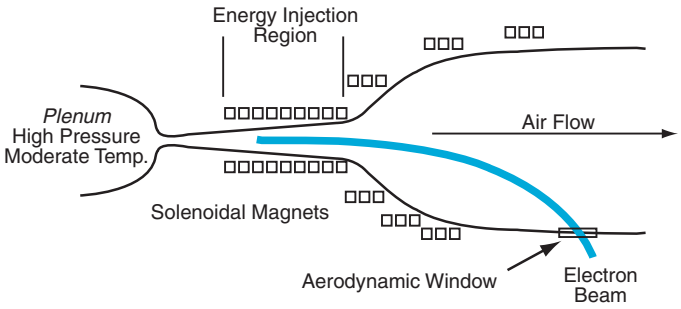

a. Cross Section of Expansion Nozzle and Energy Injection Region

b. Beam Bending Demonstrated During Blowdown Experiments

Figure 45. Beam Transportation and Confinement System

Figure 46. Differential Pumping Section that Forms the Vacuum Beam Window for Upcoming 1-MW, 1-s Blowdown Experiments

3.4.3.3.4 D-C High-Voltage Power Supply

Several d-c accelerator power supply concepts were studied under an SNL contract by the Delta Division of the Efremov Institute in St. Petersburg, Russia. The Delta group was selected because of their industrial experience with inductively coupled transformer accelerator systems. Figure 47 shows a three-phase, iron-core rectifying transformer concept for a 2-MV, 100-MW power supply. A 2-MeV accelerator column and differential pumping system for a foil-less window are shown to the left of the high-voltage power supply. Although the high-voltage output must be insulated from the grounded core in this design concept, the coupling of flux from the primary windings around each vertical core to the high-voltage secondary is very high. Closed-core concepts can have electrical efficiencies greater than 95 percent. The power supply and accelerator are insulated with SF6 and would use commercially available 25-kV diodes in the rectifier assembly. A similar transformer concept will be tested during the 1-MW, 1-s blowdown experiments.

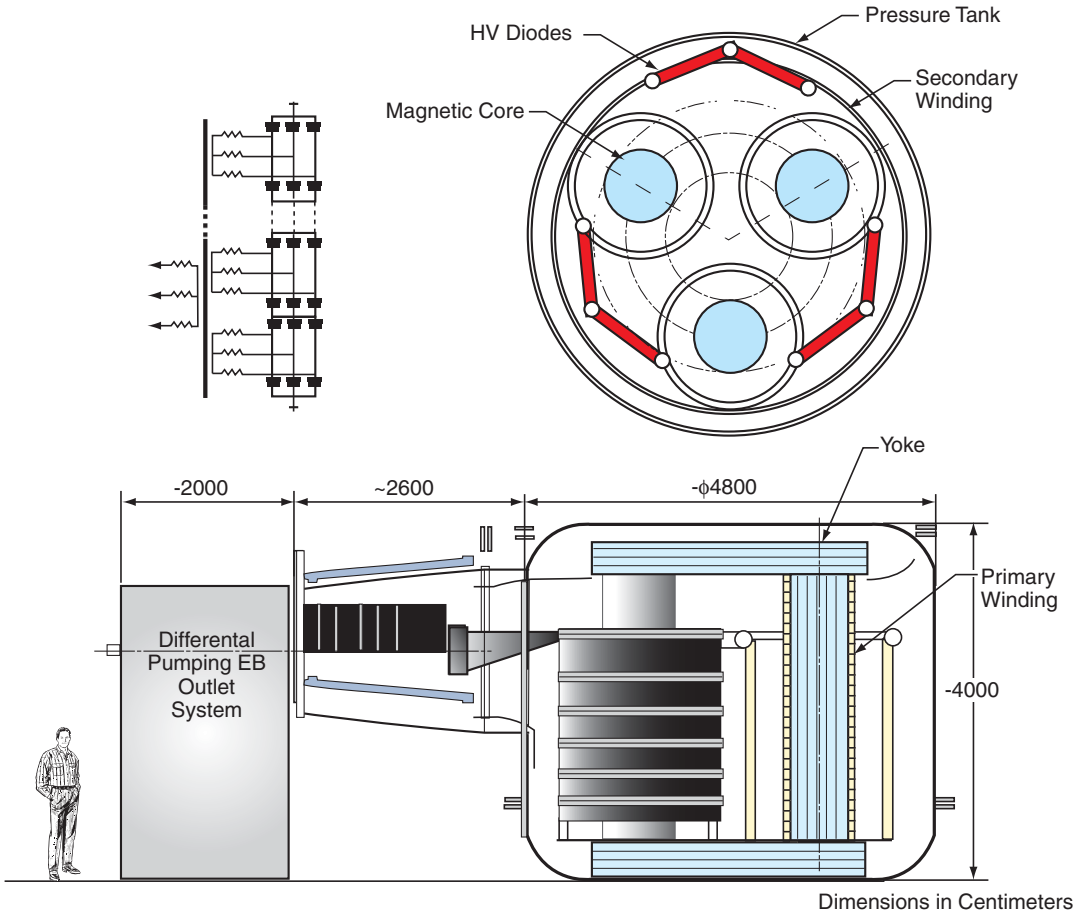

Figure 47. 2-MeV, 100-MW D-C Rectifying Transformer Power Supply Concept

3.4.4 Future Research

The major effort in energy addition has been directed towards the demonstration experiments in incrementally increasing powers. Next in the sequence will be the short- and long-duration 1-MW experiments. The accelerator being constructed for these experiments will also serve as a pathfinder for the higher power accelerators (same voltage) that will be required for the MSHWT. Successful completion of the short- and long (1-s)-duration 1-MW experiments will serve to provide code validation data and establish the long-term stability of the energy addition. Concomitant with the 1-MW experiments is the demonstration of the differential pumping system that will allow the e-beam to exit the accelerator into the atmosphere and, with subsequent magnetic guidance, into the airflow.

Following the successful conclusion of the 1-MW experiments, demonstration of energy addition into a high-pressure environment such as will be provided by the 20- to 30-MW ITS system demonstrator is necessary. This demonstration will validate the approach to create the UHP environment, the nozzle flow, the electron beam, an aerodynamic window for insertion of the e-beam into the nozzle flow, and beam-steering magnets, all within the same experiment. Additionally, this experiment will increase the energy addition roughly another order of magnitude and will provide the next increment of validation of power addition. The system demonstrator will also represent the first energy addition at the ultra-high pressures representative of the MSHWT and thus will be the first demonstration of the flow chemistry that can be expected from the energy-addition region in a completed facility.

One of the figures of merit for successful experiments is that the test medium air contains insignificant amounts of contaminant species. Since the primary energy addition mechanism is the collision of an energetic electron beam with air molecules, ionized, electronically excited and dissociated species are common in the energy-addition region. Thermalization of the energy into the flow properties occurs with the subsequent recombination of species and other chemical processes. The demonstration experiments before the ITS are all necessarily at lower stagnation pressures than envisioned for the MSHWT. The chemistry of the energy addition and the subsequent thermalization of these demonstration experiments are consequently at lower densities than will be present in the MSHWT, and the current state of the art in chemical kinetics modeling should be adequate.

The addition of significant e-beam energy at the ultra-high pressures envisioned for the MSHWT facility presents some issues that may have significant effect on the air chemical composition in the test section of a facility. Briefly, as shown earlier, the generation of a true-temperature test condition above Mach 10 will require plenum pressures on the order of 2000 MPa (300,000 psi). With energy addition at Mach 1.5 to 2, this means that the static pressure at the entrance to the energy addition region will be about 200 MPa (30,000 psi), with a corresponding density of about 0.6 g/cm^3 and a temperature of about 400K (260°F). The compressibility at this pressure and temperature is $Z \sim 2.5$.

At this density, there are about 1.25×10^{22} molecules/cm^3 (molecular weight of 29, 6.02×10^{23} molecules/mole) or a volume of about 8×10^{-23} cm^3/molecule. Considering this volume to be spherical, one knows that it has a radius of about 2.5×10^{-8} cm, giving an intermolecular spacing of 5×10^{-8} cm. This is compared to a molecular radius of $1.8 – 2 \times 10^{-8}$ cm derived from thermodynamic data. As the flow traverses the energy-addition region, temperature increases, pressure decreases, density decreases, and the nozzle expansion is adjusted to increase axial velocity to keep the Mach number in the 1 to 2 range. By some calculations, the density will have decreased by a factor of 50 (~0.012 g/cm^3) at the exit of the energy addition region, giving a number density of about 2.5×10^{20} molecules/cm^3, a molecular volume of 4×10^{-21}cm^3/ molecule, or an intermolecular distance of 2×10^{-7} cm (four times greater than the entrance to the heating region). Compressibility has decreased to ~1. The length of the heating region is generally taken to be about 50 cm.

The significance of this is that the molecular spacing through a significant portion of the energy-addition region is so small that the molecular potentials will be affected. This is especially illustrated by the compressibility factor of 2.5 at the entrance to the energy-addition region. Density is so high that the molecular shapes are being deformed and the molecular interactions are no longer isolated, and as if the molecules were in their undisturbed configuration. This means that the energy transfer and chemistry properties that are derived from lower pressure considerations may be suspect. This includes the products of the interaction of the high-energy electron beam with the air and the Arrhenius rate coefficients used for calculation of the subsequent air chemistry. This should be especially true for the electronically excited species, the most important ones in air chemistry. Multibody reaction rate constants that are so insignificant as to be unexplored at low pressures may be important at the higher pressures.

Another issue of concern is the effect, if any, of the magnetic field on the molecular orientation and the resultant reaction rates. Although the ground state of N_2 has no magnetic moment, excited electronic states and the ion states do have magnetic moments. Ground and excited-state oxygen also have magnetic moments. Consequently, those species important to chemistry may be influenced by the magnetic field. In the simplest model, the period of oscillation of a bar magnet in a magnetic field is:

$$T = 2\pi\sqrt{\frac{I}{B\mu}}$$

where I is the moment of inertia (kg m^2), B is the magnetic field strength [1 Tesla = 1 Weber/m^2 = 1 Newton/(amp m^2) = 10^4 Gauss], and μ is the magnetic moment of the molecule (amp m^2). The moment of inertia can be found from the rotational constant,

$$B_{mol} = \frac{h}{8\pi^2 cI}$$

which for N_2 and O_2 ranges from around 1.5 to 2 cm^{-1}. The magnetic moment of a molecule is related to the Bohr Magneton, μ_0

$$\mu_0 = \frac{\bar{h}}{2m_e}$$

or 9.27×10^{-24} amp m^2. Using these values and assuming a 1-Tesla field, an oscillation period of about 2.5×10^{-12} s is found. Although the analysis and assumptions used here are extremely crude and refinement in analysis will yield more defensible numbers, there will not be orders-of-magnitude change in the result. Furthermore, most of the assumptions have been such that the actual period will be shorter. Thus, the response of the molecules in the flow to the magnetic field will be practically instantaneous with respect to flow times. (Flow time scales are six to nine orders of magnitude larger). In addition, the classical collision frequency at the high-density condition mentioned above is around 10^{-12} s/collision and at the low density condition is around 10^{-10} s/collision. The molecules are therefore subjected to very few (i.e., from less than one to a maximum of 10) collisions during one period of motion in the magnetic field. Thus, there will be a bias in the orientation of the molecules in the flow. This means that orientation during chemistry producing collisions is no longer random, and molecular collisions will no longer uniformly distribute over all collision angles. This bias in the collision orientation may influence effective chemical reaction cross sections and rates in an unknown way.

Finally, the magnetic fields are strong enough to influence the coupling of the sundry energy states in the molecular structure (e.g., Zeeman Effect), and the influence of this influence on resultant chemistry is unknown.

These phenomena need to be examined theoretically to ensure that the assumption that the chemical reactions involving charged species will be very rapid with respect to flow times and that thermal chemistry at lower densities downstream of the energy addition region will still prevail. Under these assumptions, maintaining the static temperature below about 2500K will ensure that the production of NO will not be significant. Theoretical cross-section calculations with the intermolecular potential functions derived from the high-pressure equation of state would be a possibility and a starting place.

3.5 MHD ACCELERATOR ENERGY ADDITION

The purpose of the MHD energy addition is to augment the test Mach number capability of the airstream above that which can be provided by the supersonic thermal-energy-addition technique by using electromotive body forces (J × B). For the MSHWT, the ultimate goal is to achieve an equivalent flight Mach number of 15 and a dynamic pressure of 2000 psf (96 kPA) in the flow behind the bow shock wave to create the equivalent of a 5-deg inlet wedge. This concept represents a new application regime for MHD, and analytical performance tools need to be developed and validated.

3.5.1 Background and Summary

As noted earlier, the thermal-energy-addition concept appears to be limited to about Mach 12 for an RDHWT-type facility because of the pressure limitations. Preliminary analyses have indicated that the addition of an MHD accelerator system has the potential to extend facility performance to about Mach 15. Early in the program (Ref. 52) the suggestion was made to use electron beams as a means to create the necessary conductivity for MHD velocity augmentation in the relatively low-pressure, low-temperature environment of the expanded flow downstream of the e-beam energy addition region. Work proceeded on the concept (e.g., see Ref. 53) and developed far enough to plan experimental verification (Ref. 54). A segmented e-beam conductivity enhancement system (concept shown in Fig. 48) was developed for the present program, but electrode failures in the e-beams have precluded its use on this program to date.

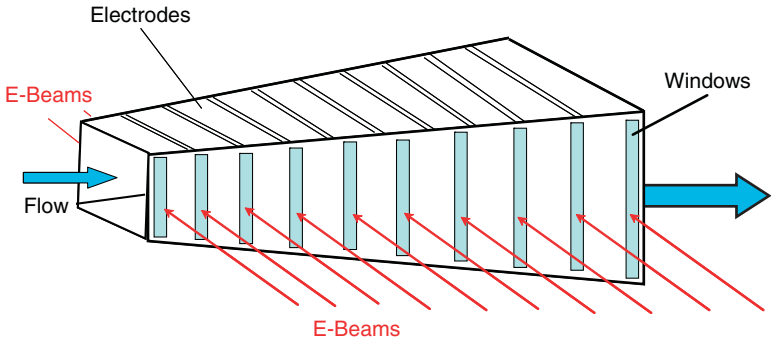

Figure 48. MHD Channel with Segmented E-Beam Conductivity Enhancement Concept

During this reporting period, work continued on this effort (e.g., Refs. 24 and 55); however, progress was slowed because a higher priority was established for other aspects of the work, especially the UHP and e-beam energy addition experiments. The MARIAH II program has benefited from other agencies' funding of research into application of MHD to flow control and other aerospace sciences applications.

3.5.2 Critical Technical Issues

Identified critical issues include:

1) **Operating regime of MHD accelerators**. MHD accelerators have been operated successfully at static pressures from 101 to 404 kPa (1 to 4 atm) and at static temperatures above 2500 K (4000°F) that produced an equilibrium electrical conductivity in seeded flow. However, the exit entropy levels were much too high (i.e., high-altitude simulation was too high) to achieve the lower altitude performance goals needed for hypersonic, air-breathing propulsion testing. To overcome this problem, the channel inlet entropy must be much lower, which means that the static pressure must be much higher,

the static temperature must be much lower, and/or some adequate combination of lower temperature and higher pressure must be used.

The constraint on entropy precludes operation at high temperatures and moderate pressures, as has been done in MHD channels with electric arc preheating at stagnation pressures up to approximately 10 MPa (100 atm). Operation of seeded MHD accelerators at very high static pressures and high temperatures has been suggested, but never demonstrated nor believed possible because of materials limitations and chemistry issues. Low-static-temperature (below 500 K), low-static-pressure (below 1 atm) operation of MHD accelerators is an attractive option, provided that nonequilibrium electrical conductivity is sufficient and can be achieved and sustained. But this, also, has not been demonstrated.

Two MHD operating regime options, A and B, are considered.

Option A is for low static pressure and temperature, where it is believed feasible to achieve sufficient conductivity with e-beams injected perpendicular to the flow. To achieve the low static temperature and pressure, a rather high channel-inlet supersonic Mach number is expected.

Option B is for a higher inlet static pressure and temperature. For Option B, means other than e-beams, such as diffused arcs, probably will be required to establish flow conductivity. Option B has the potential of being more thermodynamically efficient and also offers a potentially lower channel-inlet Mach number, but there is some risk of creating unwanted species such as NO, depending upon the ionization method used, as well as increased channel wall heating.

2) **Electrical conductivity issues.** Electrical conductivity must be sustained in the gas flow through the accelerator at a level sufficient to ensure electromotive force acceleration. External means of establishing and maintaining conductivity (i.e., to achieve values of conductivity of 0.1 mhos/m) are expected to be required. Reference 15 presents more detail on the electrical conductivity work.

3) **Channel boundary-layer issues.** Overheating of the channel walls may be a major issue. However, the flow entering the channel will have a heated, high-velocity core surrounded by an unheated, low-velocity flow between the heated core and the channel walls. Wall recovery temperature, heat loads, and thermal boundary-layer management must be addressed. The degree to which the boundary layer is an issue depends on channel inlet conditions, the boundary-layer electrical conductivity, and the mode of operation in the MHD accelerator. Both velocity and thermal overshoots in the boundary layer are to be avoided. Thermal overshoots can result in high electrical conductivity near the electrode walls and sidewalls. This may in turn cause inter-electrode shorting axially along the electrode walls, as well as transverse shorting in the sidewall boundary layers. The latter effect (sidewall shorting), if sufficiently pronounced, can produce relatively

high accelerating MHD forces in the boundary layer compared to those in the core flow, clearly an undesirable situation. Tailoring the flow conductivity to prevent overacceleration of the boundary layer on the electrode walls may be required if the cold inlet outer flow does not sufficiently offset the increased conductivity effect in the boundary layer. A 2D analytical investigation is needed to assess the magnitude of boundary-layer issues.

3.5.3 Progress

A summary of the research appropriate to the MARIAH II program for this reporting period can be found in Ref. 15. Briefly, it has been shown through modeling that levels of conductivity necessary for MHD augmentation could be accomplished with electron beams in the relatively low-pressure, low-temperature environment expected in the MSHWT. Early modeling also has suggested that the necessary e-beam current may be relatively low, thus allowing a simple foil as a window rather than the more complicated plasma porthole, which is problematic in a high magnetic field.

Experimental validation using e-beams was postponed, however, because the fabrication of an e-beam array, being accomplished under other funding, did not proceed according to expectations and was not delivered for implementation (An array is necessary to obtain an adequate volume of conducting flow.)

Meanwhile, a Mach 3 cold air MHD channel (Ref. 55), developed under another program, has provided some insight into the MHD process applicable to the MARIAH concept. Since an electron beam array was not available, an alternate approach to providing “cold” or nonequilibrium ionization, use of a high-voltage pulser, was investigated for laboratory proof-of-principle demonstrations. This work was successful in that a uniform discharge across the flow was produced that sustained the necessary conductivity. Magnetohydrodynamic effects were produced by placing a bias voltage across the channel and observing the current vs. time at several voltages and with the direction of the magnetic field switched to change the sense of the MHD-generated field. In the cases where the MHD-generated field and the bias field opposed each other, the current across the MHD channel was small. In the cases where the bias and MHD voltage were added, significant currents were measured. In these latter cases, the current generated a force opposing the flow. These experiments served to demonstrate that MHD effects were present and could be measured using this approach.

That proof-of-principle work was accomplished with a single continuous electrode, and subsequent modeling of a segmented electrode case, suggests that adaptation to the segmented electrode may not be straightforward. The modeling suggests that the cathode sheath current in the segmented case falls significantly more quickly than it does in the single continuous electrode case, resulting in quicker current cutoff. Electron beams as ionizers are predicted not to show this behavior. Modeling codes have been developed and need to be validated. Experimental work funded by other programs has provided some proof-of-principle demonstrations. An experimental observation of an MHD electric field in an MHD generator with nonequilibrium ionization in

cold supersonic flows was accomplished. Demonstration with an ionization source (electron beams) or a segmented channel has not been accomplished.

3.5.4 Future Work

Although modeling and experimental work accomplished under other funding are promising for application to the RDHWT/MARIAH II program, there has been no validation or experimental demonstration of the principle. This work should be accomplished. Specifically, the establishment and maintenance of a large volume of ionization in the low-density flow should be demonstrated. At present, this appears to require the completion and application of the electron beam array. Although an MHD effect has been demonstrated in low-density flows, this demonstration was the production of voltage caused by MHD effects rather than by acceleration of the flow. The ability to accelerate the flow needs to be demonstrated.

With the demonstration of the maintenance of large-volume ionization and MHD acceleration, the limit of air densities and temperatures allowing the phenomena needs to be explored and established. If MHD acceleration will work at less than Mach 12 test conditions (higher pressures and densities), the UHP environment producing the flow will be less highly stressed. Significant performance enhancements and cost reduction may be achieved if MHD acceleration can be applied at a Mach number lower than the current Mach 12-to-15 goal.

4.0 SYSTEMS DEFINITION AND INTEGRATION

The research effort to this point has involved development and scaling of individual components or subsystems seen as necessary for achieving the final goal, determination of design criteria for an MSHWT. These experiments have been described in previous sections. Although these experiments have been conducted essentially independently, they have proceeded with the knowledge that, at a future date, the individual components would have to be combined into a single, working system. To this end, systems integration studies have accompanied the other work to incorporate the latest findings of the individual investigations into the system definition and to provide feedback to the individual experiments for planning of demonstrations and directions that will be necessary in the future. A good deal of the results of this systems integrations work has already been seen in the earlier discussions. A summary of the results and system definitions as currently understood is included here.

It is recognized that, in addition to the demonstrations of individual components of the technology, a system demonstration would also be necessary. To this end, an ITS is planned as a final demonstration in the energy-addition experiments. The ITS definition is necessarily more fluid than the MSHWT definition since, while the ITS requirements are driven by developing technology, the MSHWT requirements are driven by flight simulation conditions. Both the ITS and the MSHWT systems are described below. Current understanding of the ITS is given in some detail, and the MSHWT is presented in summary form. Details of the MSHWT system definition are included below.

4.1 INTEGRATED TEST SYSTEM

The Integrated Test System (ITS) has three interrelated but distinct objectives. These objectives are not precisely defined, but they include:

- *Demonstrate UHP Air Supply System Technology*. This demonstration includes the UHP facility with both air and nitrogen (if needed) supply and two-flow systems at sufficiently high pressures to inspire confidence in building the MSHWT UHP system.
- *Demonstrate High-Performance E-Beam Aerodynamic Heating*. This includes demonstration of e-beam heating at pressures representative of the MSHWT and with enthalpy addition similarly representative of the MSHWT. This includes production of representative flow chemistry. This can be done in a short-duration experiment with time scales adequate for flow stabilization.
- *Demonstrate System Integration*. This includes demonstrating the systems operating as a single-facility simulation, although not necessarily at the maximum operating conditions of the subsystems, for a time of up to one second.

4.1.1 Approach

With the foregoing three objectives in mind, the approach proposed is to accomplish the system integration demonstration at slightly less stressing requirements than those for MSHWT and then to upgrade the equipment to enable the high-performance UHP and energy-addition demonstrations. Thus the approach is as follows:

1) Provide the UHP air supply required for the system integration demonstration to the maximum pressure level consistent with MSHWT requirements and budget limitations. This operational testing would include the UHP system only with flow exhausting to atmosphere.

2) Upgrade the e-beam and magnet system required for the system integration demonstration to a voltage level and power level consistent with the high-performance operation and within the UHP air supply limits given above. Achieve specific enthalpies approaching MSHWT requirements but at a smaller mass flow. Power levels on the order of 50 MW are expected, but test times would be short (~ 5 ms).

3) With UHP and energy-addition systems operating together, provide a systems integration demonstration by generating flow conditions appropriate for the entrance to a test section of a subscale facility. The test section and associated components are not necessary for the system demonstration, but the system should provide flow conditions appropriate for such a facility. This is currently thought to require the addition of a 20 to 30-MW rectified power supply, operating for one second, with pressure levels consistent with power level and throat size limitations.

4.1.2 Configuration Development

With this approach and the general objectives given, some initial trade studies of possible configurations were conducted. Results for two sample system integration demonstrations are given in Tables 10 and 11, below. In both cases the throat was set at 7 mm, as was necessary to achieve uniform energy-addition profiles and shielding of the e-beam from the channel walls. Stagnation temperature was set at 1000 K (1340°F), and run time was set at 1 s.

Two additional parameters are required to completely specify the flow; in Tables 10 and 11 these are noted as the test section Mach number and the dynamic pressure, q, respectively. In Table 10, the Mach number is at a fixed M = 10, and the dynamic pressure, q, is varied (1000, 1500, and 2000 psf) (48, 72, and 96 kPa). All other parameters result from these choices. Relative costs** shown are for two stagnation heating configurations. The baseline configuration is stagnation heating with ceramic heaters in the pressure intensifiers (Section 3.2.3), and the other is for a storage heater system (Section 3.2.3.4). A Mach 10, q=1500 psf (72 kPa) facility is the baseline facility for cost comparisons.

Table 10. Dynamic Pressure (q) Variation

Test Section q, psf	1000	1500	2000
Mach	10.00	10.00	10.00
d Test Core, mm	467.1	400.4	359.9
Time Run, s	1	1	1
Air Supply			
Press, MPa	604	685	751
Temp, K	1000	1000	1000
mdot, kg/sec	21.4	23.9	25.9
d* Total, mm	7.0	7.0	7.0
UHP Base System			
Preheat, K	550	550	550
Time Overhead, s	0.5	0.5	0.5
UHP Vol, liters	102	104	105
Charge Press, MPa	44	49	54
UHP	1.0	1.0	1.0
UHP Storage Heater System			
UHP Vol, liters	37	41	45
Stor Heat Vol, liters	23	27	30
E-Beam			
Power, MW	18.0	19.0	19.9
Voltage, MW	1.37	1.42	1.50
Cost Factor - System Integration			
Base	0.95	1.0	1.05
Storage Heater	0.69	0.74	0.80

** Unpublished cost estimates of the basic MSHWT were made by ASE, St. Paul, Minnesota. Scaling algorithms were developed by Ring Technical Services to calculate the cost factors shown.

It is seen, that contrary to intuition, the power levels and relative costs increase only slightly with increasing q. On closer examination, it is seen that this is the result of a complex interaction of real-gas thermodynamics (air becoming incompressible) and changing temperature in the atmosphere (significantly higher enthalpies at the lower q's). However, the conclusion is that the value of q can be selected over a wide range for the design of the ITS. This conclusion also means that the facility can be operated over a range of q values. Note that there is a significant reduction in cost when a storage heater system is used.

Table 11 shows the same results for a fixed q = 1500 psf (72 kPa) and Mach numbers varied (M = 9, 10, 11, and 12).

Table 11. Mach Number Variation

Test Section Mach No.	**9.00**	**10.00**	**11.00**	**12.00**
q, psf	1500	1500	1500	1500
d Test Core, mm	296.4	400.4	511.3	620
Time Run, s	1	1	1	1
Air Supply				
Press, MPa	375	685	1113	1714
Temp, K	1000	1000	1000	1000
mdot, kg/s	14.6	23.9	35.3	47.3
d* Total, mm	7.0	7.0	7.0	7.0
UHP Base System				
Preheat, K	550	550	550	550
Time Overhead, s	0.5	0.5	0.5	0.5
UHP Vol, liters	101	104	111	116
Charge Press, MPa	27	49	80	124
UHP Storage Heater System				
UHP Vol, liters	24	41	63	86
Stor Heat Vol, liters	14	27	46	71
E-Beam				
Power, MW	9.3	19.0	33.8	53.4
Voltage, MW	1.11	1.42	1.72	1.97
Cost Factor - System Integration				
Base	0.66	1.0	1.51	2.0
Storage Heater	0.41	0.74	1.25	2.15

Here it is seen that the power levels and costs increase rapidly with increasing Mach number. Thus, for a constrained power level and/or cost level, there is little latitude in the choice of Mach number. Again, note the significant reduction in cost when a storage heater system is used, except for the Mach 11 and 12 cases.

Table 12 shows results for upgrade of the system integration UHP to higher pressures for the UHP demonstration. The upgraded UHP levels are set at 1500 and 2046 MPa (217,556 and 296,747 psi). It is assumed that the Base System (M = 10, q = 1500 psf) is used with the volume of the UHP and d* held fixed, and the UHP pressure vessels and the hydraulic system are upgraded to the higher pressure levels. For the Storage Heater System, d* is held fixed at 7.0 mm while the UHP volume and storage heater volume are increased to provide the required flow. Two cost factors are shown: the cost of the upgrade alone, and the resulting total cost of the system integration plus the UHP demonstration. Again, the costs are relative to the base M = 10, q = 1500-psf (72-kPa) system.

Table 12. UHP Upgrade

Test Section			
Mach	10.00	10.00	10.00
q, psf	1500	1500	1500
d Test Core, mm	400.4	400.4	400.4
Time Run, s	1	1	1
Air Supply			
Press, MPa	685	1500	2046
Temp, K	1000		
mdot, kg/s	23.9		
d* Total, mm	7.0	7.0	7.0
UHP Base System			
Preheat, K	550	550	550
Time Overhead, s	0.5	0.5	0.5
UHP Vol, liters	104	104	104
Charge Press, MPa	49	153	381
UHP Storage Heater System			
UHP Vol, liters	41	81	106
Stor Heat Vol, liters	27	64	93
E-Beam			
Power, MW	19.0		
Voltage, MV	1.42		
Cost - System Integration – Base System			
UHP Increment		0.43	0.78
Sys Int + UHP	1.0	1.43	1.78
Cost - System Integration – Storage Heater System			
UHP Increment		0.59	1.18
Sys Int + UHP	0.74	1.33	1.92

Here it is seen that the costs increase rapidly with increasing UHP system pressure levels. A reduced throat size for the UHP demonstration may reduce costs. This has not been considered here but should be considered before a final decision is made on design of the experiment.

The costs of the high-performance e-beam and aerodynamic heating demonstration have not been studied and will need to be included in the considerations. The power level is envisioned at 50 to 60 MW for a 5-ms pulse and is expected to add nearly 10 percent to the cost.

Based on these preliminary trade studies, it is recommended that the ITS configuration be as follows:

- A system integration demonstration (UHP and energy addition) providing M = 10, q = 1500-psf (72-kPa) airflow with a d* = 7-mm (0.28-in.) throat for 1-s flow time.
- A UHP system demonstration centered around UHP pressure of 1500 MPa (217,556 psi) with a d* = 7.0 mm (0.28 in).
- A high-performance e-beam and aerodynamic heating demonstration centered around 5–ms, 50- to 60-MW, capacitor-driven operation, d* = 7.0 mm (0.28 in.), providing near-MSHWT conditions.

Additional calculations and trade studies need to be accomplished to establish the details of performance and operating conditions. Feasibility and impact of using smaller throat sizes need to be assessed. It is thought that the performance should not change greatly from the figures given above.

4.2 MEDIUM-SCALE HYPERSONIC WIND TUNNEL

The Medium-Scale Hypersonic Wind Tunnel (MSHWT) has been chosen as a target facility for which to develop design criteria with the RDHWT/MARIAH II program. To be a useful facility, the MSHWT must provide duplication of flight conditions at hypersonic speeds and run durations beyond those currently available with other facilities. The requirements for the MSHWT have evolved through the course of the research and are currently defined as follows:

- Maximum performance design point of q = 2000 psf (96 kPa) at Mach 12;
- Nominal additional operating points of Mach 8 and Mach 10 at q = 2000 psf (96 kPa);
- Minimum q = 500 psf (24 kPa);
- Capability of full duplication (i.e., altitude-matched temperature);
- Uncontaminated, clean air;
- Insignificant flow nonequilibrium;
- Ability to test aerodynamic and propulsion systems;
- Useful test flow of 1-m (39-in.) diam;
- Useful test time of 10 s; and
- 210-MW, 3-MV, 70-A e-beam heating system.

4.2.1 MSHWT Facility Design Approach

The design approach for the baseline MSHWT is as follows:

- UHP air supply based on single-stroke intensifier system;
- UHP vessel internal ceramic heaters to preheat the air to 550 K (530°F);
- UHP system sized for the Mach 12, q = 2000-psf (96-kPa), 10-s flow-time operating point;
- Throat protection based on using a nitrogen layer around the central air flow in approximately the same radial extent for each (approximately 4:1 area proportions);
- Wall protected from e-beam heating by a cold flow layer where the layer represents approximately 75 percent of mass flow at Mach 12 conditions, as well as 3 mm (0.12 in.) at throat for Mach 10 and Mach 8 conditions; this layer may be the nitrogen layer used for film protection of the nozzle;
- Utility grid-based, rectifier power supply system; and
- Exhaust to atmosphere with a steam ejector-driven exhaust system.

Since the air supply is sized for 10-s operation at Mach 12 and q = 2000 psf (96 kPa), the resulting run times at both the Mach 8 and Mach 10 conditions are slightly under 10 s for q = 2000 psf (96 kPa) but greater than 10 s for q less than 1500 psf (72 kPa).

A more detailed MSHWT description is given in Appendix C.

4.2.1.1 Baseline Air Supply System Alternate Approach

Using an inline storage heater rather than the UHP internal resistance heater also is being considered for the MSHWT. In addition to potentially reducing cost, the flow quality might be improved in terms of temporal uniformity. The storage heater operating concept consists of:

- Heating the storage heater core matrix to the facility operating temperature;
- Charging the UHP vessel plus the storage heater, not to exceed 344.6 MPa (50,000 psi); the air in the UHP vessel would come to room temperature (293 K) (68°F), the UHP vessel temperature;
- Compressing at constant temperature to the operating pressure. The compression would be slow, so that the air would again be cooled to the steel temperature, allowing only a minor rise in the temperature of the steel;
- Heating the air at constant pressure as it passes through the storage heater to the operating temperature; and
- Having the hydraulic system drive out the flow for operation.

The 344.6-MPa (50,000-psi) compression limit corresponds to that of available commercial compressors.

A more detailed description of the storage heater concept is given in Section 3.2.3.4.

4.2.1.2 Nozzle Protection Concept

A two-flow concept is being considered for the MSHWT to provide throat/nozzle heat and oxidation protection, as well as channel protection from e-beam heating. This raises the question of the extent of the shear layer at the nitrogen-air interface. To further sort out the issues from a system point of view, calculations of the shear velocity between the nitrogen and the air layers were made for the MSHWT design case and the A2LM design case. The nitrogen temperatures were taken to give a minimum shear velocity in the total region from the reservoir to a Mach number 2.5 flow. A slightly positive shear was taken at the throat.

The results show that the shear velocity (the difference between the air and nitrogen stream velocities) is less than 2 m/s for the total range of both flows except for the A2LM above Mach 1.5. The shear velocity is less than 0.5 percent of the flow velocity over the total range for both flows, implying that mixing of the air and nitrogen should not be significant and that degradation of the useful test core should be limited.

A more detailed description of this shear-layer mixing is given in Appendix D.

4.2.2 MSHWT Performance

A 1D aerodynamic system simulation model was developed with equilibrium and real-air thermodynamics and includes e-beam heating addition. The model is described in more detail in Appendix B. This model computes:

- Flow from the UHP reservoir;
- Flow through the nozzle throat;
- Expansion to the start of e-beam heating;
- Supersonic e-beam heat addition;
- Expansion to the test section at a matched altitude condition, specified test section pressure level, or specified test section area;
- Pressure recovery through the diffuser; and
- Pressure drop and cooling in the heat exchanger for a specified pressure loss coefficient and heat exchanger temperature, providing the required exhauster pumping requirements.

The system simulation model incorporates a number of features:

- A two-flow model (i.e., an inner core e-beam heated flow with an outer film flow that is unheated). This allows 1D simulation of the 2D case where a cold flow is used to shield the channel walls from the fringe e-beam column heating.
- Calculation of the e-beam heating using the Lipinski-Anderson equation (Ref. 56) to compute the e-beam heating.
- Design calculations for which the thermodynamic path is specified and the resulting e-beam voltage and channel length are determined.

- Off-design performance calculations for which the channel geometry as well as the e-beam voltage and current are specified and the resulting flow is computed. The flow thermodynamic path is computed rather than specified.

The system simulation model can be used to design flow channels with 1) constant Mach number; 2) constant temperature; 3) constant channel expansion angle (a cone); 4) a specified pressure gradient; or 5) any combination of the above with appropriate modifications of the iteration scheme.

An initial examination was made of the influence of channel configuration on the performance of the MSHWT operating at the Mach 12, q = 2000-psf (96-kPa) conditions. Specifically, the investigations were directed towards 1) determining the minimum e-beam voltage that can be used, and 2) determining the effect of deviating from the ideal theoretical nozzle area distribution. The conclusion of this investigation was that a minimum of 2.0 MV is required but that 3.0 MV gives a better, more conservative channel design. It was also found that a nozzle starting with a rapidly expanding area at the entrance followed by a conical flow provides a good overall design.

A more detailed description of the MSHWT nozzle flow is given in Appendix E.

It is highly desirable to minimize nozzle hardware configuration changes for different test conditions. Thus the project team attempted to develop some feel for the practicality of this objective while making performance map calculations. The performance map of the MSHWT was computed with the assumption that the MSHWT facility will be sized and designed for the Mach 12, q = 2000-psf (96-kPa) operating point, with the exception of the exhaust system, which will be designed for 500-psf (24-kPa) dynamic pressure operation and the inclusion of both a Mach 8 and a Mach 10 nozzle. The facility will be operated off-design to provide an operating map. This appears to be a reasonable approach considering both performance and cost. The results of this performance analysis are given in Appendix F. From these calculations one is led to conclude that it seems feasible to consider using conical nozzles with interchangeable nozzle throat inserts to vary Mach number. However, much more study of interaction of the e-beam energy deposition for various densities and a fixed nozzle expansion is needed before reaching a final conclusion.

In Appendix F, the Mach 8 and Mach 10 maximum operating points were taken as greater than 2000 psf (96 kPa) dynamic pressure insofar as the facility has that capability. However, it is not clear that there is a testing need for such flows. An improved operating map can be obtained by limiting the Mach 8 and Mach 10 maximum operating points to q = 2000 psf (96 kPa).

4.2.3 MSHWT Cost Estimate and Trade Model

On the basis of the MSHWT description as given in Appendix C, a cost estimate of the MSHWT facility was developed and will be reported in a separate government document.††

5.0 SUMMARY, REMAINING RESEARCH NEEDS, AND CONCLUDING REMARKS

Principal accomplishments during this reporting period can be listed as follows:

1) Design, construction, checkout, and use of the Ultra-High-Pressure Test Facility (UHPTF).

2) Design, fabrication, checkout, and use of the A-2 Lite pressure intensifier. During static operations (no blowdown), a pressure of 1200 MPa (174,000 psi) was achieved, which is the highest pressure ever reported for the volume (~ 1 l). Blowdown experiments for nozzle survivability were begun, but pressure conditions had not reached failure limits for the materials by the close of the period.

3) A design concept for a hypersonic test facility structure was developed, using the forces of the pressure intensifier to provide sealing forces at the intersection of high-pressure containment pieces. Design calculations showed that estimated stresses were within material property limits.

4) A design concept for accomplishing film cooling of the throat and nozzle was developed. This will use nitrogen as an inert gas around the air core to reduce the recovery temperature, suppress ignition events between core flow air oxygen, and act as an additional flow to absorb residual e-beam energy. A new iridium material developed under a separate program shows promise in accepting a higher recovery temperature and, if tests confirm predictions, will obviate the need for film cooling. Fabrication and testing of such a nozzle have not been accomplished.

5) An approach to extract the e-beam from the vacuum of the accelerator to the atmosphere was developed. This approach, using differential pumping, was developed following failure of the originally planned plasma porthole.

6) Energy addition to a supersonic flow at power levels near 1 MW was accomplished. The experiments were of short duration and did not have a stable e-beam at the high powers. The e-beam instability was thought to be caused by interactions of the e-beam and the hastily crafted aperture following the plasma porthole failure. Relatively stable e-beam operation was accomplished at lower powers (approximately 400 kW), and useful data

†† Laster, M. L. “Acquisition Alternatives for Mach 6-12 R&D and T&E Hypersonic Wind Tunnel Capabilities Using the RDHWT Approach.” AEDC-TMR, Arnold Engineering Development Center, Arnold Air Force Base, TN. To be published.

were obtained. The power addition and nozzle flow were stable at the reduced power over the length of the e-beam pulse (~5 ms), which was long enough for the heated flow to fully fill the nozzle. Stable operation at approximately 800kW was also inferred, but the energy addition at this level was accomplished over a shorter time period.

7) Using the lessons learned from the short duration experiments, equipment upgrades to accomplish long-duration (1-s) energy addition at 1 MW was begun.

8) Preliminary requirements for a demonstrator facility, the Integrated Test System (ITS) were established. This facility will demonstrate the use of the high-pressure intensifier, magnet technology, and e-beam energy addition in a single system at the 20- to 30-MW power levels.

Before concept and design criteria can be written for the ITS demonstrator and the MSHWT facility, a number of remaining issues should and/or must be addressed in demonstration experiments. The ITS will be the systems-level demonstration that will also be used to address any remaining technical issues. The following known technical issues remain to be addressed and solved:

1) The pressure intensifier approach must be experimentally demonstrated up to 2100 MPa (304,579 psi) pressure. Also, a scale model of the MSHWT air supply concept, currently the octahedral concept, must be demonstrated at 2100 MPa (304,579 psi) pressure.

2) The advantages and disadvantages of a storage heater in series with the pressure intensifier must be studied and thoroughly understood. An experimental demonstration of this approach may be required if such a system has advantages over a heated pressure intensifier alone.

3) The A-2 Lite nozzle survivability experiments need to be completed in order for investigators to know the limits of nozzle survivability with air and nitrogen and with candidate nozzle throat materials (currently maraging steel and an iridium alloy). The wall recovery temperature in the nozzle throat should be measured and the recovery factor determined in these experiments.

4) A combination air/nitrogen intensifier system with coaxial flow needs to be demonstrated at UHP conditions. This need is subject to the results of the A-2 Lite experiments mentioned earlier.

5) The physics of the electron beam energy-addition process to flowing air needs to be understood, adequately modeled, and experimentally validated.

6) Nozzle heat transfer from the combination of fluid dynamic and electron beam heating must be understood, and strategies must be developed to cope with the heating problem as necessary.

7) Stable electron beam operations and energy addition to air flow need to be demonstrated at run times of one second or greater, with energy-addition efficiencies of near 100 percent.

8) The nozzle aerodynamic window concept for penetration of the electron beam through the nozzle wall needs to be developed and experimentally demonstrated.

9) Reliable prediction codes need to be developed and validated as follows:

   a) Spatial energy deposition from the electron beam. (A code needs to be fast and robust for facility studies as well as for accurately predicting the energy deposition.)

   b) Models that predict the electron beam energy exchange and release process in air.

   c) Models of the flow composition resulting from e-beam energy addition in the high-pressure, high-magnetic-field environment.

   d) Prediction of nozzle heat transfer from fluid dynamic, radiation, and electron beam heating.

   e) Prediction of nozzle boundary-layer growth at UHP conditions.

   f) Prediction of the nitrogen/air coaxial mixing process.

   g) UHP air and nitrogen equation of state.

   h) UHP systems structural models.

   i) UHP systems fatigue-life models.

   All of these codes have yet to be fully developed and validated. Some coded models do exist, but they have yet to be sufficiently validated.

10) Flow diagnostics instrumentation must be developed to support further experiments, operations of the energy addition experiments, the ITS, and future operations of the MSHWT.

Although not required for the ITS demonstrator or the MSHWT specifications to achieve a Mach 12 flow, MHD is required to accelerate the flow beyond Mach 12. The research has been given a lower priority than the other aspects of the work, and much remains to be done. The research that has been accomplished is promising, and the work to demonstrate the production of

large-volume, low-density ionization should be accomplished as well as demonstration of MHD acceleration. If MHD can be applied at lower Mach numbers than the Mach 12 design goal for MSHWT, this should be established before design criteria are written. The application at lower Mach numbers represents an opportunity for significant performance enhancement at significantly less stressful facility conditions and subsequent lower cost.

In conclusion, no fundamental flaws in the RDHWT/MARIAH II MSHWT concept have been identified from the experimental and analytical investigations conducted during this program. Additionally, no insurmountable problems were identified during the thermal energy addition and UHP air supply research, although the performance demonstration goals for the air supply, nozzle survivability, and energy addition have not yet been achieved. Thermal energy addition experiments and modeling have led to the conclusion that stable energy addition to the supersonic flow can be achieved, at least to the power densities achieved in these experiments. While e-beam accelerator technology must be developed to produce an accelerator for the MSHWT with an average power level that is two orders of magnitude greater than those demonstrated to date, experimental results and analysis of accelerator components have led to the conclusion that the concept is viable.

Although there is a considerable amount of research to be accomplished, most of the work remaining can be described as development and scaling rather than fundamental proof or demonstration of principle. At program termination, the work is poised to move from demonstrations at benign physical conditions to conditions not produced in any other ground test facility. The hardware necessary to effect these extrapolations will provide a capability for research and testing at conditions not otherwise possible.

REFERENCES

1. “Requirements for Hypersonic Test Requirements.” United States Air Force Scientific Advisory Board, May 1989.

2. “Air Force 2025: America’s Vigilant Edge.” Air University, Air Education and Training Command, Maxwell Air Force Base, AL, 1996.

3. “Aerospace 2020.” AGARD Advisory Report No. 360, North Atlantic Treaty Organization, NASA Center for Aerospace Information, Linthicum Heights, ND, 1997.

4. “Review and Evaluation of the Air Force Hypersonic Technology Program.” National Research Council, ISBN 0-309-06142-3, National Academy Press, Washington, D. C., 1998.

5. Ritchey, G. K. and McKinney, L. W. “Hypersonic Test Investment Plan (HTIP) – A Development Plan and Investment Strategy for U. S. Hypersonic Test Capabilities and Facilities.” AEDC-TR-94-4, Arnold Engineering Development Center, Arnold Air Force Base, TN. December 1994.

6. "DoD Aeronautical Test Facilities Assessment Study." OUSD(A&T)/DTSE&E Study, J. M. Griffin, J. D. Berry, and D. P. McErlean, Co-Chairs, March 1977.

7. Laster, M., L., Simmons, G., Fetterhoff, T., and Jordan, J.L., "A Research Program for the Development of a True-Temperature Mach 8-15 Medium Scale Wind Tunnel." AIAA-2000-0157, 37th Aerospace Sciences Meeting and Exhibit, Reno, NV, January 10-13, 2000.

8. Fetterhoff, T. P., Jordan, J. L., and Laster, M. L., "RDHWT/MARIAH II Program: Overview and Technical Status." AIAA-2002-3125, 22nd AIAA Advanced Measurement Technology and Ground Testing Conference, St. Louis, MO, June 24-26, 2002.

9. Miles, R. B., Brown, G. L., Lempert, W. R. , Yetter, R. , Williams Jr., G., Bogdonoff, S. M., Natelson, D., and Guest, J. R. "Radiatively Driven Hypersonic Wind Tunnel." *AIAA Journal*, Vol. 33, No. 8, 1995, pp. 1463-1470.

10. Vuonadonna, V. R., Knight, C. J., and Hertzberg, A. "The Laser Heated Wind Tunnel – A New Approach to Hypersonic Laboratory Simulation." AIAA Paper No. 73-211, 11th Aerospace Sciences Meeting, Washington, DC, January 10-12, 1973, p. 12.

11. Baughman, Jack A., Micheletti, David A., Nelson, Gorden L., and Simmons, Gloyd A. "Magnetohydrodynamics Accelerator Research Into Advanced Hypersonics (MARIAH) Final Report." NASA/CR-97-206242/PT1 and PT2, October 1997.

12. Simmons, Gloyd A. (Editor). "Radiatively Driven Hypersonic Wind Tunnel Program, Magnetohydrodynamic Accelerator Research Into Advanced Hypersonics (MARIAH) Fiscal Year 1998 Annual Report." AEDC-TR-00-5 (AD-A397435), September 2001.

13. Simmons, Gloyd A. (Editor). "Radiatively Driven Hypersonic Wind Tunnel (RDHWT)/Magnetohydrodynamics Accelerator Research Into Advanced Hypersonics (MARIAH) Program Progress Report (June 15, 1999 through January 15, 2001), AEDC TR-05-29.

14. Wilson, R., Laster, M. L., Jordan, J. L., and Limbaugh, C. C. "Plans and Status of the RDHWT/MARIAH II Facility Research Program." AIAA-2004-2479, 24th AIAA Measurement Technology and Ground Testing Conference, Portland, OR, June 28 - July 1, 2004.

15. Macheret, M., Schneider, R., Murray, Zaidi, S., Vasilyak, L., and Miles, R. "MHD Modeling and Experiments Review." AIAA Paper 2004-2485, 24th AIAA Aerodynamics Measurement Technology and Ground Testing Conference, Portland, OR, June 28 - July 1, 2004.

16. Miles, R., Mansfield, D., Girgis, I., and Brown, G. "RDHWT/MARIAH II Energy-Addition Modeling and Experiments Review." AIAA Paper 2004-2480, 24th AIAA Aerodynamics Measurement Technology and Ground Testing Conference, Portland, OR, June 28 - July 1, 2004.

17. Constantino, M., and Darnel, I. “Ultra High Pressure Modeling and Experiments Review.” AIAA Paper 2004-2482, 24th AIAA Aerodynamics Measurement Technology and Ground Testing Conference, Portland, OR, June 28 - July 1, 2004.

18. Ring, L. E. “RDHWT/MARIAH II Systems Integration Studies Review.” AIAA Paper 2004-2486, 24th AIAA Aerodynamics Measurement Technology and Ground Testing Conference, Portland, OR, June 28 - July 1, 2004.

19. Brown, G. L., Girgis, I. G., Jiang, F., and Lockner, T. L. “A Review of the RDHWT/ MARIAH II Fluid Mechanics Modeling and Experiment.” AIAA-2004-2481, 24th AIAA Aerodynamic Measurement Technology and Ground Testing Conference, Portland, OR, June 28 - July 1, 2004.

20. Schneider, L., Glover, S., Lipinski, R., Lockner, T., Pena, G., and Reed, K. “Progress Towards a 200MW Electron Beam Accelerator System for the RDHWT/Mariah II Program.” AIAA Paper 2004-2484, 24th AIAA Aerodynamics Measurement Technology and Ground Testing Conference, Portland, OR, June 28 - July 1, 2004.

21. Tarrant, S., Lofftus, D., Pusich-Lester, J., Tourikis, J., Simmons, G., Liu, C. T., Easton, D. S., Schneibel, J., and Felderman, E. J. “Radiatively Driven Hypersonic Wind Tunnel/Magneto-hydrodynamics Accelerator Research Into Advanced Hypersonics (RDHWT/MARIAH II) Ultrahigh-Pressure Technology and Nozzle Survivability Experiments Review.” AIAA Paper 2004-2483, 24th AIAA Aerodynamics Measurement Technology and Ground Testing Conference, Portland, OR, June 28 - July 1, 2004.

22. Schneibel, J. H. and Felderman, E. J. “Development and Testing of New Materials for Aerospace Applications.” AIAA 2004-2593, 24th AIAA Aerodynamics Measurement Technology and Ground Testing Conference, Portland, OR, June 28 - July 1, 2004.

23. Girgis, I. G., Brown, G. L., Mansfield, D. K., Miles, R. B., and Lipinski, R. J. “Unsteady Numerical Simulation of the 1-MW Radiatively-Driven Hypersonic Wind Tunnel Experiments.” AIAA 2004-1136, 42nd AIAA Aerospace Sciences Meeting & Exhibit, Reno, NV, January 5-8, 2004.

24. Murray, R. C., Zaidi, S. H., Carraro, M. R., Vasilyak, L. M.,Macheret, S. O., Shneider, M. N., and Miles, R. B. “Observation of MHD Effects with Non-Equilibrium Ionization in Cold Supersonic Air Flows.” AIAA 2004-1025, 42nd AIAA Aerospace Sciences Meeting and Exhibit, Reno, NV, January, 5-8 2004.

25. Mansfield, D. K., Miles, R.B., Howard, P.J., Luff, J. D., Girgis, I. G., Brown, G. L., Lipinski, R. J., Pena, G. E., Schneider, L. X., Grinstead, J., and Howard, R. “Results of the 1 MW Radiatively-Driven Hypersonic Wind Tunnel Experiments.” AIAA Paper No. 2004-1134, 42nd AIAA Aerospace Sciences Meeting and Exhibit, Reno, NV, January 5-8, 2004

26. Tirres, C. “The Future of Hypersonic Wind Tunnels.” AIAA-99-0819, 37th Aerospace Sciences Meeting and Exhibit, Reno, NV, January 11-14, 1999.

27. Tirres, C., Bradley, M., Morrison, C., and Edelman, R. “A Flow Quality Analysis for Future Hypersonic Vehicle Testing.” AIAA-2002-2706, 22nd AIAA Aerodynamic Measurement and Ground Testing Conference, St. Louis, MO, June 24-26, 2002.

28. Simmons, G., Nelson, G., Miles, R., Brown, G., Barker, P., Macheret, S., Costantino, M., and Lipinski, R. “Progress Toward a Radiative and MHD Driven High Enthalpy, High Pressure, Long Duration Test Facility.” AIAA 2000-0158, 38th AIAA Aerospace Sciences Meeting and Exhibit, Reno, NV, January 10-13, 2000.

29. “Evaluation of the National Aerospace Initiative.” Air Force Science and Technology Board, 2004.

30. “Report of the Ad Hoc Committee on Hypersonic Air-Breathing Vehicle Technology.” Air Force Scientific Advisory Board, June 1992.

31. Laster, Marion L. And Bushnell, Dennis M. “A National Study for Hypersonic Facility Development.” AIAA-1994-2473, AIAA Aerospace Ground Testing Conference, Colorado Springs, CO, June 20-23, 1994.

32. verBrugge, R., Schouten, J. A., and Trappeniers, N. J. “Static Seal for High Gas Pressures.” *Rev. Sci. Instr.*, Vol. 56, 1985, pp. 625-626.

33. Stishov, S. M. and Zil’bershtein, V. A. “A Seal for Pressure-Amplifier Pistons,” translated from *Pribory i Tekhnika Eksperimenta*, No. 4, July-August 1966, p. 216.

34. Stishov, S. M. and Zil’bershtein, V.A. “Sealing the Piston of a Pressure Booster to 30 Katm (tech.) with a Rubber Ring,” translated from *Pribory i Tekhnika Eksperimenta*, No. 6, November-December 1966, pp. 209-210.

35. Raman, K. S., “Nozzle Boundary Layer and Heat Transfer Measurement at Reynolds Numbers from 10^9 to 10^{10}.” Dissertation, Princeton University, January 2001.

36. Anderson, John D, Jr. *Hypersonic and High Temperature Gasdynamics*, McGraw-Hill, New York, 1988, p. 225.

37. White, F. M., *Viscous Fluid Flow*. McGraw-Hill, New York, 1991, 2nd Edition.

38. Morgan, A., Barker, P., Anderson, R., Grinstead, J., Brown, G., and Miles, R. “Preliminary Experiments in the Development of the Radiatively Driven Wind Tunnel.” AIAA 98-2498, 20th AIAA Advanced Measurement and Ground Testing Technology Conference, Albuquerque, NM, June 15-18, 1998.

39. Barker, P., Grinstead, J., Morgan, A., Anderson, R., Howard, P., Brown, G., Miles, R., Lipinski, R., Reed, K., Pena, G., and Schneider, L. “Radiatively Driven Wind Tunnel Experiment with a 30 kW Electron Beam.” AIAA-99-0688, 37th AIAA Aerospace Sciences Meeting and Exhibit, Reno, NV, January 11-14, 1999.

40. Barker, P., Grinstead, J., Howard, P., Anderson, R., Brown, G., and Miles, R. “A 150kW Electron Beam heated Radiatively Driven Wind Tunnel Experiment.” AIAA-2000-0159, 38th AIAA Aerospace Sciences Meeting and Exhibit, Reno, NV, January 10-13, 2000.

41. Barker, P., Lipinski, R., Grinstead, J., Howard, R., Miles, R., and Brown, G. “Proof of Principle Energy Addition Experiments for the RDHWT/MARIAH II Hypersonic Wind Tunnel.” AIAA-2000-2276, 21st Aerodynamic Measurement Technology and Ground Testing Conference, Denver, CO, June 19-22, 2000.

42. Mansfield, D. K., Grinstead, J., Howard, P., Brown, G., Girgis, I., Miles, R., Lipinski, R., Pena, G., Schneider, L., and Howard, R. “A 1MW Radiatively-Driven Hypersonic Wind Tunnel Experiment.” AIAA Paper No. 2002-3130, 22nd Aerodynamic Measurement Technology and Ground Testing Conference, St. Louis, MO, June 24-26, 2002.

43. Girgis, I. G., Brown, G. L., Miles, R. B., and Lipinski, R. J. “Inviscid and Viscous Predictions for an E-Beam Heated Hypersonic Wind Tunnel (Invited).” AIAA 2002-3129, 22nd AIAA Advanced Measurement Technology and Ground Testing Conference, St. Louis, MO, June 24-26, 2002.

44. Girgis, I. G., Brown, G. L., and Miles, R. B. “Heat Transfer and Boundary layer Growth for Ultra High Reynolds Number Turbulent Boundary Layers for A Radiatively Driven Hypersonic Wind Tunnel.” AIAA-2002-0575, 40th AIAA Aerospace Sciences Meeting & Exhibit, Reno, NV, January 14-17, 2002.

45. Girgis, I. G., Brown, G. L., Miles, R. B., and Lipinski, R. J. “Fluid Mechanics of a Mach 7-12, Electron-Beam-Driven, Missile Scale Hypersonic Wind Tunnel: Modeling and Predictions,” *Physics of Fluids*, Vol. 14, No. 11, November 2002, pp. 4026-4039.

46. Hershcovitch, A., "A Plasma Window for Transmission of Particle Beams and Radiation from Vacuum to Atmosphere for Various Applications.” *Physics of Plasmas,* Vol. 5, No. 5, May 1998, pp. 2130-2136.

47. Miles, R. B., Mansfield, D. K., Howard, P., Luff, J., Girgis, I., Brown, G., Lipinski, R., Pena, G., Schneider, L., and Howard, R. “A 1MW Radiatively-Driven Hypersonic Wind Tunnel Experiment: Preliminary Results.” AIAA Paper No. 2003-0090, 41st AIAA Aerospace Sciences Meeting and Exhibit, Reno, NV, January 6-9, 2003.

48. Mansfield, D. K., Howard, P. J., et al. “The 1 MW Radiatively-Driven Hypersonic Wind Tunnel Experiments Final Report.” AEDC-TR-05-3, January 2005.

49. Howard, R. P., Dietz, K. L., McGregor, W. K. and Limbaugh., C. C. “Non-Intrusive Nitric Oxide Density Measurements in the Effluent of Core Heated Air Streams.” AIAA-90-1478, AIAA 21st Fluid Dynamics, Plasmadynamics, and Lasers Conference, Seattle, WA, June 18-20, 1990.

50. Limbaugh, C. C. “Calculations of Air Chemistry in the Electron-Beam Heated Hypersonic Wind Tunnel II. Current Experiments.” AIAA Paper No. AIAA-2002-3131, 22nd AIAA Advanced Measurement Technology and Ground Testing Conference, St. Louis, MO, June 24-26, 2002.

51. Halblieb, J. A., Kenesek, R. P., Mehlhorn, T. A., Valdez, G. D., Seltzer, S. M., and Berger, M. J. “ITS Version 3.0: The Integrated TIGER Series of Coupled Electron/Photon Monte Carlo Transport Codes.” SAND91-1634, Sandia National Laboratories, Albuquerque, NM, June 1994.

52. Macheret, S. O., Shneider, M .N., Miles, R. B., Lipinski, R. L., and Nelson, G. L. “MHD Acceleration of Supersonic Air Flows Using Electron Beam Enhanced Conductivity.” Paper AIAA-98-2922, 29th Plasmadynamics and Lasers Conference, Albuquerque, NM, June 15-18, 1998.

53. Simmons, G. A., Nelson, G. L., Cambier, J.-L., Macheret, S. O., Shneider, M. N., Lipinski, R. J., and Reed, K. W. “Electron Beam Driven MHD for the RDHWT/MARIAH II Hypersonic Wind Tunnel.” AIAA Paper 2000-2277, 21st AIAA Aerodynamic Measurement Technology and Ground Testing Conference, Denver, CO, June 19-22, 2000.

54. Lee, Y. M., Simmons, G. A., Ring, L., Macheret, S. O., and Shneider, M. N. “MHD Accelerator Performance Predictions And Plans For Experimental Verification.” AIAA 2002-3132, 22nd AIAA Aerodynamic Measurement Technology and Ground Testing Conference, St. Louis, MO, June 24-26, 2002.

55. Murray, R. C., Zaidi, S. H., Carraro, M. R., Vasilyak, L. M.,Macheret, S. O., Shneider, M. N., and Miles, R. B. “Investigation of a Mach 3 Cold Air MHD Channel.” AIAA 2003-4282, 34th AIAA Plasmadynamics and Lasers Conference, Orlando, FL, June 23-26 2003.

56. Anderson, R. W. and Brown, G. L. “Performance Models and Predictions for the RDHWT/MARIAH II Hypersonic Wind Tunnel.” AIAA 2000-2274, 21st AIAA Aerodynamic Measurement Technology and Ground Testing Conference, Denver, CO, June 19-22, 2000.

APPENDIX A
IMPLIED HEATING DISTRIBUTION FROM THE 1-MEGAWATT EXPERIMENT

INTRODUCTION

As has been noted (e.g., Refs. A-1 and A-2), the 1-MW experimental results differed significantly from predictions. In particular, the wall pressure measurements were consistent with an energy deposition profile that is significantly different from that used for calculations. These differences can have significant implications on the design of the ITS and the MSHWT. Some analysis was done to develop an understanding of these differences. The referenced 1-MW data are reported in Ref. A-1, the final report on the experiment.

REFERENCE DATA

The data used for this analysis are the same three medium-power shots used by the Princeton group for their detailed performance calculations. For reference, the three shots are: 746/4371, 748/4379, and 753/4396. Tables 7-1 and 7-2, in Ref. A-1, give measured airflow properties as follows:

Plenum Properties

Plenum Pressure:	2147 psi
Plenum Temperature:	605 K

Exit Properties with Power On

Mach Number:	1.08 ± 0.01
Flow Speed:	926 ± 80 m/s
Pressure Rise:	31.5 ± 2.0 psi

Exit Pressure with Power Off

Pressure Rise:	53.5 ± 5.2 (psi)

Table 4.8.2-A4, Ref. A-1, gives the average current and power for the three shots as follows:

Current:	0.6 amps
Power:	352 kW

The implied voltage is 587 kV.

Delta pressures for power are obtained from Fig. 7.4, Ref. A-1, as follows:

Channel 1	0 cm	0 psi
Channel 2	190 cm	2 psi
Channel 3	315 cm	18 psi

Channel 4	443 cm	34 psi
Channel 5	512 cm	32 psi

The 1-MW channel geometry was taken from previous 1-MW design calculations. From these, the throat is d* = 11.46 mm, mdot = 2.49 kg/s, and channel length is 519 mm. The area distribution was that for a constant Mach 1.5 for the design calculations.

PERFORMANCE

The channel exit core conditions were computed from the exit: Mach number, velocity, and pressure. The core temperature was thus found to be 2003 K.

Using a two-flow model, cold flow at reservoir conditions expanded to the exit pressure plus a core flow with the above conditions, one can compute the flow fraction in the core and cold flow to obtain a total flow area equal to the exit flow area. The result is a value of 4.97 percent of the mass flow in the core flow, with the remaining in the cold flow. The corresponding core diameter is 22.3 percent of the total flow diameter prior to heating. It is to be noted that the core mass flow with the core enthalpy rise gives a power. This power is found to be 260 kW, compared to the e-beam power of 352 kW. This would suggest that 74 percent of the e-beam power got into the flow stream.

With a core flow/total flow ratio established, the channel heating performance can be computed for a range of assumptions.

In the cases that follow, the core mass flow fraction was held at 4.97 percent, the energy addition was held at 260 kW, and the channel geometry was fixed.

1) L-A Base

"A" base channel performance properties are computed using the Lipinski-Anderson (L-A) e-beam deposition model (Ref. A-3). It was found that, when the 260 kW was added, the entropy rise was less than that found in the experiments. To achieve the experimental exit conditions, it was necessary to increase the entropy rise by 24 percent (i.e., there is an implied loss mechanism which increases the entropy an additional 24 percent above that attributable to the heating itself). One can only speculate what the mechanism might be.

The resulting pressure distribution is shown in Fig. A-1 as a pressure increase from the no-heating case. It is seen to be grossly different from the experimental points. In particular, the heating is far too forward in the channel.

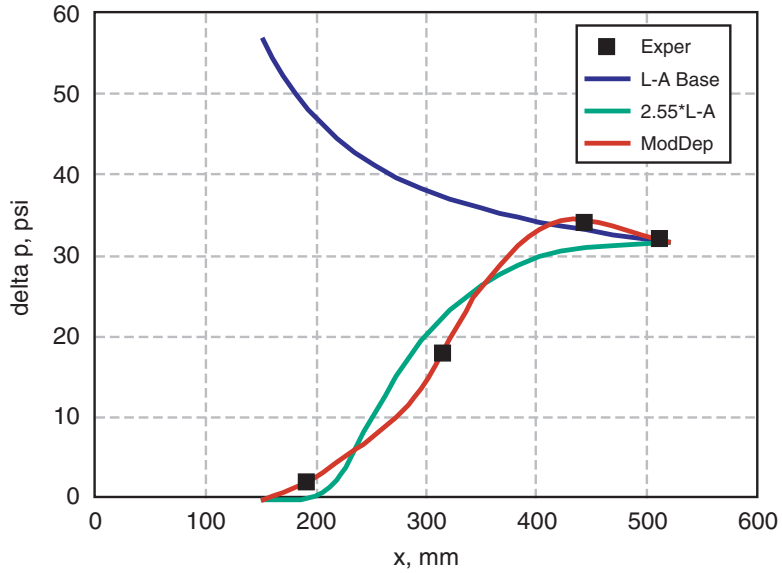

Figure A-1. Channel Pressure Distribution

2) 2.55*L-A

The channel performance is computed using the L-A e-beam deposition model modified by assuming the heat deposition is 2.55 times the base model. This corresponds to assuming that the heating occurs in 39 percent of the L-A computed distance. It is significant that this computation required no assumption regarding increased entropy rise. That is, the channel exit entropy rise was automatically achieved.

The resulting pressure distribution is also shown in Fig. A-1 as a pressure increase from the no–heating case. It is seen to come closer to the experimental points, but a mismatch remains. The heating is now in the right general area of the channel.

3) ModDep

The channel performance is computed using a “Modified Deposition” e-beam deposition. Specifically, the heating was chosen to match the experimental pressure distribution.

The resulting pressure distribution is also shown in Fig. A-1 as a pressure increase from the no-heating case. It is no surprise that the calculation matches the experimental pressure distribution. However, what is extremely significant is that this matching required no assumption as to entropy rise. That is, the channel exit entropy rise was again automatically achieved.

Briefly, it is shown that there is an axial energy deposition that, when used with the above experimental inputs, gives the experimental pressure distribution and exit flow conditions, including entropy rise in the core flow.

For reference, the Mach number distributions and heating distributions corresponding to the above cases are shown in Figs. A-2 and A-3.

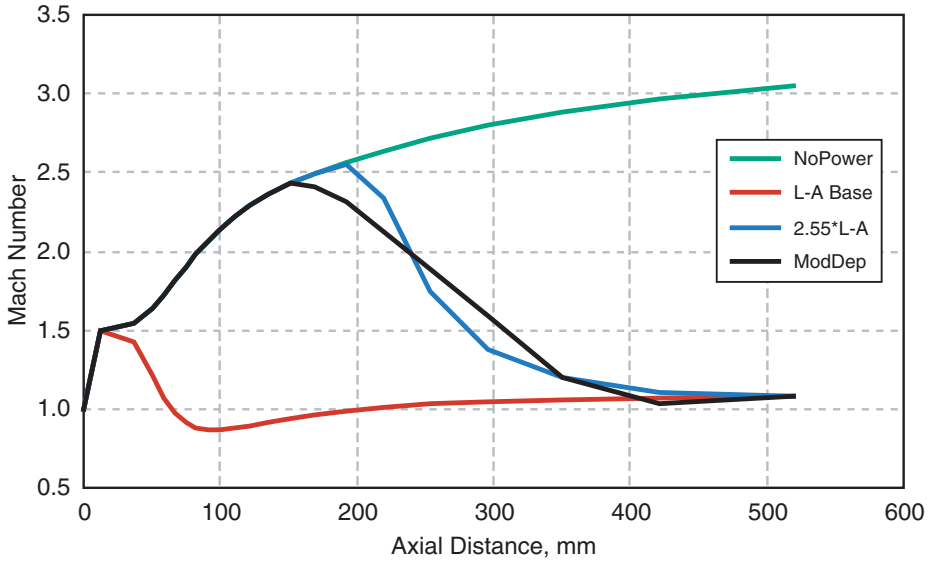

Figure A-2. Mach Number Distribution

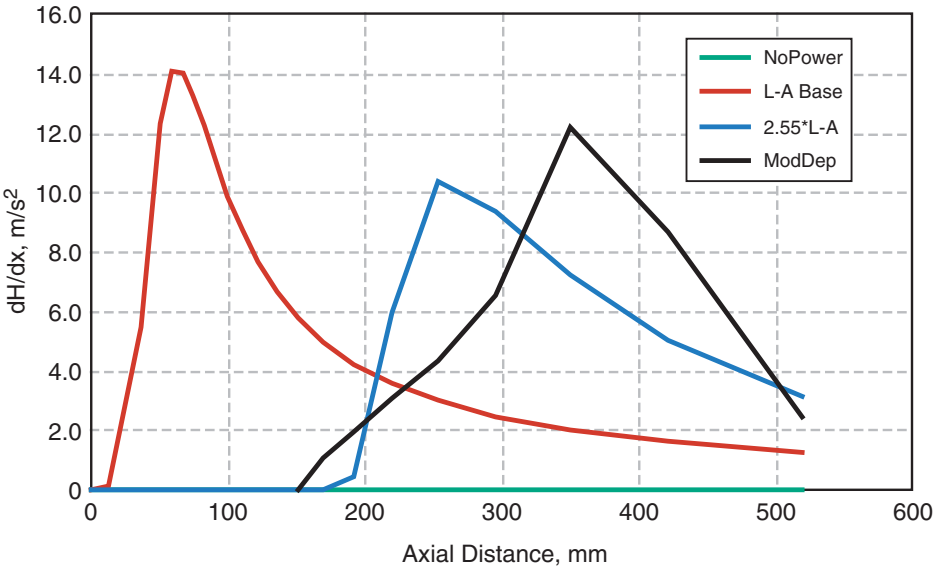

Figure A-3. Channel Heat Addition Distribution

SUMMARY

From this analysis, one can see that there are four numbers that characterize the flow:

- Mass flow fraction that is heated: 5 percent
- Fraction of e-beam power deposited in the flow: 74 percent
- Increased deposition rate above the L-A predictions: 2.5 times
- In addition, a deposition rate similar to but different from the L-A predictions improves the axial pressure distribution.

It remains to be shown whether these results are valid over a general range of operation or if they merely explain an isolated experiment. Furthermore, it seems evident that the analysis results would change for detailed 2D flow calculations. However, it seems more than coincidental that for the assumed heating distribution the entropy rise equals that of the experiment.

Because of the agreement with the data, it seems evident that the thermodynamic performance of the channel is fairly represented by the above calculations—even though they are only 1D. A plausible explanation of a mechanism leading to the differences in data and prediction, and consistent with the above heating profile result, has been offered in Ref. A-2. In this analysis, the electron beam appears to be impinging upon the edges of the aperture, deflecting and losing energy, and thus resulting in a heating profile similar to the one assumed here.

REFERENCES

A-1. Mansfield, D. K., Howard, P. J., et al. “The 1-MW Radiatively-Driven Hypersonic Wind Tunnel Experiments Final Report.” AEDC-TR-05-3, January 2005.

A-2. Mansfield, D. K., Miles, R. B., Howard, P. J., Luff, J. D., Girgis, I. G., Brown, G. L., Lipinski, R. J., Pena, G. E., Schneider, L. X., Grinstead, J., and Howard, R. “Results of the 1-MW Radiatively-Driven Hypersonic Wind Tunnel Experiments.” AIAA Paper No. 2004-1134, 42nd AIAA Aerospace Sciences Meeting and Exhibit, Reno, NV, January 5-8, 2004.

A-3. Anderson, R. W. and Brown, G. L. “Performance Models and Predictions for the RDHWT/MARIAH II Hypersonic Wind Tunnel.” AIAA Paper 2000-2274, 21st AIAA Aerodynamic Measurement and Ground Testing Conference, June 19-22, 2000, Denver, CO.

APPENDIX B
SYSTEM SIMULATION MODEL

INTRODUCTION

Attributes of the system simulation model include:

1) Incorporation of a two-flow model, an inner core e-beam-heated flow with an outer flow that is unheated. This allows 1D simulation of the 2D case where a cold flow is used to shield the channel walls from the fringe e-beam column heating.

2) Calculation of the e-beam heating.

3) Design calculations for which the thermodynamic path is specified and the resulting e-beam voltage and channel length are determined.

4) Off-design performance calculations in which the channel geometry as well as the e-beam voltage and current are specified and the resulting flow computed. The flow thermodynamic path is computed rather than specified.

More specifically, the simulation model incorporates two separate calculations:

- **Design** calculations, in which input includes:
  Reservoir p_o and T_o
  Core flow and total flow throat diameters
  Entrance Mach number
  Thermodynamic heating path (p, T, or Mach number distribution)
  Input power, or test section Mach number at matched altitude
  E-beam voltage

  and computed output includes:

  All thermodynamics through the e-beam heating region
  Test section Mach number at matched altitude, or the input power
  Channel area distribution
  Channel length distribution
  E-beam current

- **Performance** calculations, in which input includes:
  Reservoir p_o and T_o
  Core flow and total flow throat diameters
  Channel length distribution, x
  Channel area distribution as a function of x
  E-beam voltage

E-beam current

and computed output includes:

All thermodynamics through the e-beam heating region
Test section Mach number at matched altitude

In addition, diffuser recovery and exhauster pumping requirements are computed. The simulation program does not include the capability of MHD energy addition.

The model is based on 1D aerodynamics, with equilibrium, real-air thermo-dynamics. It computes the flow:

- from the UHP reservoir,
- through the throat,
- expansion to the start of e-beam heating,
- supersonic heat addition,
- expansion to the test section, at a matched altitude condition, specified test section pressure level or specified test section area,
- pressure recovery through the diffuser,
- pressure drop and cooling in the heat exchanger, for a specified pressure loss coefficient and heat exchanger temperature, giving the required exhauster pumping requirements.

FLOW COMPUTATION LOGIC

The computational logic is as described below for each step in the flow process, with actual calculation flow on the spreadsheet in the order of the following steps. Input quantities at each step are shown in bold.

1) The reservoir conditions, in terms of ***pressure*** and ***temperature***, are input. Other reservoir thermodynamic quantities are computed from these inputs.

2) The flow expands to the throat. The throat location is found by minimizing the area while the Mach number is 1.0.

3) For reference, throat recovery conditions are computed to display the approximate adiabatic recovery temperature. The expression $h_{aw} = h + sqrt(Pr) * (H – h)$ is used. With the

computed enthalpy, other thermo quantities are computed. A value of ***Pr = 0.9*** is used as the default Prandtl number for these high Reynolds number flows

4) The flow expands at constant entropy to an assumed pressure ratio for the start of e-beam heating.

5) E-beam energy is then added to the supersonic flow. A value of the pressure ratio at each channel point is assumed for integration. A 20-step integration process is used, a parameter η with $(1 - \eta)$ being the ratio of entropy rise to the theoretical value of entropy rise for heat addition to the flow. A negative value corresponds to higher than theoretical entropy rise and can be used to account for flow inefficiencies. A default value of $\eta = -0.07$ was used to give a performance margin corresponding to 2D calculations.

   With assumed energy addition given and the assumed pressure distribution given as a function of H, the flow process is determined through the e-beam heating with all quantities, including the area ratio, as a function of the total enthalpy, H. At this point H, not length (x), is the independent variable.

6) The flow is expanded at constant entropy to the test section. The atmospheric pressure level corresponding to the entropy level is computed. This is the matched altitude level. With this pressure and entropy, all remaining thermodynamics are found.

   If a desired test section pressure level is desired, that pressure is input.

   The dynamic pressure, q, is computed at these test section conditions. In addition, the corresponding geometric altitude is found from the test section pressure.

7) Pressure recovery in the diffuser is found using a given fraction of normal shock recovery at the test section flow conditions. The full normal shock values are computed. The diffuser recovery is obtained by multiplying by the ***Diffuser Recover*** factor. Following Lukasiewicz, Ref. B-1, on the basis of AEDC hypersonic experiments, a default value of 30 percent is used. Note that these calculations require real-air thermo because the static temperature can reach 5000 to 6000 K in this region.

8) Following the diffuser, a finned tube heat exchanger is assumed. For the heat exchanger, inputs of ***pressure drop*** and ***final temperature*** are required. Default values of 25 percent total pressure loss and a final temperature of 400 K are used. The exhauster requirements in terms of pressure level and volume flow rate are then computed.

9) This then completes the flow calculation through the flow channel. With the input of the throat diameter, ***d****, the mass flow and power are computed. The channel diameter distribution and power addition distribution are computed along the flow channel.

FLOW CHANNEL INTEGRATION

The channel flow is computed with given values of pressure distribution and total enthalpy distribution. Enthalpy, H, is the independent variable. All of the calculations are straightforward, with the exception of the channel integration. In the case of the flow channel, the formulation is as follows:

The entropy rise can be expressed as follows:

$$dS = (1 - \eta)/T\ dH = 1/T\ dh - ZR\ d(\ln p)$$

where η is the conversion efficiency and dH is the enthalpy and total energy addition. This is expressed as

$$dh = (1 - \eta)\ dH + ZRT\ d(\ln p)$$

A simple second-order integration process was used within the above formulation. With the new values of pressure and enthalpy, all other quantities are found.

Again the problem is reduced to determining the pressure distribution through the channel heating.

E-BEAM COMPUTATION LOGIC AND INTEGRATION

The basic e-beam heating expression is that taken from the MARIAH II / RDHWT 1999 annual report, Eq. (7-1), Ref. B-2. This can be written as:

$$dH / dx = J\ \rho\ 10^5/mdot * \{Xi * \exp[-(t - to)2] + 1.5 * \exp(-t2)\} \qquad \text{Eq. (B-1)}$$

where: H = total enthalpy
x = axial distance measured in the flow direction
J = total e-beam current
ρ = flow density
mdot = heated core mass flow
Xi = [12.5/sqrt() – 1.5]/[1 + ERF(t_o)]
$t = - 0.625/E_o * \rho\ dx$
$t_o = 1.25 * E_o\text{^}0.22$

All quantities are in standard MKS units except E_o, which is in MV (constants have dimensions). This can be integrated to give:

$$H = J\ Eo\ sqrt()\ 0.8*10^5/mdot * [Xi*ERF(t - to) + Xi*ERF(to) + 1.5*ERF(t)\}] \qquad \text{Eq. (B-2)}$$

This gives H as an explicit function of the scaled distance t measured from the exit of the heating region. A tacit but critical assumption in Eq. (B-2) is that mdot is a constant. This implies that the e-beam column is tailored to meet the flow area through the heating area. For the ***Design*** case, this is an obvious assumption; for the ***Performance*** (off-design) case, this implies that the magnets are adjusted to meet the resulting flow diameters as one moves to off-design conditions.

It is noted that the quantity Xi is given in Ref. B-2 as:

$$Xi = 2.2 + 0.8/E_o \qquad \text{Eq. (B-3)}$$

Equation B-2 has been changed here to normalize the energy (i.e., to make the total energy addition equal to the input power when integrating to infinity). Thus, at t = infinity,

$$H = J\ E_o\ 10^6 / \text{mdot} \qquad \text{Eq. (B-4)}$$

The change is not great, but it was made to allow mathematical convergence in the total energy addition. This is critical in the details of the entrance region of the e-beam heating.

The computational logic is as described in the following:

- E_o is specified. For the ***Design*** case, J is then computed from the total input power. For the ***Performance*** case, J is specified.

- For the ***Design*** case, we have H and need to find t. This is done using Eq. (B-2) with a pseudo integration/iteration technique to find t = t(H). With t = t(H), one finds x by integrating

  $$x = -1.6\ E_o\ 1/\rho\ dt$$

  With x = x(H), all quantities are expressed as a function of the distance, x.

  For the ***Performance*** case, x is given. One finds t by integrating its definition [given in Eq. (B-1)] to obtain t = t(x).

  $$t = -0.625/E_o\ \rho\ dx$$

  With t = t(x), a new distribution, H = H(x), can now be computed from Eq. (B-1) to produce an improved H distribution.

ITERATION TO SOLUTION FOR PRESSURE AND ENTHALPY DISTRIBUTION

It remains to iterate to find the correct pressure distribution and energy-addition distribution.

For the ***Design*** case, an iteration procedure is used to find the pressure distribution in order to achieve the desired thermodynamic path: constant Mach number, constant temperature, or

some other path. This is done by including the appropriate expression that must be iterated to convergence (e.g., Mach = 2.0).

For the ***Performance*** case, an iteration procedure is used to find the pressure distribution in order to achieve the correct area distribution. A second iteration on enthalpy, H, is used to make the assumed enthalpy distribution equal to the computed enthalpy distribution. One note: the e-beam equation, Eq. (B-2), achieves total e-beam energy deposition in the flow only with an infinite-length channel. This shows up mathematically as a singular point in the function x = x(H) at the channel entrance. To remove this singularity, integration is stopped at 99 percent of the total enthalpy addition. In practice, the remaining 1 percent will be deposited between the throat and the channel entrance.

A related point is that in a ***Performance*** calculation, a major fraction of the input energy remains in the e-beam at the channel entrance if too high a value of E_o is specified. In practice, the excess energy is deposited upstream of the channel entrance, perhaps into the wall at the throat. This can be checked by the e-beam power ratio. If this ratio is less than 1.0, the e-beam voltage must be reduced to prevent undesirable heating of the throat.

SUMMARY SHEET

Operational Note

These calculations contain a large number of iterations and use thermodynamics over a large range. It is very easy to provide inputs that make the calculation physically impossible. It is advisable to start with a valid calculation and change in small increments to the new case of interest. For example, one may find that the test section is at a pressure above atmosphere (i.e., below sea level). On the other hand, the expansion in the nozzle may go below the air condensation limit.

REFERENCES

B-1. Lukasiewicz, J. *Experimental Methods of Hypersonics*. M. Dekker, New York, 1973.

B-2. Simmons, Gloyd A. (Editor) “Radiatively Driven Hypersonic Wind Tunnel Program, Magnetohydrodynamic Accelerator Research Into Advanced Hypersonics (MARIAH) Fiscal Year 1998 Annual Report.” AEDC TR-00-5 (AD-A397435), September 2001.

APPENDIX C
MSHWT DESCRIPTION

Following is a description of the MSHWT as envisioned at the close of the program (2004). This definition will serve as the basis for the forthcoming cost estimate for the MSHWT.

Included is a "Performance/Design Approach" section, which gives the parameters upon which the description is based, as well as an "MSHWT Facility Description" section, which describes the main subsystems and components of the facility.

MSHWT Performance/Design Approach

The MSHWT Performance is summarized below:

Based on a UHP facility with 2100 MPa at 750 K
Maximum performance design point of 500 psf q 2000 psf at M = 12
Nominal operating points of M = 8 and M = 10 at 500 psf q 2000 psf
1-m-diam test section flow
Useful test time of 10 s
A 210-MW, 3-MV, 70-amp e-beam heating system

The MSHWT design approach is based on the following:

UHP facility based on single-stroke intensifier system
Internal ceramic heaters to preheat the UHP vessel air to 550 K
Throat protection based on utilizing a 50-percent nitrogen, 50-percent air flow by mass
UHP system sized for the M = 12, q = 2000-psf operating point
Wall protected from e-beam heating by a cold flow layer
- layer represents 75 percent of mass flow at M = 12 operation‡‡
- layer represents 3 mm at throat for M = 10 and M = 8 operations

Utility-grid based, rectifier power supply system
Exhaust to atmosphere with a steam ejector-driven exhaust system

The MSHWT includes buildings and Environmental, Safety, and Health (ES&H) for the above.

‡‡ Only 50 percent of the air is heated by the electron beam, thus 75 percent of the mass flow (100 percent of the nitrogen and 50 percent of the air) is cold flow.

MSHWT Facility Description

UHP Air/Nitrogen Supply

Performance

The MSHWT will be designed around a UHP single-stroke intensifier system with a maximum performance of p_o = 2100 MPa at T_o = 750 K. At this maximum operating point, the system will have an 11.9-mm-diam throat requiring a combined air/nitrogen flow of 166 kg/s delivered for 10 s.

The system will operate down to p_o = 75 MPa to provide the q = 500 psf at the M = 8 operating point.

The UHP system is based on using nitrogen to protect the throat/nozzle from oxygen, and on using this nitrogen, plus part of the air flow, to protect the e-beam heating channel from electron beam heating. The total flow will be 50 percent air and 50 percent nitrogen. The air and nitrogen pressures and temperatures will be nominally the same.

The UHP air supply system will be designed and sized to provide a 10-s run time at the M = 12, q = 2000-psf performance point. The run times at lower Mach numbers may be limited by the air supply to something less than 10 s.

General Description

The UHP air supply system will consist of:

- High-pressure nitrogen storage tanks to store the nitrogen, which will drive the hydraulic fluid for the hydraulic rams which, in turn, will drive the UHP intensifiers.
- Hydraulic fluid tanks, which store the hydraulic fluid; these have a membrane to separate the nitrogen from the hydraulic fluid, and they serve as the supply to drive the hydraulic rams.
- UHP intensifiers, which include a hydraulic ram, an intensifier piston, and the UHP vessel itself.
- An octahedral-type containment structure to contain multiple (four) intensifiers in a “layer” module.
- A manifold system to connect the multiple (four) layers to the stilling chamber.
- UHP vessel internal ceramic electrical heaters, which will be used to heat the air charge to a uniform air temperature of 550 K prior to completing the temperature rise through the heat of compression.
- A hydraulic pumping system, which will pump the hydraulic fluid, after each facility run, from the intensifier systems back into the hydraulic fluid storage tanks, and in turn pump the nitrogen back into the high-pressure nitrogen storage tanks for the next facility run.

The UHP nitrogen supply system will be essentially a duplicate of the air system.

The nitrogen and air flows will be delivered in a concentric, axial flow just upstream of the throat.

Operation

The air system design will be at the p_o = 2100 MPa and T_o = 750 K conditions. This M = 12, q = 2000-psf operating point has the highest mass flow requirement of any operating point. Therefore, it is anticipated that operation of this air supply system off-design will provide all other facility operating points.

The operating sequence of the air/nitrogen supply systems will be as follows:

- Charge the high-pressure nitrogen tanks to their operating pressure.
- Charge the intensifiers, air and nitrogen, to their precompression pressures.
- Heat the air/nitrogen charge to its precompression temperature, nominally 550 K.
- Start the intensifier pistons in motion to compress and heat the air/nitrogen.
- At the operating pressure, open a quick opening valve to initiate air/nitrogen flow. The nitrogen flow leads the air flow slightly in time to ensure that no high-pressure air impinges on the nozzle throat or nozzle.
- Terminate the run by stopping the motion of the intensifier pistons.
- Return the pistons to their pre-run positions by pumping the hydraulic fluid back into the hydraulic reservoirs.

Throat/Nozzle/E-Beam Heating Channel

General Description

The general design approach used to protect the throat/nozzle/e-beam heating channel from heat/oxidization is to:

1) provide thermal protection by the use of wall materials able to withstand the aerodynamic recovery temperatures, absent an oxidizing atmosphere, and

2) provide oxygen protection by the use of a nitrogen layer between the air flow and the wall.

The general design approach used to protect the e-beam heating channel from electron beam heating is the use of high-intensity magnetic fields to control electron motion coupled with a cold, nonheated flow layer between the heated core flow and the wall. The heated flow will be about 25 percent of the total flow at the M = 12 conditions, and it will increase to 49 percent of the total flow at the M = 8 conditions.

Each throat/nozzle/e-beam heating channel will be comprised of a single integrated unit. Three interchangeable units are required, one each for M = 8, 10, and 12 operation. Each unit will have mechanical separation points as may be required by the mechanical designs.

The nozzle throat diameters will be approximately 20.0 mm for M = 8, 14.3 mm for M = 10, and 11.9 mm for M = 12.

The air/nitrogen supply systems will deliver air/nitrogen in a concentric axial flow configuration just upstream of the throat. The concentric flow will pass through the throat and continue downstream.

Note that the heated core flow is 25 percent of the total flow for the M = 12 operations, while the air flow is 50 percent of the total flow. Therefore, the shear layer separating the air/nitrogen will be contained within the cold-flow layer.

The channel lengths will vary from about 200 mm for M = 12 to 570 mm for M = 8. Each channel will consist of a rapid expansion downstream of the throat before going into an approximately conical flow of 11 to 14 deg half-angle expansion to the exit of the e-beam heating.

The throat/nozzle/e-beam heating channel must provide space for and accommodate the high-strength magnetic fields required for the e-beam heating.

The throat/nozzle/e-beam heating channel must be electrically conducting to accommodate the e-beam current return path.

Operation

There is no operation connected to the throat/nozzle/e-beam heating channel. It is a passive unit.

The units must provide for easy exchange between the three units.

E-Beam Energy Addition

General Description

The e-beam energy addition system includes the total system required to deliver e-beam energy to the flow. This includes the e-beam accelerator; the power supply for the e-beam accelerator; a power supply for the electron injector, the magnet system, and its power supplies; and all supporting equipment. It is a nominal 210-MW, 3-MV system, but it can operate down to 0.8 MV and at any current from zero up to the maximum design current.

The e-beam system is assumed to be powered from a utility grid, with the grid having the capability to accommodate a 210-MW, 10-s^2 pulse.

E-Beam Accelerator

The e-beam accelerator will be a single e-beam unit designed to operate at up to 3 MV and at currents up to 70 amps.

The e-beam accelerator will be housed in a high-pressure SF_6 tank to withstand the high voltages. An SF_6 system will be part of the e-beam accelerator system.

The e-beam accelerator will operate at a preset, constant voltage for each run. This voltage control will be through tap adjustment on the low-voltage side of the rectifier-transformer prior to initiation of the run.

The e-beam current will be controlled separately by varying the injector voltage, and it will operate from zero to its set current value during each run. The e-beam current will be continuously variable, controlled by the injector power supply.

The injector configuration will be capable of providing the best possible top-hat electron current distribution in the heating channel.

Power Supply

The e-beam accelerator power supply will have the following characteristics:

- multiple modules, each with about 20 MW of power
- each module will have a step-changing (low-voltage side) transformer, with 10 steps to change the voltage between 0.8 and 3 MV, or about 16 percent voltage increase with each step
- the rectifier-transformer will be a six-phase transformer with windings connected by a bridge-rectifying circuit using 25-kV diodes
- voltage ripple requirements will be met without additional filtering
- the assembly will be housed in an insulated SF_6 high-pressure tank

Aerodynamic Window

The electron beam will enter the aerodynamic nozzle through an aerodynamic window, which is an opening in the nozzle wall. The window will be configured to minimize aerodynamic disturbances.

The e-beam accelerator will be direct-connected to the aerodynamic window in the second nozzle (see below) at a point where the maximum operating static pressure is approximately one

atmosphere. A differential pumping system with a series of orifices will provide the vacuum environment required for the e-beam accelerator.

Magnet System

A magnet system consisting of multiple conventional and superconducting magnets will be used to focus and control the e-beam trajectory. Magnetic fields up to 20 Tesla will be required.

These magnets will constrict the e-beam diameter when it passes through orifices, turn the beam to align it with the e-beam heating channel, and control the e-beam diameter to meet the area distribution of the e-beam heating channel.

DC power supplies and cryogenic systems will be required to support the magnet system and are part of the magnet system.

Operation

The e-beam system operating sequence will be as follows:

- Activate the differential pumping system with the beam exit valve closed.
- Energize the magnet system and allow the magnets to come up to strength and penetrate the nozzle.
- Open the beam exit valve
- Energize the e-beam accelerator power supply at its preset voltage.
- Energize the injector power supply, starting at low voltage, and bring up injector current to its set value over a time of about two flow times of the flow through the e–beam heating channel (about 0.5 ms) to allow stable flow during the starting process.
- At the end of the run, reverse the steps.

Second Nozzle/Test Section

Second Nozzle

A second nozzle will expand the flow from the exit of the e-beam heating channel to the test section. The channel at the exit of the e-beam heating will be expanding between 11 and 14 deg. The flow will continue to expand at this rate and then, with a contoured nozzle, have nearly parallel flow in the test section. The test flow diameter will be a nominal 1 m as it enters the test section. For some tests, a simple conical nozzle or a direct connect to a propulsion system combustor may be used.

The e-beam current will enter the channel through an aerodynamic window in the second nozzle.

The second nozzle length will be between 2 and 3 m, and will include backside water cooling for thermal protection. Three nozzles will be required, one for each of the three nominal operating Mach numbers (8, 10, and 12).

Test Section

The test section will be an open jet housed in a cylindrical tank, 3 m in diameter and 3 m long, providing a 2-m space for the test article between the nozzle exit and the diffuser lip. No active cooling is anticipated except for the leading edge of some model support components. The test tank will include multiple windows for visual observation of the test article and for the use of optical instrumentation.

Diffuser/Exhaust System

General Description

The MSHWT, like conventional hypersonic wind tunnels, will require an exhauster system to discharge the flow to atmosphere. It is envisioned that the exhauster system will utilize a hypersonic diffuser to maximize pressure recovery and that the resulting flow will be pumped with a steam ejector system. A steam ejector system with steam accumulators would be used since operating time of the ejector would be less than a minute to support the multisecond run time of the MSHWT.

Diffuser

The diffuser will consist of a converging section, a constant area section, and a diverging section exhausting into a settling chamber. The geometry is yet to be determined, but the inlet will be on the order of 2 m in diameter, the constant area section about 1 m diameter, and the overall length will be on the order of 15 m. It will require an active cooling system. At the M = 12 conditions, the diffuser exit temperature will approach 2700 K. A spray cooling system at the exit of the diffuser will cool the flow and protect the exhaust settling chamber.

Ejector System

For the M = 12 conditions at q = 2000 psf, the recovery pressure for the core flow will be about 0.54 atm. Assuming that the cold flow will be uniformly mixed with the core flow in the diffuser, the recovery pressure will be reduced by a factor of four, to 0.14 atm. Thus an ejector system to pump 166kg/s of air/nitrogen with a pressure ratio of 7 is required. This could entail a steam flow rate of 1200kg/s. For MSHWT operation at a reduced q = 500 psf, the recovery pressure is further reduced, by a factor of four, to 0.036 atm and represents the maximum exhauster requirement.

The M = 8 and M = 10 flows require somewhat less pumping capacity than do the M = 12 conditions.

Thus the operating exhauster pumping pressure ratio will be about 30. A somewhat higher pressure ratio, about 60, will be required during the starting process. Thus a two-stage steam ejector system is envisioned.

Steam Supply System

Since relatively short runs are required in the MSHWT, a steam accumulator system is envisioned to drive the ejector system. The steam accumulator capacity needs the capacity to drive the ejectors during the facility starting, operating, and shutdown process. The steam ejector system is envisioned to operate for about 10 s during the facility starting process, 10 seconds during the run proper, and 5 s during the facility shutdown process for a total operating time of 25 s.

Alternately, it may be more economical to oversize the UHP air or nitrogen storage and use this air or nitrogen to drive the ejector system.

Control System

General Description

The control system will be composed of a master controller and a distributed PLC system located on individual components and subsystems. The PLCs will be controlled by the master controller, which will control and sequence the total operation of the facility through a predetermined operating sequence. The master controller will shut down the facility in the case of an off-normal event.

Operational Logic/Sequence

The facility operating sequence is envisioned as follows:

- Charge the UHP intensifiers to the required air and nitrogen pressure with the throat valve closed.
- Heat the air/nitrogen charge to the required precompression temperatures.
- Turn on the exhauster steam ejector system and pump down the nozzle, test section, and diffuser system to the ejector blank-off pressure.
- Activate the e-beam differential pumping system, and allow it to reach its blank-off pressure.
- Energize the e-beam magnet system, and allow magnetic fields to penetrate nozzle walls.
- Open the e-beam exit valve.
- Turn on the e-beam accelerator voltage.
- Activate the UHP hydraulic piston drive system, and start pumping up the main plenum.

- As the UHP operating pressure is reached, open the main throat valve. This will allow the UHP air and nitrogen flow to commence. The hydraulic piston drive system will continue on its prescribed path, maintaining the plenum conditions.
- Allow the cold flow (no e-beam heating) to be established through the nozzle, diffuser, and exhaust system. The pressures are such that the flow at the e–beam heating exit will be above atmospheric pressure and the temperature above the air condensation limit. The air temperature will reach the condensation limit, and a condensation shock will develop in the expansion nozzle between the e-beam heating exit and the test section. However, the exhauster pressure ratio will be insufficient to establish supersonic flow through the test section, causing a shock wave to reside in the expansion nozzle.
- Turn on the e-beam current and establish the test flow conditions.
- At the completion of the test, shut down the facility by reversing the above steps.

Buildings/Site

General Description

The MSHWP facility will be housed in a building with appropriate protection for operating personnel. This will include a control room shielded from UHP explosion hazards and radiation from the e-beam system.

Flow Train Operating Conditions

Flow train aerodynamic calculations were made under the following assumptions:

- Three operating channel configurations were developed: M = 12, M = 10, and M = 8, all for q = 2000 psf. The UHP pressures were selected to give the q = 2000 psf at a UHP temperature of 750 K. The thermodynamic path was taken as M = 2 with temperature limits of 2400, 1700, and 1200 K for the Mach 12, 10, and 8 cases, respectively. The mass flow was taken so as to provide the 1.0-m-diam flow.
- Each channel was then modified to a “modified conical configuration” having the same performance.
- Off-design performance was then computed for each of the three channel configurations for q = 1500, 1000, and 500 psf. The UHP pressure, e-beam voltage, and e-beam current were selected so as to provide the same e-beam current penetration, the same 1.0-m-diam flow, and the specified q levels.
- The exhaust system requirements were computed under the assumptions of 30-percent normal shock recovery of the core flow, no recovery of the cold layer flow, and mixing of these two flows. It was found that the M = 12 condition at q = 500 psf represents the maximum exhauster requirements.

Details of these flow calculations, which represent the performance map of the MSHWT, are shown in Table C-1.

Table C-1. MSHWT Detailed Performance Calculation

	M = 12 Channel Configuration				M = 10 Channel Configuration				M = 8 Channel Configuration			
Summary												
UHP Press, MPa	2045	1392	795.8	339.6	992.9	688.9	429.2	180.1	362.2	255.1	158.2	74.8
UHP Temp, K	750	750	750	750	750	750	750	750	750	750	750	750
Test Sec Diam, mm	1000	1000	1000	1000	1000	1000	1000	1000	1000	1000	1000	1000
Test Sec M	12.00	11.58	11.20	10.90	10.00	9.78	9.57	9.38	8.00	7.89	7.79	7.64
Test Sec q, psf	2000	1500	1000	500	2000	1500	1000	500	2000	1500	1000	500
E-Beam												
Voltage, MV	2.75	2.43	2.00	1.30	2.50	2.16	1.69	1.04	2.25	1.86	1.39	0.79
Current J, amps	67.6	60.4	52.5	43.6	63.8	57.9	51.7	45.2	57.0	53.2	48.9	44.8
Power, MW	185.9	146.9	104.8	56.6	159.5	124.9	87.4	47.0	128.3	98.9	67.8	35.2
Channel Length, mm	196.6	196.6	196.6	196.6	328.3	328.3	328.3	328.3	567.5	567.5	567.5	567.5
Max Expansion, deg	11.3	11.3	11.3	11.3	13.3	13.3	13.3	13.3	12.4	12.4	12.4	12.4
UHP												
Press, atm	20,183	13,734	7854	3352	9799	6799	4236	1777	3575	2517	1561	739
Temp, K	750	750	750	750	750	750	750	750	750	750	750	750
Enthalpy, H, kJ/kg	2338	1867	1406	1025	1563	1320	1102	890	1044	952	871	806
mdot Core, kg/s	41.4	32.0	21.7	10.9	50.0	38.2	25.8	12.8	62.9	47.6	32.0	16.0
mdot Total, kg/s	165.6	127.8	86.9	43.5	147.6	112.8	76.1	37.8	128.5	97.3	65.4	32.6
Throat												
Diam Core, mm	5.96	5.96	5.96	5.96	8.35	8.35	8.35	8.35	13.97	13.97	13.97	13.97
Diam Total, mm	11.92	11.92	11.92	11.92	14.35	14.35	14.35	14.35	19.97	19.97	19.97	19.97
Press, atm	5452	3836	2614	1281	3025	2354	1552	768	1348	1008	693	358
Temp, K	513	522	549	588	535	558	582	599	586	591	603	617
Recovery Temp, K	1590	1351	1086	882	1177	1037	924	808	893	843	798	763
Start Heating												
Mach	2.00	1.92	1.79	1.68	2.70	2.51	2.31	2.03	3.10	2.87	2.63	2.40
Press, atm	1564	1291	988	573	518	456	361	222	148	126	97	56
Temp, K	364	392	429	476	349	372	385	409	314	328	349	365
Diam Core, mm	6.39	6.39	6.40	6.40	9.95	9.95	9.95	9.95	20.08	20.08	20.08	20.07
Diam Total, mm	12.76	12.76	12.76	12.76	17.06	17.06	17.06	17.06	28.65	28.65	28.65	28.65

Table C-1. Continued

	M = 12 Channel Configuration				M = 10 Channel Configuration				M = 8 Channel Configuration			
End Heating												
Mach	3.19	3.00	2.81	2.66	3.20	3.07	2.95	2.86	2.97	2.90	2.84	2.76
Press, atm	64.1	55.3	43.2	25.6	19.4	16.1	11.8	6.5	7.8	6.1	4.3	2.3
Temp, K	2230	2280	2374	2527	1568	1596	1641	1732	1120	1134	1152	1198
Enthalpy, H, kJ/kg	6829	6464	6227	6231	4756	4590	4496	4561	3085	3030	2992	3009
dia core, mm	42.49	41.75	40.68	39.11	77.03	76.02	74.80	73.33	129.78	129.13	128.37	127.73
dia total, mm	46.37	46.37	46.37	46.37	83.72	83.72	83.72	83.72	139.83	139.83	139.83	139.83
Test Section												
Mach	12.00	11.58	11.20	10.90	10.00	9.78	9.57	9.38	8.00	7.89	7.79	7.64
Press, atm	9.37E-03	7.54E-03	5.38E-03	2.84E-03	1.35E-02	1.06E-02	7.36E-03	3.84E-03	2.11E-02	1.63E-02	1.11E-02	5.78E-03
Temp, K	228	231	238	250	226	227	232	244	223	224	227	236
Velocity, m/sec	3633	3531	3461	3459	3010	2954	2920	2938	2393	2369	2351	2355
Enthalpy, H, kJ/kg	6829	6464	6227	6231	4756	4590	4496	4561	3085	3030	2992	3009
dia core, mm	1000	1000	1000	1000	1000	1000	1000	1000	1000	1000	1000	1000
q, psf	2000	1500	1000	500	2000	1500	1000	500	2000	1500	1000	500
Press Alt, km	31.4	32.9	35.2	39.7	29.0	30.6	33.0	37.6	26.1	27.8	30.3	34.7
Exhauster Pumping												
Recovery P, atm	0.142	0.107	0.072	0.036	0.191	0.144	0.096	0.048	0.272	0.204	0.136	0.068
Recovery T, K	2646	2443	2218	2024	2251	2107	1976	1884	1818	1761	1714	1694
Exhauster P, atm	0.107	0.080	0.054	0.027	0.143	0.108	0.072	0.036	0.204	0.153	0.102	0.051
Exhauster T, K	400	400	400	400	400	400	400	400	400	400	400	400
Pumping, ft^3/s	62,046	63,656	64,697	64,451	41,233	41,942	42,332	41,919	25,227	25,458	25,620	25,528
UHP Heating System												
Charge												
p, MPa	380.5	230.6	120.9	40.5	159.2	98.9	52.4	24.5	43.3	31.7	22.2	11.5
atm	3756	2276	1193	400	1571	976	517	242	427	313	219	113
T, K	293	293	293	293	293	293	293	293	293	293	293	293
Heating												
p, MPa	704.6	463.8	267.4	101.3	338.0	224.9	127.1	57.0	107.6	78.3	50.3	24.0
atm	6954	4578	2639	1000	3336	2220	1255	563	1061	773	496	237
T, K	550	550	550	550	550	550	550	550	550	550	550	550

Table C-1. Concluded

	M = 12 Channel Configuration				M = 10 Channel Configuration				M = 8 Channel Configuration			
Compression												
Vol ratio	0.799	0.777	0.753	0.643	0.768	0.735	0.663	0.600	0.648	0.625	0.587	0.520
Flow Vol req'd, m3/s	0.1427	0.1222	0.0984	0.0680	0.1557	0.1340	0.1078	0.0809	0.1953	0.1736	0.1507	0.1236
UHP Vol, liter	1875	1875	1875	1875	1875	1875	1875	1875	1875	1875	1875	1875
SQ Wave Time, s	10.50	11.93	14.35	17.74	9.25	10.29	11.54	13.90	6.22	6.75	7.31	7.89

APPENDIX D
NITROGEN-AIR SHEAR LAYER MIXING***

Calculations of the shear velocity between the nitrogen and the air layers have been made for the proposed MSHWT design case and for the proposed A2LM design case. The specific conditions are as follows:

MSHWT

Air	2100 MPa and 750 K
Nitrogen	2100 MPa and 618 K

A2LM

Air	900 MPa and 750 K
Nitrogen	900 MPa and 639 K

The air conditions are current design points for the MSHWT and A2LM, respectively. The nitrogen temperatures are taken to give a minimum shear velocity in the total region from the reservoir to M = 2.5 flow. A slightly positive shear was taken at the throat.

The results are shown in Figs. D-1, D-2, and D-3.

Figure D-1 shows that the shear velocity is less than 2 m/s for the total range of both flows except for the A2LM above Mach 1.5.

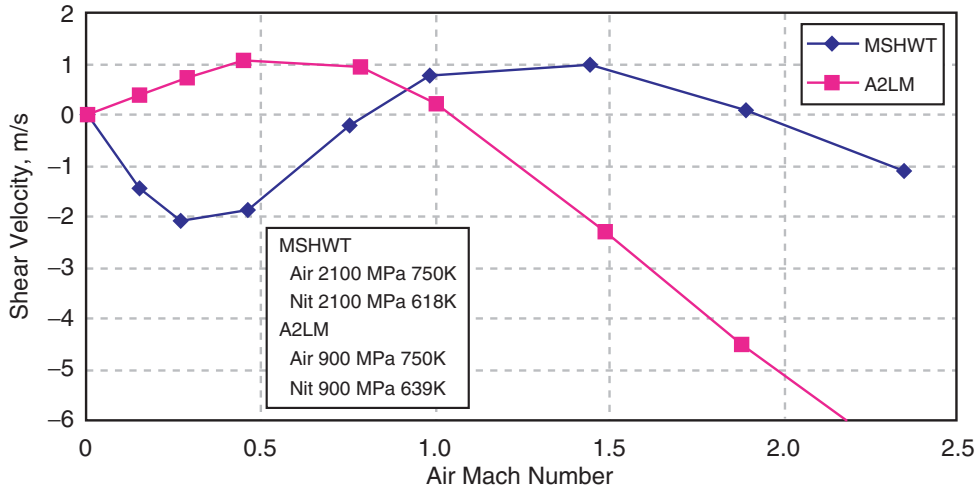

Figure D-1. Nitrogen-Air Shear Velocity

*** Private communication. There has been discussion concerning the mixing layer between the air core and the nitrogen wall-shielding layer. In addition, Merkle at AEDC has made some preliminary calculations of the mixing layer. Merkle's calculations show that about 2/3 of the mixing, in the sense of the total flow between the 5- and 95-percent concentration levels, occurs just downstream of the coaxial flow injector in the low subsonic portion of the converging nozzle. This supports the argument that the mixing is highly dependent upon the details of the injection process itself.

Figure D2 shows that the shear velocity is less than 0.5 percent over the total range for both flows.

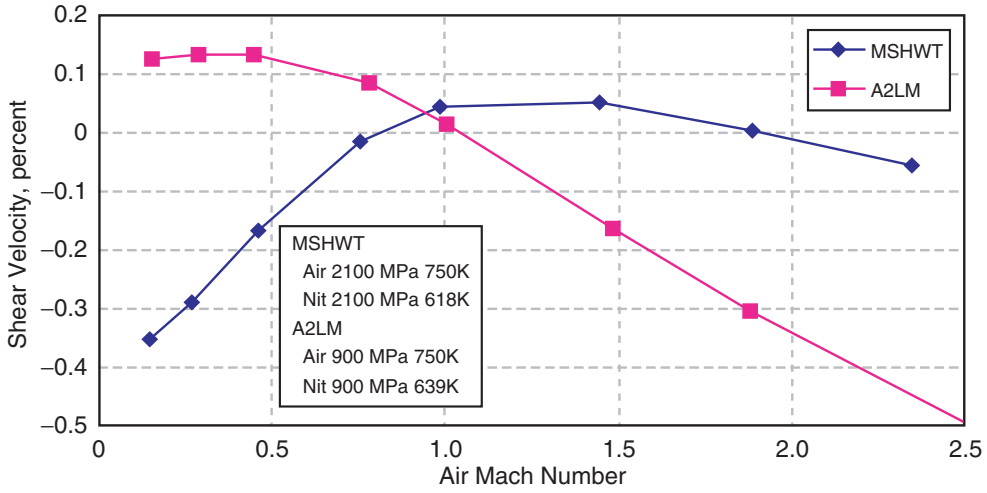

Figure D-2. Nitrogen-Air Shear Velocity, percent

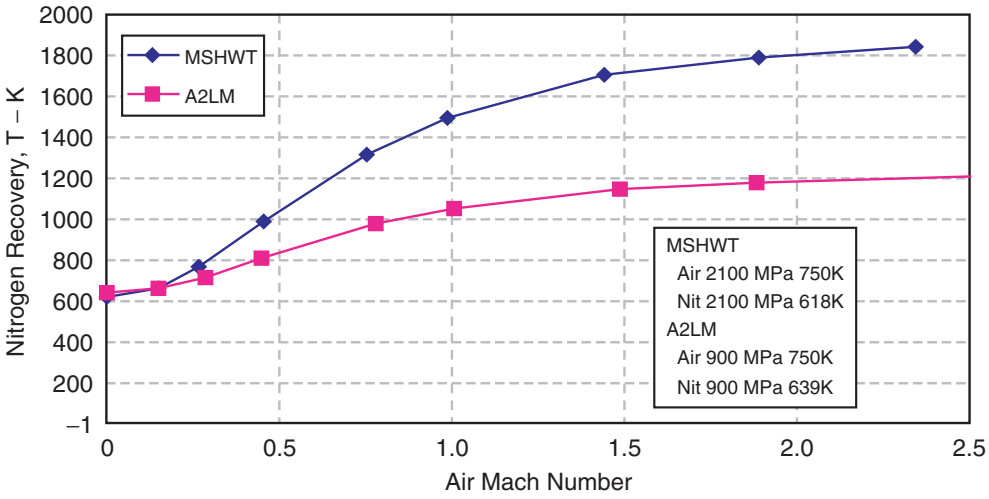

Figure D-3. Nitrogen Recovery Temperature

Thus it is easy to conclude that the mixing will be dominated by the injection process and the mixing in the nozzle, where the core velocity increases because of the e-beam heating. The injection details will be studied in the A2LM (using Princeton's calculations performed during the design of the A2LM) and then measured in the A2LM experiments. Thus the injection details in the A2LM should be consistent with expectations for the MSHWT.

The mixing in the nozzle can only be studied at the present time by Princeton's 2D viscous calculations. The first experimental information will come from the 20-MW ITS Experiment.

This experiment emphasizes that the 20-MW ITS must have an air-nitrogen system even though the throat cooling may not require the nitrogen.

Figure D-3 shows the wall nitrogen recovery temperature, which is about 200 K less than the equivalent air recovery temperature would be. This reduces the wall problem in the throat area. However, the recovery temperature will be high in the nozzle. Thus the nozzle will require special attention to protect the walls.

APPENDIX E
MSHWT NOZZLE CONFIGURATION

INTRODUCTION

An initial examination has been made of the influence of nozzle configuration on the performance of the MSHWT. The two questions of interest are these:

1) What is the minimum e-beam voltage that can be used?

2) Can a simple cone be used for the nozzle rather than the more complex contours previously considered?

The system previously considered was an early, base MSHWT configuration designed for M = 12 conditions. These conditions use a stagnation pressure of 2300 MPa rather than the 2100 MPa currently being used as the design objective (Appendix C). Although calculations at the correct conditions are necessary for any final design decisions, the present calculations are adequate to address the phenomenology of the questions posed.

The performance calculations use the system simulation model described in Appendix B. These calculations include the deposition of the e-beam energy so that the required nozzle length is found and all quantities are expressed in terms of the axial nozzle distance, x.

CALCULATIONS SUMMARY

For all cases, the system utilizes a UHP system operating at 2300 MPa and 750 K, a two-flow model whose heated core flow is 25 percent of the total mass flow, and the same throat diameter, d*, for all cases. The distance from the throat to the start of the e-beam heating was taken to be x = 2 d*. An inefficiency factor of 7 percent was included to allow performance degradation in going from these idealized 1D calculations to the more realistic 2D calculations.

The calculations included are summarized below:

1) MSHWT-3E (idealized case, 3 MV). This is the base case facility for M = 12, q = 2000 psf, with a 1.0-m test section and a UHP operating point of 2300 MPa and 750 K. The thermodynamics are based on a nozzle contour that heats at constant M = 2.0 until a temperature of 2500 K is reached, and then continues to heat at a constant temperature of 2500 K. For the heating length calculation, the investigators used an e-beam voltage of 3 MV, which is similar to the value being used in other e-beam heating investigations.

   The MSHWT-3E case is used as a base reference case throughout this Appendix.

2) MSHWT-3EC (simple cone, 3 MV). Case 3EC uses a 3-MV e-beam voltage but replaces the area contour with a simple cone from the start of heating (x = 2 d*) to the exit.

   In Case 3EC, two changes have been made relative to the base Case 3E, as follows:

   a) The Mach number at the start of the heating is reduced from M = 2.0 to M = 1.5, and the exit area ratio is increased from 11.1 to 14.0 so that the matched test section flow remains M = 12. The reduced Mach number at the start of the heating is used because the rapid expansion of the flow will allow stable flow during the heating even at the lower Mach number.

   b) The area profile is modified in the initial heating region. This is because the entropy rise is slightly higher than the base Case 3E, with the test section q reduced to q = 1900 psf. A detailed examination of the flow in the initial heating region shows that the pressure is dropping rapidly, the Mach number is increasing, and the area is increasing; therefore, one can expect stable flow. The more significant issue is the abrupt change in nozzle half angle from 0.8 deg upstream of the start of the heating to 9.7 deg in the heating region. In addition to the resulting flow quality question, this produces a higher Mach number than is desired in the initial heating region.

      It is found that the Mach number diminishes slightly in the early portion of the nozzle immediately following the transition to the cone flow. Since there is a strong positive pressure gradient in this same region, it is assumed that the flow, including the boundary layer, remains stable in this region.

3) MSHWT-3EC2 (modified cone, 3 MV). This is the same as Case 3EC above, except that the area distribution in the initial 10 mm (a distance of approximately one throat diameter) has been modified to a smooth curve, with an approximately constant radius of curvature. Beyond this point, the nozzle is a simple cone.

   The resulting flow provides a slightly reduced entropy rise, so the test section flow essentially matches the base Case 3E. Thus there is a slightly modified cone with the same nozzle length and e-beam voltage giving the same test section flow as the base Case 1.

   It may be desirable to make the transition region somewhat longer than that used here. This would reduce the Mach number overshoot and increase the overall nozzle performance slightly.

4) MSHWT-2EC2 (reduced voltage, 2 MV). The voltage is reduced from 3 to 2 MV, and correspondingly the nozzle heating region is reduced in length by a scale factor of 0.6. The e-beam current is increased to prevent any change in total power. All other input quantities remain unchanged from the modified cone Case 3EC2 above.

All flow quantities are found to be essentially unchanged from the modified cone Case 3EC2, except at a reduced length scale. The nozzle half-cone angle is 16.3 deg, compared to a value of 9.9 deg for Case 3EC2.

5) MSHWT-2EC2R (reduced current). This is an "off-design" case. All input conditions are the same as those for the reduced voltage Case 2EC2 above, except that the current is reduced by a factor of two. Since the voltage is unchanged, the power level is reduced by this same factor of two.

   The nozzle flow is reasonable in all details. The penetration of the heating into the nozzle is reduced, but hardly noticeable. Thus operation in this off-design condition is entirely feasible.

   The only critical point for this case is that the entropy rise is greatly reduced, and the matched altitude is thus achieved at a greatly reduced test section flow diameter: 380 mm, compared to 1000 mm for the design case. Thus operation at this off-design condition will require a changed UHP operating condition in addition to the reduced e-beam current if a 1-m test section is to be utilized. This remains to be examined.

The results of these five cases are summarized in Table E-1.

Also, the following curves are shown in Figs. E-1 thorugh E-4. respectively:

1) The thermodynamic path through the heating region,

2) Nozzle pressure distribution as a function of distance, x,

3) Nozzle Mach number as a function of distance, x, and

4) Nozzle diameter as a function of distance, x.

CALCULATIONS SUMMARY

Three main issues are presented here:

1) What is the minimum e-beam voltage that can be used?

   The cost of the e-beam accelerator, the e–beam power supply, and the magnets is highly dependent upon the required voltage level. The required strength of the magnets, for example, varies with the square of the e-beam voltage. The 2-MV voltage level cases (2EC2 and 2EC2R) seem acceptable, but there is probably a lower limit to be considered. A key issue is the minimum length nozzle in terms of nozzle cone half angle. The 2-MV case gives a half angle of 16.3 deg, which is probably pushing the upper limit in nozzle expansion angle. A second issue is the minimum length for which the magnets can be designed. Again, 110 mm of active heating, about 10 d*, seems to be a lower limit.

Table E-1. Summary

	MSHWT -3E	MSHWT -3EC	MSHWT -3EC2	MSHWT -2EC2	MSHWT -2EC2R
Summary					
UHP Press, MPa	2300	2300	2300	2300	2300
UHP Temp, K	750.0	750.0	750.0	750.0	750.0
Throat Diam C, mm	5.728	5.728	5.728	5.728	5.728
Test Sec Diam, mm	998	1018	996	975	382
Test Sec M	12.00	11.99	12.00	12.01	10.12
Test Sec q, psf	2009	1933	2020	2105	11284
Power					
Power UHP, MW	104.2	104.2	104.2	104.2	104.2
Power Heat, MW	178.8	178.8	178.8	178.8	89.4
Total, MW	283.0	283.0	283.0	283.0	193.6
E-Beam					
Voltage, MV	3.0	3.0	3.0	2.0	2.0
Current J, amps	59.6	59.6	59.6	89.4	44.7
Nozzle Length, mm	204.7	204.7	204.7	132.0	132.0
Max Expansion, deg	13.5	9.7	9.9	16.3	16.3
Energy Ratios					
H EB/H UHP	2.715	2.715	2.715	2.715	1.858
Delta Enthalpy, kJ/kg	4313.3	4313.3	4313.3	4313.3	2156.6
UHP					
Press, MPa	2300	2300	2300	2300	2300
atm	22,699	22,699	22,699	22,699	22,699
psi	333,589	333,589	333,589	333,589	333,589
Temp, K	750.0	750.0	750.0	750.0	750.0
Enthalpy, H, kJ/kg	2514.8	2514.8	2514.8	2514.8	2514.8
Entropy, S/R	16.410	16.410	16.410	16.410	16.410
mdot Core, kg/s	41.452	41.452	41.452	41.452	41.452
mdot Total, kg/s	165.809	165.809	165.809	165.809	165.809
Throat					
Diam Core, mm	5.728	5.728	5.728	5.728	5.728
Diam Total, mm	11.456	11.456	11.456	11.456	11.456
Press, atm	6084	6084	6084	6084	6084
Temp, K	507.4	507.4	507.4	507.4	507.4
Velocity, m/s	1,766	1,766	1,766	1,766	1,766
Recovery Temp, K	1677.1	1677.1	1677.1	1677.1	1677.1

Table E-1. Concluded

	MSHWT -3E	MSHWT -3EC	MSHWT -3EC2	MSHWT -2EC2	MSHWT -2EC2R
Start Heating					
Mach	2.00	1.54	1.50	1.50	1.51
Press, atm	1702	2875	2971	3004	2966
Temp, K	358.0	428.3	414.2	420.6	413.4
Velocity, m/s	2,052	1,968	1,966	1,963	1,967
Enthalpy, H, kJ/kg	2519.1	2528.4	2515.7	2519.3	2515.2
Entropy, S/R	16.483	16.619	16.424	16.480	16.416
Diam Core, mm	6.14	5.94	5.87	5.88	5.87
Diam Total, mm	12.25	11.79	11.74	11.74	11.74
End Heating					
Mach	2.87	3.04	3.08	3.11	3.66
Press, atm	112.2	80.0	78.6	77.3	50.4
Temp, K	2500.0	2349.8	2317.3	2289.0	1271.9
Velocity, m/s	2,776	2,850	2,866	2,880	2,571
Enthalpy, H, kJ/kg	6828.1	6828.1	6828.1	6828.1	4671.4
Entropy, S/R	27.626	27.668	27.620	27.576	25.379
Diam Core, mm	34.95	39.52	39.49	39.46	38.58
Diam Total, mm	38.19	42.86	42.86	42.86	42.86
Test Section					
Mach	12.00	11.99	12.00	12.01	10.12
Press, atm	9.42E-03	9.07E-03	9.47E-03	9.85E-03	7.44E-02
Temp, K	228.1	228.3	228.0	227.7	216.7
Velocity, m/s	3,633	3,633	3,633	3,633	2,985
Enthalpy, H, kJ/kg	6828.1	6828.1	6828.1	6828.1	4671.4
Entropy, S/R	27.626	27.668	27.620	27.576	25.379
Diam Core, mm	998	1018	996	975	382
q, psf	2,009	1,933	2,020	2,105	11,284
Press Alt, km	31.4	31.6	31.3	31.1	18.0

2) Can a simple cone be used for the e-beam heating nozzle rather than the more complex contours previously considered?

   These calculations indicate that the answer is yes. The calculations show that the transition from the slowly increasing area downstream of the throat to the cone is critical. However, a simple radius-of-curvature in the initial e-beam heating area is probably acceptable. With the rapid expansion in this area, heating can probably be started at M = 1.5 with a stable heating region because of the rapid decrease in pressure, increase in Mach number, and increase in nozzle area. It can be argued that this case is more stable than the constant Mach-number-2.0 heating that has been considered.

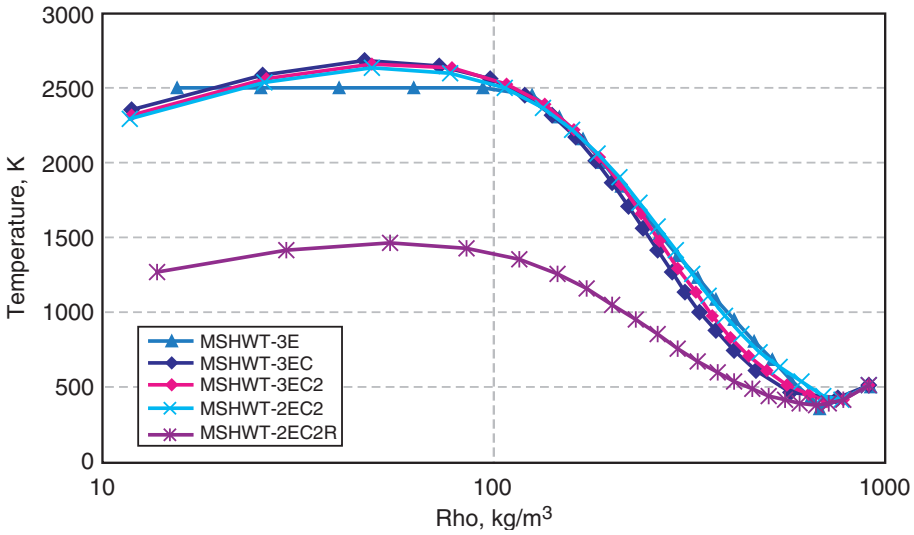

Figure E-1. Channel Thermo Paths

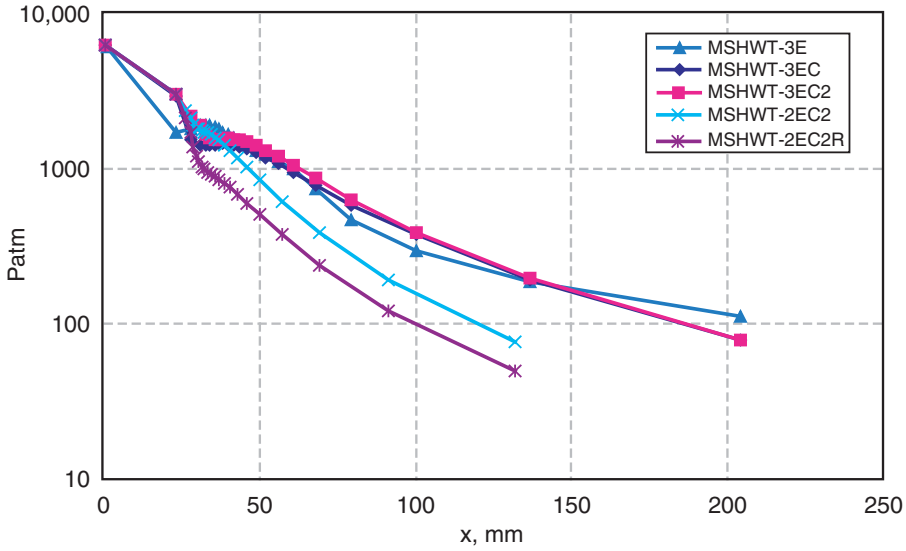

Figure E-2. Channel Pressure Distribution

The peak nozzle temperature is 2630 K, slightly higher than the base case of 2500 K. However, the nozzle exit temperature is about 2300 K, lower than the base case 2500 K. Thus one might expect that the flow chemistry would be as good or better than the base case.

It seems clear from these initial calculations that the nozzle transition from the throat to the conical heating area is a short distance, but critical in the area distribution. Also, it is important to match the e-beam voltage to the UHP system pressure level and the nozzle length so that the e-beam penetration reaches the beginning of the nozzle heating region but does not penetrate into the throat region. Choking will occur if the beam is allowed to penetrate into the throat region.

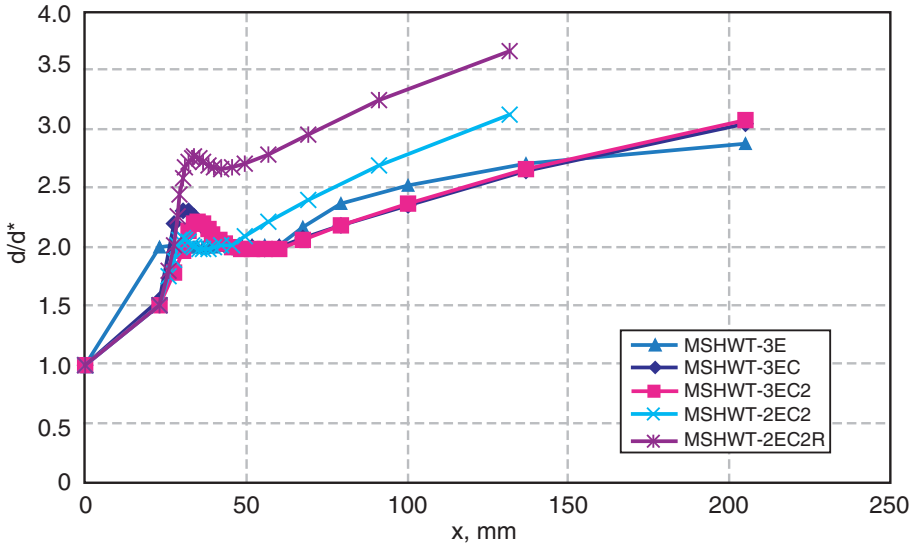

Figure E-3. Channel Mach Number

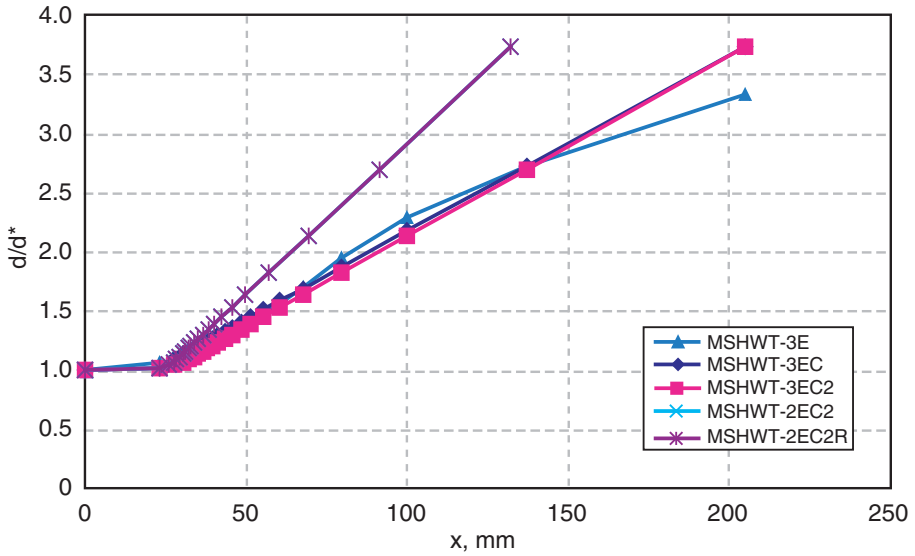

Figure E-4. Channel Geometry

3) Can a useful test can be achieved at off-design conditions?

This question needs much additional study, but the initial indication is that it can. In general, it appears that any off-design operation requires a voltage level that is dependent upon the UHP pressure level, and that the UHP pressure level needs to be adjusted with power level in order to achieve a matched altitude condition with expansion to the same 1-m test section flow diameter.

APPENDIX F
MSHWT OFF-DESIGN PERFORMANCE

INTRODUCTION

Performance calculations for the MSHWT have been made in an effort to define the operating map of the MSHWT and to determine the number of hardware configurations required to cover the map. The approach was to:

1) Develop a base design for the M = 12, q = 2000-psf case.

2) Develop base designs for M = 10 and M = 8, with the highest q possible, subject to the limitation of using the same e-beam system and UHP air supply system as that required for the M = 12 base case. The cold air mass flow was taken to give a 3-mm layer of cold air at the throat.

3) For each of the three base designs, compute off-design performance by varying the UHP conditions (p_o and T_o) and the e-beam power supply setting (E_o and J). For each case, the conditions are constrained so that the expansion to a 1-m test core corresponds to a matched altitude condition.

The matrix of conditions developed for the three Mach numbers is:

1) M = 12 hardware: q = 2000, 1500, and 1000 psf.

2) M = 10 hardware: q = 3000, 2000, 1000, and 500 psf.

3) M = 8 hardware: q = 4000, 3000, 2,000, 1000, and 500 psf.

THREE BASE DESIGNS

The design for the M = 12 base case was taken as the “Mod Cone” configuration as previously developed and reported in Ref. F-1 and Case 3EC2 in Appendix E. This uses a UHP 2300 MPa, 750-K system and a 2.47-MV e-beam voltage with a core power of 186 MW. The e-beam voltage was selected to give a nozzle expansion half angle of 15 deg aft of the maximum heating point.

For the M = 8 and M = 10 base cases, the e-beam was thus taken to be 2.5 MV at a power of 190 MW in the core flow. The cold flow was taken as a 3-mm layer of cold air at the throat.

An indication of the conditions and performance that can be achieved for the M = 8 case can be seen in Fig. F-1, taken from Ref. F-1. On this basis a value of q = 4000 psf was selected, as indicated above. For M = 8 and q = 4000 psf, the test section total enthalpy, entropy, and mass flow are determined. The UHP temperature was taken as T_o = 800 K. The UHP p_o is then found

such that 190 MW of power gives the correct test section total enthalpy. With the entropy level in the UHP and the test section now known, the required entropy rise also is known. It remains to develop a thermodynamic path for the e-beam heating such that it will produce this required entropy rise.

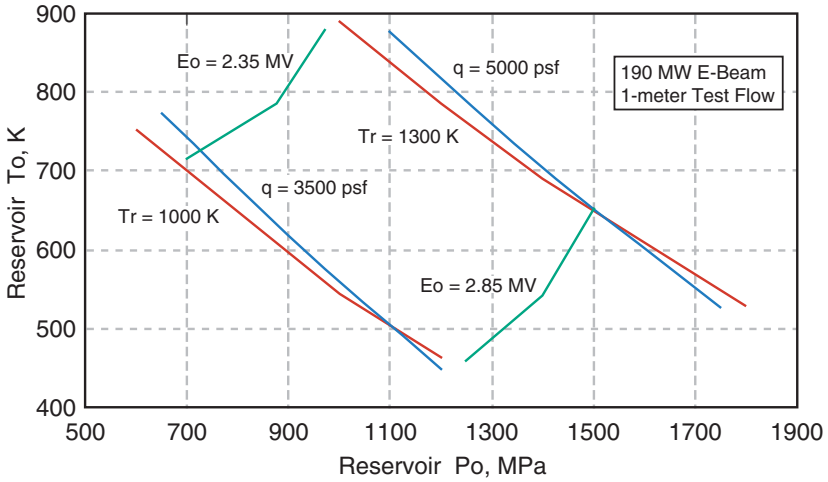

Figure F-1. Mach 8 Performance Map

Any thermodynamic path that produces the required entropy rise is acceptable thermodynamically. However, an arbitrary thermodynamic path can result in excessive nozzle expansion angles, adverse pressure gradients, and undesirable Mach number gradients. For the M = 12 base case, the criteria used to select the thermodynamic path were: 1) dp/dx 0, 2) dM/dx 0, and 3) dα/dx 0. For the M = 8 base case, no solution could be found that met these three criteria. The reasons turn out to be 1) greatly reduced real gas effects caused by the reduced pressure level; hence, changed gas thermodynamic derivatives and 2) the high entropy rise in the M = 8 case, which required low static temperatures; hence, high Mach numbers in the initial nozzle heating region. Thus the thermodynamic path selected was one that had a very slowly decreasing pressure in the initial heating region and then transitioned into a conical flow for the aft portion of the nozzle heating.

It is to be noted that either 1) increasing the UHP temperature T_o or 2) reducing the value of the test section q reduces the nozzle mass flow and improves the nozzle expansion angle and Mach number distributions.

The same design procedure was used to develop the M = 10 base case. Here a value of q = 3000 psf and a UHP temperature of T_o = 775 K were used.

A summary tabulation of three base cases is shown below in Tables F-1, F-2, and F-3. Curves of the conditions are shown in Fig. F-2.

Table F-1. Mach 12 Base Design/Configuration

	q = 2000	q = 1500	q =1 000
Test Section			
Mach	12.00	11.43	10.97
q, psf	2,081	1,500	1,000
Diam Core, mm	1000	1000	1000
Press Alt, km	31.1	32.7	34.9
UHP			
Press, MPa	2300.0	1511.0	866.1
Temp, K	750	750	750
mdot Total, kg/s	172.4	129.7	88.9
Throat			
Diam Core, mm	5.8	5.8	5.8
Diam Total, mm	11.7	11.7	11.7
T Recovery, K	1677	1398	1118
E-Beam			
Voltage Eo, MV	2.47	2.12	1.74
Current J, amps	75.1	66.3	57.5
Power Heat, MW	185.6	140.3	100.1
Chan Length, mm	175.4	175.4	175.4
Start Heating			
Mach	1.65	1.63	1.52
Press, atm	2495	1866	1417
Temp, K	399	419	458
End Heating			
Mach	3.41	3.13	2.90
Press, atm	46.1	39.8	31.6
Temp, K	2059	2115	2200

OFF-DESIGN CASES

For each of the three base cases, off-design performance was computed under the assumption that:

1) The hardware was fixed: throat diameter, e-beam heating nozzle area distribution and length, and test section diameter.

2) UHP temperature could increase slightly as the pressure is decreased:
   M = 12, T_o = 750 K
   M = 10, T_o = 775 K
   M = 8, T_o = 800 K

3) E-Beam voltage and current would not exceed those for the M = 12 base case.

Table F-2. Mach 10 Base Design/Configuration

	q = 3000	q = 2000	q = 1000	q = 500
Test Section				
Mach	10.00	9.44	8.96	8.72
q, psf	3,000	2,000	1,000	500
Diam Core, mm	1000	1000	1000	1000
Press Alt, km	26.3	28.2	32.1	36.5
UHP				
Press, MPa	1774.1	1049.7	459.6	194.0
Temp, K	775	775	775	775
mdot Total, kg/s	220.1	154.8	80.7	40.4
Throat				
Diam Core, mm	8.5	8.5	8.5	8.5
Diam Total, mm	14.5	14.5	14.5	14.5
T Recovery, K	1520	1224	962	840
E-Beam				
Voltage Eo, MV	2.50	2.14	1.48	0.93
Current J, amps	76.0	64.7	51.7	44.9
Power Heat, MW	190.0	138.3	76.5	41.5
Chan Length, mm	303.6	303.6	303.6	303.6
Start Heating				
Mach	4.02	3.43	2.78	2.37
Press, atm	343	327	251	161
Temp, K	280	315	353	390
End Heating				
Mach	3.13	2.81	2.52	2.39
Press, atm	32.4	26.6	16.6	9.3
Temp, K	1592	1636	1706	1802

The computational procedure to develop the reduced performance was to:

1) Pick a reduced q as the target performance number.

2) Iterate on the UHP pressure, p_o, to get the q value.

3) Iterate on the e-beam voltage to get the same e-beam penetration. This criterion was applied by requiring 99.9 percent of the e-beam energy deposition to be downstream of the "start of nozzle heating" point and 0.1 percent upstream of this same point.

   The exception to this was for the M = 12 cases, where the 99.9 percent was increased to 99.95 percent to get slightly less penetration and give more margin for choking near the throat.

4) Iterate on the e-beam current, J, to adjust the power so that expansion to the 1000-mm test section was at a matched altitude condition.

Table F-3. Mach 8 Base Design/Configuration

	q = 4000	q = 3000	q = 2000	q = 1000	q = 500
Test Section					
Mach	8.00	7.73	7.46	7.18	7.02
q, psf	4,000	3,000	2,000	1,000	500
Diam Core, mm	1000	1000	1000	1000	1000
Press Alt, km	21.6	23.0	25.1	29.2	33.5
UHP					
Press, MPa	867.0	626.8	400.3	176.5	83.8
Temp, K	800	800	800	800	800
mdot total, kg/s	258.2	199.9	137.4	70.7	35.6
Throat					
Diam Core, mm	14.1	14.1	14.1	14.1	14.1
Diam Total, mm	20.1	20.1	20.1	20.1	20.1
T Recovery, K	1163	1057	959	857	817
E-Beam					
Voltage Eo, MV	2.50	2.16	1.71	1.07	0.61
Current J, amps	76.0	69.2	61.7	52.8	48.1
Power Heat, MW	190.0	149.7	105.4	56.2	29.2
Chan Length, mm	469.7	469.7	469.7	469.7	469.7
Start Heating					
Mach	5.12	4.49	3.86	3.20	2.91
Press, atm	94	90	78	53	31
Temp, K	230	250	273	299	320
End Heating					
Mach	2.55	2.37	2.18	1.97	1.86
Press, atm	30.9	26.2	20.1	11.8	6.4
Temp, K	1303	1327	1358	1406	1458

Note that the above three iterations were in addition to and simultaneous with the two model simulation iterations (the nozzle pressure distribution to match the specified area distribution, and the energy-addition distribution to match the e-beam heating equations). Simultaneous convergence of these five iterations required special consideration, but it was accomplished.

Summary tabulations of the off-design cases are shown below in Tables F-1, F-2, and F-3. Curves of the conditions are shown in Figs. F-3 through F-5. Figure F-6 gives the resulting performance map. The UHP operating conditions are shown in Fig. F-7.

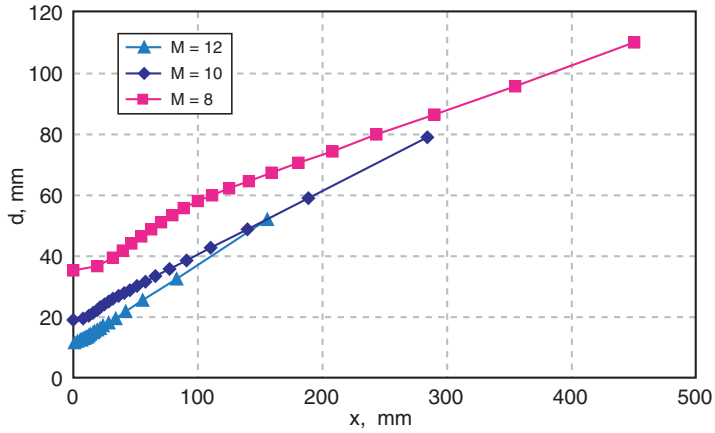

a. Nozzle Diameter vs. Distance

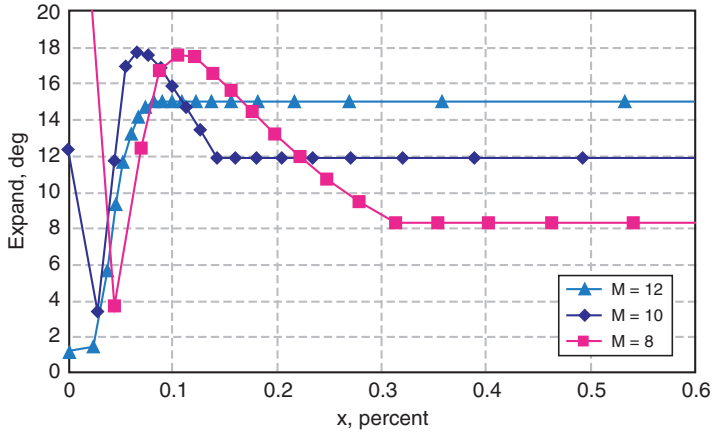

b. Nozzle Expansion vs. Percent Nozzle Length

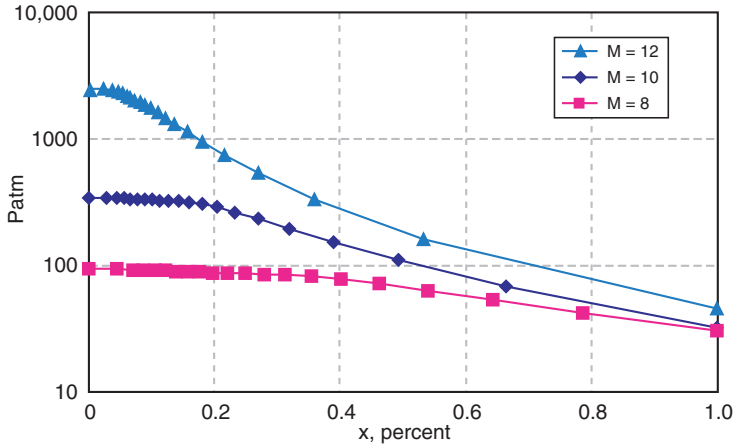

c. Nozzle Pressure vs. Percent Nozzle Length

Figure F-2. M = 12, 10, and 8 Base Cases

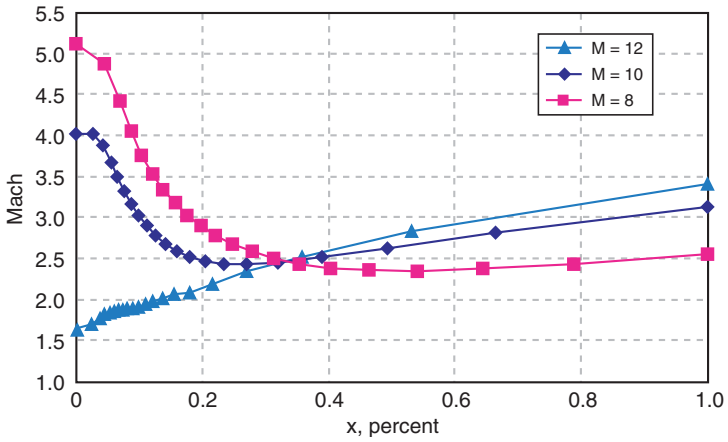

d. Nozzle Mach Number vs. Percent Nozzle Length

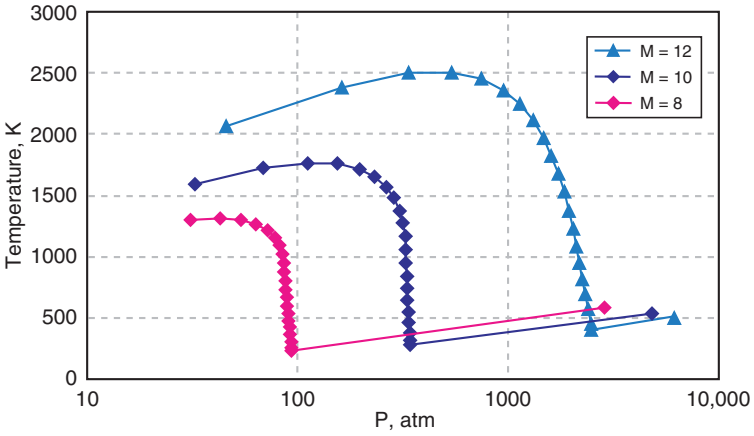

e. Nozzle Thermodynamic Paths

Figure F-2. Concluded

DISCUSSION

Several points are worth noting:

1) Figure F-2a shows that the nozzle length increases with reduced Mach number. This is a consequence of the UHP pressure decrease for the reduced Mach numbers and the constraint of using the same 2.5 MV, thus requiring increased length. Note that the nozzle geometry remains well behaved.

2) Figure F-2b shows the nozzle expansion angle distribution to be greatly changed at the lower Mach number compared to the M = 12 case. This is the result of 1) greatly reduced real gas thermodynamic effects and 2) the need to operate at higher heating Mach numbers to get low temperature and the required large entropy rises.

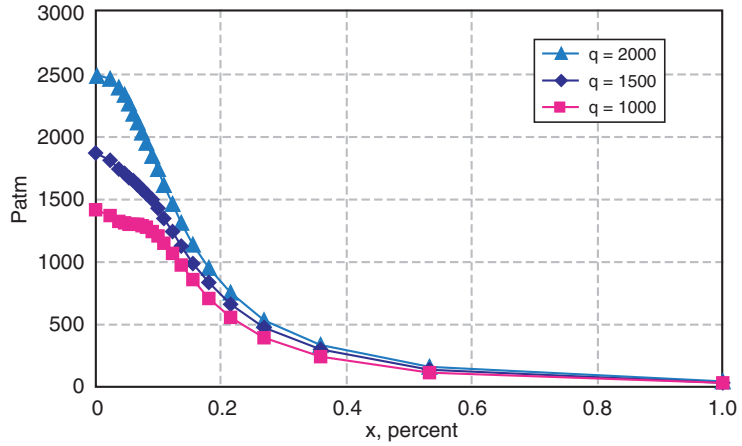

a. Nozzle Pressure vs. Percent Nozzle Length

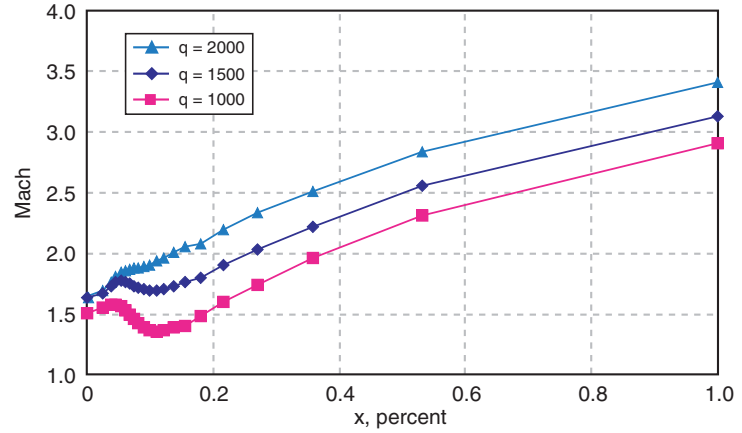

b. Nozzle Mach Number vs. Percent Nozzle Length

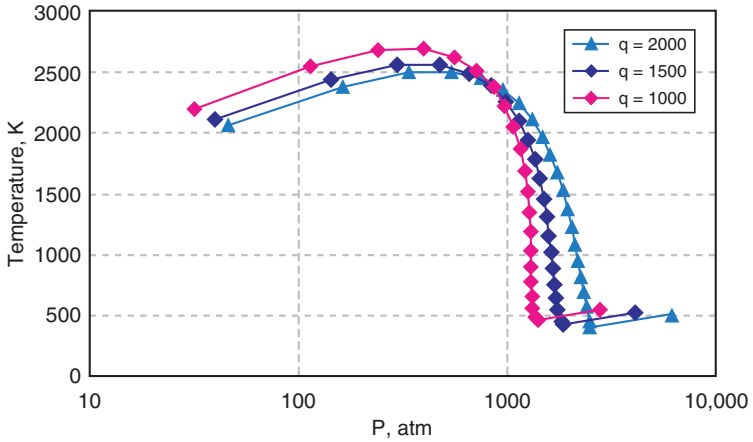

c. Nozzle Thermodynamic Paths

Figure F-3. M = 12 Configuration

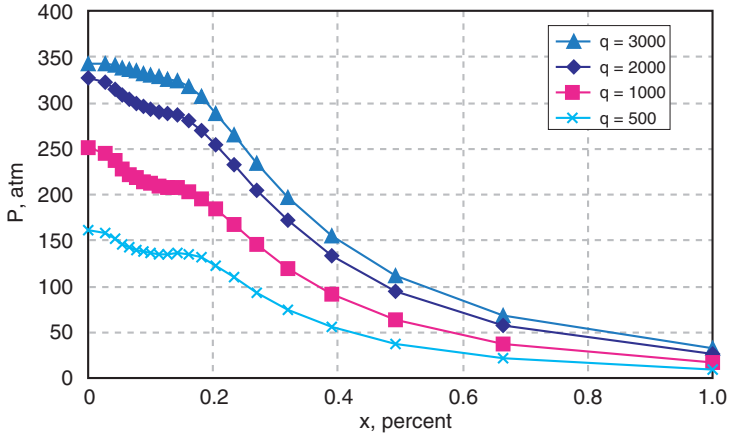

a. Nozzle Pressure vs. Percent Nozzle Length

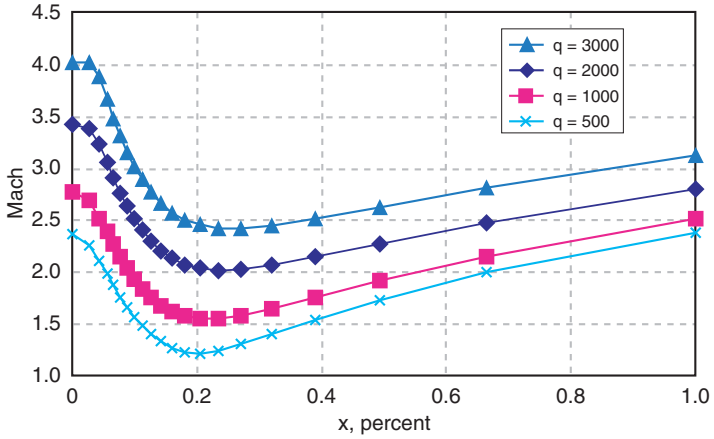

b. Nozzle Mach Number vs. Percent Nozzle Length

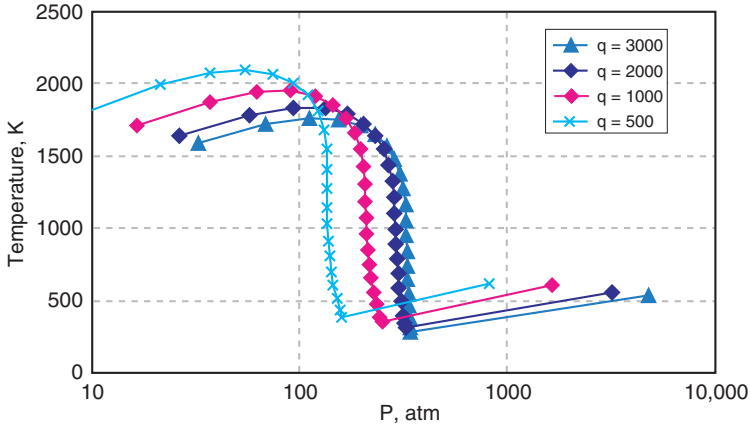

c. Nozzle Thermodynamic Paths

Figure F-4. M = 10 Configuration

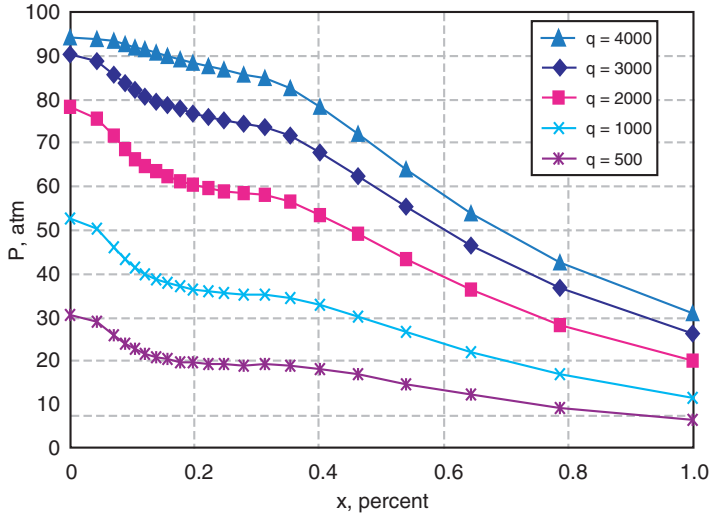

a. Nozzle Pressure vs. Percent Nozzle Length

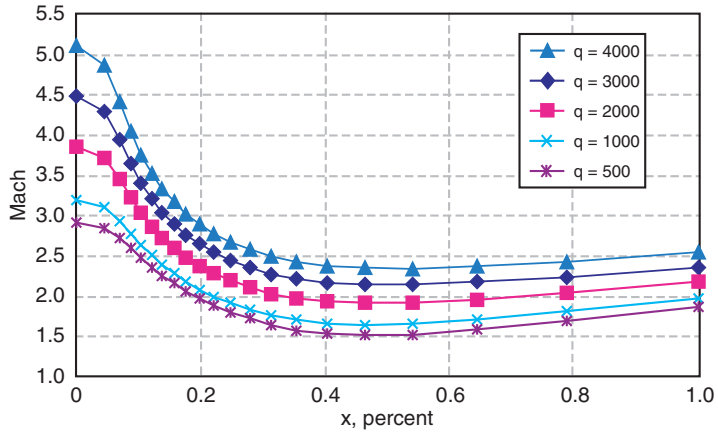

b. Nozzle Mach Number vs. Percent Nozzle Length

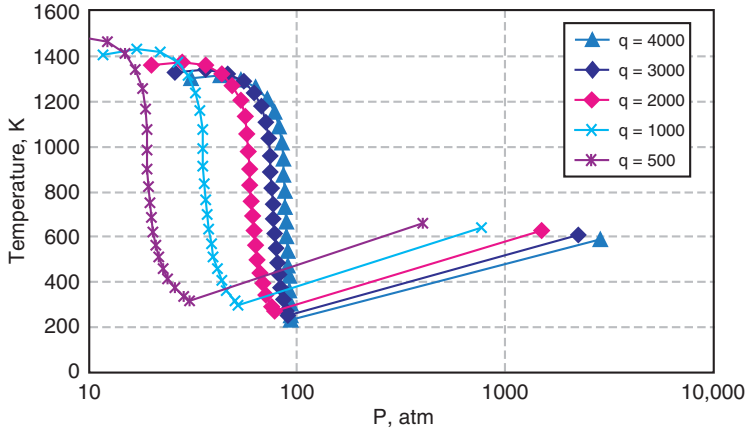

c. Nozzle Thermodynamic Paths

Figure F-5. M = 8 Configuration

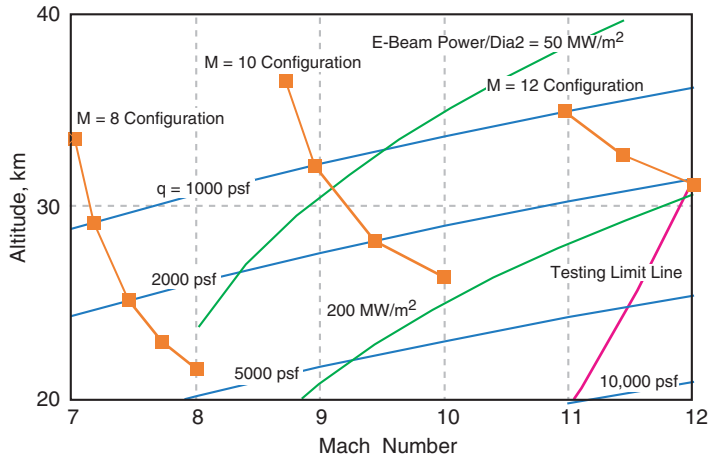

Figure F-6. Off-Design Performance Map, M = 8, 10, and 12 Configurations

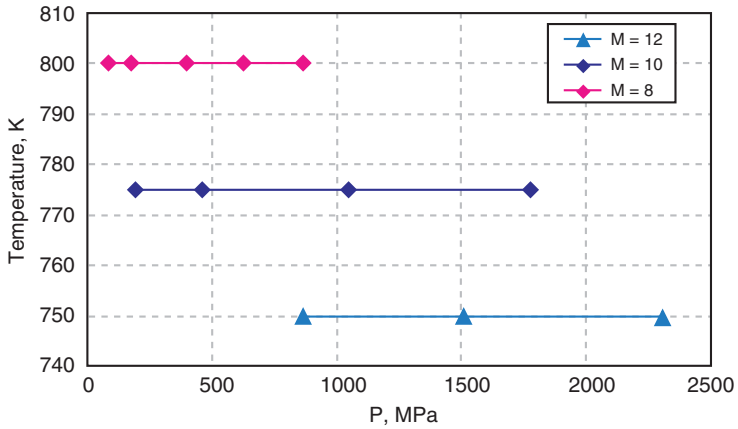

Figure F-7. UHP Operating Points, M = 8, 10, and 12 Configurations

3) At M = 12, the emphasis is to keep the entropy rise as small as possible. At M = 8, the emphasis is to make the entropy rise as large as possible to meet matched altitude conditions. The greatly changed Mach numbers are seen in Fig. F-2d. Thus a M = 8 or M = 10 nozzle is fundamentally different from the M = 12 case.

4) Figures F-3b, F-4b, and F-5b all show that off-design operation always results in reduced Mach number operation. The limit in off-design operation turns out to be when the Mach numbers get too close to M = 1 and choke.

5) In all cases, the off-design operation results in lower static temperature, which should help regarding nonequilibrium chemistry.

REFERENCE

F-1. Ring. L. E., Brown, G. L., Girgis, I. G., Schneider, L. X., and Lofftus, D. A. “RDHWT/MARIAH II Program: Facility Performance and System Integration Issues.” AIAA 2002-3126, 22nd AIAA Aerodynamic Measurement Technology and Ground Testing Conference, St. Louis, MO, June 24-26, 2002.

NOMENCLATURE

1D	One-dimensional
2D	Two-dimensional
A	Ampere
A2LM	A-2 Lite Modified
AEDC	Arnold Engineering Development Center
ANSI	American National Standards Institute
ASE	AeroSystems Engineering Corporation
ac	Alternating current
atm	Atmosphere
CFD	Computational fluid dynamics
cm	Centimeter
cm^2	Centimeter squared
cm^3	Cubic centimeter
dc	Direct current
EMF	Electromotive force
EOS	Equation of state
e-beam	Electron beam
eV	Electronvolt
FEA	Finite-element analysis
FY	Fiscal year
ft	Foot
GHz	Gigahertz
ID	Inside diameter
IPT	Integrated Program Team
ITS	Integrated test system
in.	Inch
in./s	Inches per second
keV	Kiloelectronvolt
kg	Kilogram
kHz	Kilohertz

kJ	Kilojoule
km	Kilometer
kPa	Kilopascal
kV	Kilovolt
kW	Kilowatt
L	Liter
LAN	Local area network
LLNL	Lawrence Livermore National Laboratory
lbf	Pounds force
MARIAH	Magnetohydrodynamic accelerator research into advanced hypersonics
MeV	Megaelectronvolt
MHD	Magnetohydrodynamics
MN	Meganewton
MPa	Millipascal
MSE	MSE Technology Applications, Inc.
MSHWT	Medium-scale hypersonic wind tunnel
MV	Megavolt
MW	Megawatt
m	Meter
m^3	Cubic meter
mA	Milliampere
min	Minute
mm	Millimeter
mrad	Milliradian
ms	Millisecond
NIST	National Institute of Standards and Testing
ns	Nanosecond
OD	Outside diameter
ORNL	Oak Ridge National Laboratory
PLC	Programmable logic controller
psf	Pounds per square foot

psi	Pounds per square foot
psig	Pounds per square foot gage
R&D	Research and development
RBS	Retractable Bridgman support
RDHWT	Radiatively driven hypersonic wind tunnel
RF	Radio frequency
RTS	Ring Technical Services
SNL	Sandia National Laboratories
SOTPs	System operating test procedure
s	Second
scf	Standard cubic foot
T	Tesla
T&E	Test and evaluation
UHP	Ultra-high pressure
UHPTF	Ultra-high-pressure test facility
USAF	U.S. Air Force
V	Volt